



**UNIVERSITA' DEGLI STUDI DI PADOVA**

DIPARTIMENTO DI TECNICA E GESTIONE DEI SISTEMI INDUSTRIALI

**TESI DI LAUREA MAGISTRALE IN INGEGNERIA DEI  
MATERIALI**

(Laurea Magistrale)

**MATERIALS CHARACTERIZATION FOR THE INNOVATION  
OF SKI EQUIPMENTS**

CARATTERIZZAZIONE DI MATERIALI PER APPLICAZIONI INNOVATIVE IN  
AMBITO SCIISTICO

***Relatore: Prof. Nicola Petrone***

***Correlatore: Ing. Giorgio Grandin***

***Laureando: ALEX PERSICO***

ANNO ACCADEMICO 2013-2014



# Summary

- INTRODUCTION..... 1
- 1. From Prehistoric Skis to Carving Technology ..... 3
  - 1.1 Modern skis ..... 4
  - 1.2 Skidding and carved turns ..... 5
    - 1.2.1 Ski forces..... 6
    - 1.2.2 Radius of turn ..... 8
- 2. Ski characterization devices ..... 11
  - 2.1 MTS 858 Mini Bionix ..... 11
  - 2.2 Chemnitz bench ..... 13
    - 2.2.1 Test method ..... 15
    - 2.2.2 Test output..... 15
  - 2.3 Flex bench of Tecnica Group laboratory ..... 16
  - 2.4 Torsion bench of Tecnica Group laboratory..... 18
  - 2.5 Slytech bench..... 19
    - 2.5.1 Test Methods ..... 22
    - 2.5.2 Test output..... 23
- 3. Elastic compensation superstructure, “arm” ..... 25
  - 3.1 Definition of the different part of the ski..... 25
  - 3.2 Patents..... 26
  - 3.3 Prototypes ..... 29
    - 3.3.1 ALU..... 31
    - 3.3.2 PU..... 32
    - 3.3.3 PU+C..... 35
    - 3.3.4 C H B..... 35
  - 3.4 Flex arm properties ..... 36
    - 3.4.1 Nordica arm stiffness test ..... 36
    - 3.4.2 Nordica test Results..... 36
    - 3.4.3 DII arm stiffness test ..... 37
    - 3.4.4 DII test results ..... 39

3.4.5	Comparisons.....	40
3.4.6	Comments to the results .....	42
3.5	Vibration damping.....	43
3.5.1	Procedure.....	44
4.	Work bench result influenced by arm prototypes .....	49
4.1	Dobermann Spitfire Edge load profile.....	49
4.2	Slytech bench results .....	49
4.2.1	Comments to the results .....	53
4.3	Results from Chemnitz bench.....	54
4.4	Results from Nordica flex bench .....	57
4.5	Padua – Chemnitz benches comparisons.....	58
4.6	Chemnitz – Nordica benches comparisons.....	60
4.7	Comments.....	61
4.8	Feedback from skiers.....	62
4.8.1	Test procedure .....	65
4.8.2	Form results.....	65
4.8.3	Comments to the results .....	66
4.8.4	Other comments .....	67
5.	Foam: a new device for ski load distribution acquisition.....	69
5.1	Introduction .....	69
5.2	Materials and methods.....	69
5.2.1	General mechanical properties of snow .....	70
5.2.2	MTS 858 Mini Bionix .....	73
5.2.3	Slytech edge load profile bench .....	74
5.2.4	Faro ScanArm V3.....	75
5.2.5	SmartScope ogp Flash CNC 300.....	76
5.3	Foam characterization.....	77
5.3.1	Data analysis .....	78
5.4	Test and laser acquisition .....	79
5.4.1	Execution of the test.....	79

5.4.2	Faro ScanArm laser acquisition .....	80
5.4.3	Faro ScanArm data analysis .....	81
5.4.4	SmartScope Flash CNC300 acquisition .....	82
5.4.5	SmartScope Flach CNC300 data analysis .....	82
5.5	Results .....	83
5.5.1	Foam characterization results .....	83
5.5.2	Slytech bench results .....	87
5.5.3	Scanarm results .....	89
5.5.4	Smartscope results .....	92
5.5.5	Smartscope and ScanArm results .....	94
5.6	Comments to the results .....	96
6.	Conclusions .....	97
Appendix	.....	99
	<i>PU details: Resina SG 95</i> .....	99
	<i>Vittorio Quaggiotti Patent</i> .....	101
	<i>Influence of rubber inserts</i> .....	101
Bibliography	.....	105



# INTRODUCTION

The present thesis comes from the passion for winter sports, especially alpine skiing.

Skiing is a recreational activity and competitive sport in which the participant attaches long runners or skis to boots or shoes on feet and uses them to travel on the snow. Thanks to its double nature, which combines together agonism and amusement, nowadays it has become the most popular winter season activity. Every year millions of people spend at least one day skiing on the slopes of resorts located on the mountains all over the world. That's why all the skiing equipment companies are constantly looking to evolve their products, especially in the last fifty years.

The aim of this activity was essentially to study different elastic compensation arm prototypes, fixed to the front part of the ski, useful to redistribute the forces at the ski shovel in order to improve the ski handling.

An accurate knowledge of ski structural and mechanical properties is very important for users. A key point for the comprehension of these properties is the distribution of pressure at the edge. The Edge Load Profile (ELP), a diagram representing the pressure along an effective length of the ski, is a complex study to perform, but an accurate development of different shape for different skis provides a tool for ski qualification and design improvement.

Researcher and ski manufacturer developed different types of benches and several activities were carried out for measuring the static edge pressure profile when a ski is pressed against the bench with different angles and loads.

In this work the bench used for characterize the ski during a bending test are presented: the Slytech bench, the Chemnitz bench and the Nordica bench. In this way it was possible to test experimentally the performances of elastic compensation arms applied to the ski with respect the original one. Furthermore the arm stiffness and its influence on the total system rigidity, the ski with arm, were experimentally evaluated.

Once that all experimental tests were performed, the complementary activity was to compare the engineering results with the sensations arising from in-field tests. Data obtained are not sufficient to give statistically results, but the developed procedure will be followed in further acquisitions and statistical analysis.

The final section of the thesis deals with the study of an innovative procedure to obtained the edge load profile by using foam of different density. Some foam material has been characterize that could simulate the snow's behaviors, in order to find the absorbed force during a static simulation of a curved turn.





# 1. From Prehistoric Skis to Carving Technology

Initially ski were developed as like means of transportation, facilitate the transfortation of people and objects on the snow using its characteristic extended and flat shape. First skis were made entirely by wood and bindings consisted into two tiers that allowed keeping the foot attached to the ski. A ski binding is an attachment which anchors a ski boot to the ski.

During the 1800's, skiing evolved into a sport and great advances in technique and equipment design followed. Generally skiing activity was much closer to skating, using long gliding strides. This technique required bindings that followed the skier's foot through a wider range of motion, but loosening the toe strap simply caused a fall. To address this, a second strap was added that looped from the toe around the heel of the boot, pulling it forward into the toe strap. Over time, the toe strap evolved into a metal cup that provided much greater fixation grip, and the heel strap was replaced by metal cables and springs. During downhill runs, the skier could clip the cable under small fingers near the heel of the boot, locking it down and providing better control. When the downhill portion ended, they could be unclipped to allow the normal striding motion.



**Figure 1.1** Example of an ancient cable bindings on the left, and a modern Alpine ski bindings on the right

It was not until the 1930s that the techniques for alpine and cross country skiing started to separate in earnest. The introduction of ski lifts propelled this evolution. This led to the request of bindings that would release in the case of an accident, which was more likely to cause injury during the higher speeds of a downhill descent. At the same time, the need to unclip the binding for the cross-country portion was eliminated. Cable bindings remained in use for some time for cross-country, and a limited selection are still available today. Also skis were modified introducing steel for edges having better grip during the turns. The skiing technique expected a “skid turn” to change direction. That means a combination of sliding and slipping as the skis move through the turn. Tails of the skis are making a wider path than the tips.

A very important revolution was the side-cut geometry, that allowed skier to bend the ski while edging to perform the curve. In this way the skier is able to carve the ski on the snow

describing a curve without skidding out because the imprint to the ground is just a curve with a certain radius, as will be explained better later.

## 1.1 Modern skis

Present day skis are still laminates of several material layers; the bottom layer usually consists of sintered or extruded polyethylene enframed by steel edges. Above the base layer a sandwich structure of wood or plastic core enclosed by two metal (typical aluminum or titanal) face layers follows. This sandwich structure determinates the bending and torsion stiffness of the ski; the thickness of the core material varies along the ski axis, so the stiffness distribution can be adjusted. To increase the torsion stiffness, layers of fiberglass are laminated often embedded in polyurethane. Figure 1.2 displays a simplified example of the typical composition of a modern ski usually modern skis are equipped with additional accessory features to increase torsion stiffness or enhance damping properties.

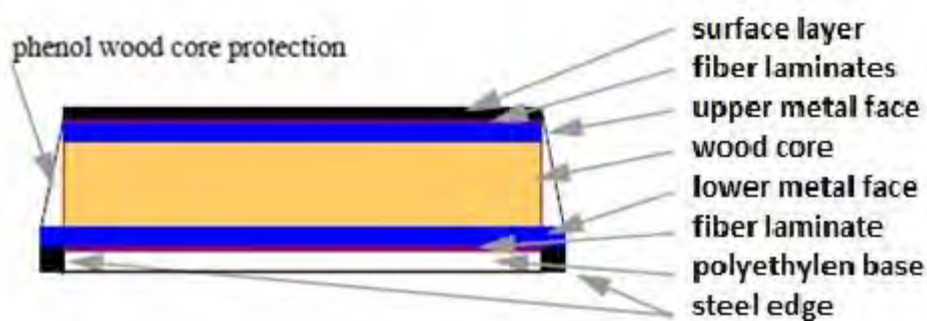


**Figure 1.2** *Simplify cross section of a sandwich structure of a modern ski.*

The material layer are glued together with a special epoxy resin by pressing: this induces a deformation and pre-stresses the sandwich structure of the ski when the layers are glued together. This pre-stressed state cause the ski to camber: if the ski is then loaded in the middle section the camber transfers the pressure to the ski end and the shovel, which improves the snow grip of the ski edges at the shovel and tail and facilitates turning.

The variable width of the ski along its length defines the ski's side cut, that is explained by the "radius" of a ski. During the turn the ski is bent until the middle section is in contact with the snow, so the side cut of the ski determinates how much the ski will be bent. The shape of the ski is chosen such that the ski during the turn ideally assumes a circular shape.

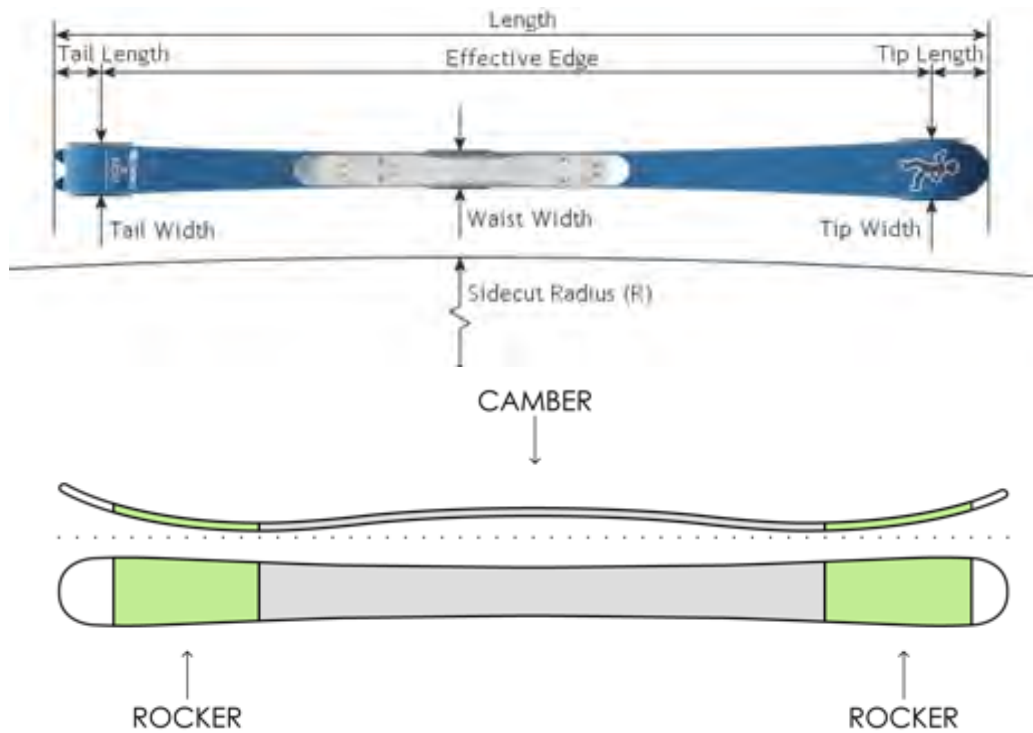


**Figure 1.3** Ski dimensions [<http://www.mechanicsofsport.com> and [www.evo.com](http://www.evo.com)]

## 1.2 Skidding and carved turns

Shaped skis, also called parabolic skis, make carve turns possible at low speeds and with short turn radius. They were first developed in 1988 by Jurij Franko in Slovenian ski producing company Elan who calculated a suitable flex pattern for new kind of skis with his colleague Pavel Skofic.

Shaped skis were almost unheard of until the early 1990s, when skiers began noticing certain advantages to the deeper sidecuts of snowboards, especially alpine snowboards, and the carving ability that this shape offered over the traditionally-shaped ski. Skis of this new shape have since become the most common, and in many areas, the only kind of recreational ski available. The idea of shaped skis was formed by approaching the occurrence of skidding from a different perspective. Two basic assumptions were applied: that the ski would bend when edged (edging is the angling of the ski running base with the snow surface) only to the point where the ski's center came in contact with snow surface. If radius of a turn is chosen together with edge angle, calculation of sidecut (intersection of snow and ski surface) is relatively easy. The final result is parabolic sidecut.

Unlike a skidding turn, which primarily uses the skidding effect to reduce speed, a perfect carve turn does not lose any speed because there is no braking action in the turns. Rather, the reduction of the average path slope angle resulting from the carve skier's S-shaped path down the slope, as opposed to a path straight down, reduces the skier's speed.

During a carved turn the ski would not “skid” only when all the points of the edge of the ski traveled through the same point on the snow surface.

For a dynamic analysis of skiing turns the interaction between ski and snow plays an essential role. In the present thesis it has been studied this interaction in a static case, with no computer simulations, which is also fundamental for carved turns. Assume that a skier performs a carved turn with a certain instantaneous turn radius and a given velocity: these two quantities determine the centrifugal force, which acts on the skier. There are also other forces that it’s not possible to neglect but are more difficult to take in account, like weighting or unweighting, leg and trunk actions, poling or skating. In a simplify model the resultant force acting on the skier is given by the vector sum of the centrifugal force and the gravitational force. To maintain equilibrium the skier tilts toward the center of the turn. He has to take such a position that the resultant force acting on his center of gravity is directed to the region between the skis, usually to the loaded edge of the outer ski. Thus, the resulting force is approximately normal to the running surface of the ski.

Further, torques about the longitudinal axis of the ski (edging torque), the transversal axis (forward or backward leaning) and the vertical axis act on the skier. Forces and torques can be transmitted from the skier to the ski in the boot-binding region only. The snow has to sustain the forces that the ski exerts onto the snow. The relation between compaction pressure and penetration could be approximated as linear, however, when the compaction pressure exceeds a certain limiting value, the yield pressure, the snow starts yielding.

The aim of this study is the evaluation of the pressure distribution under the loaded ski during purely carved turns. This permits to develop a theory that takes in account the benefits introduced with an elastic superstructure.

### 1.2.1 Ski forces

A skier’s weight is distributed over the snow by ski length, camber and stiffness.



**Figure 1.4** Resultant skier force  $R$  and ground reaction force  $F_N$

In Figure 1.4  $R$  defines the summation of the weight force and centrifugal force;  $F_N$  define lateral ground reaction force opposite to  $F$  shared along all the ski length. Obviously the summation of all forces in each direction is zero.

During a ski run a lot of forces are developed and pass through the bindings that have therefore a crucial role in transferring forces from skier's body to the ski and ground. It's now clear double task that bindings have to provide for: they have to maintain fixed contact between skis and boots opposing acting forces till a predetermined value of forces themselves; then, when this limit is exceeded, they have to break up the contact and free the boots to prevent traumas and injuries to the skier.

P. Gardin and N. Petrone had developed a specific load cell to interpose between ski and binding that record stresses on it.

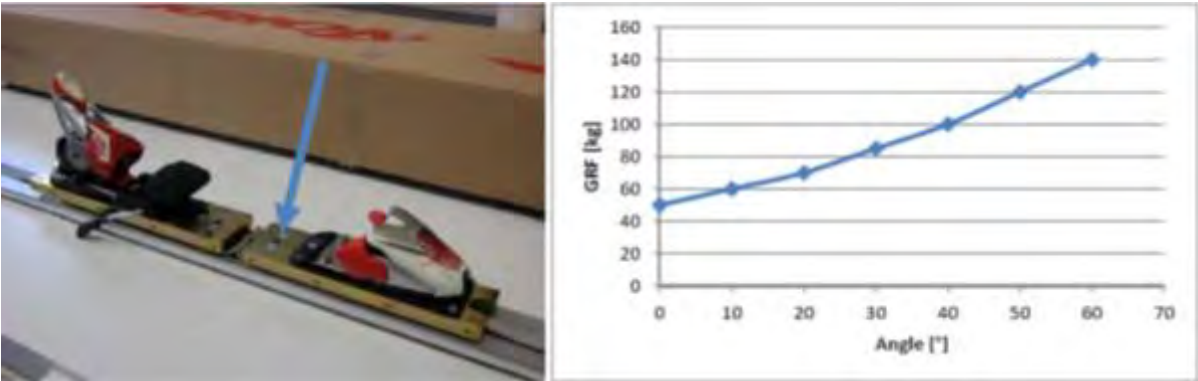


**Figure 1.5** Picture of the load cell recording the stress on bindings and the output from data analysis

The previous graph, which represents the mean Ground Reaction Force (GRF) recorded during a ski run, allows having an idea of the load transfer during a turn due to centrifugal force. We can suppose, with a good approximation, that a man of 100 kg presses a leg with different loads during a turn. When the angle  $\theta$  is  $0^\circ$ , obviously, 50 kg are applied on each leg; when angle  $\theta$  increases, loads increase. Defining  $\theta$  the angle between ground and the body in a frontal view, field test allows assuming, as previous graph represents, the next table of GRF distribution

**Table 1.1** Ground Reaction Force for different Angles

$\Theta$ [°]	GRF [kg]	GRF Ratio %
0	50	100%
10	60	120%
20	70	140%
30	85	170%
40	100	200%
50	120	240%
60	140	280%

As the angle increase, the percentage of the GRF increases proportionally; for example, in a turn with an angle of 40°, GRF is double of the entire body weight of the skier. This is an important concept because it highlights that, during a ski run, the forces acting on the bindings depends not only on the skier’s behavior, that is if he jumps or brakes hard or so on, but also on the turning angle. It also highlights that the binding’s work is very complex because it has not only to contrast a force, but varying force during the time.

**1.2.2 Radius of turn**

Each ski is determined by its radius of the turn; this parameter depends on side-cut and typifies the destination use of the ski itself. Some examples, skis for Gigant slalom have high radius of curvature (about 30 m), instead Special Slalom skis have lower radius of curvature (about 13-14 m). Radius of the turn is fundamental and influences the ski performances, it depends on:

- Side Cut
- Edging angle  $\theta$
- Load against planar surface of the ski
- Snow characteristic

Sidecut radius is defined as the distance between the narrowest point in the waist W and the chord of the circle between the widest point (H and S) of the ski that are on the circle.

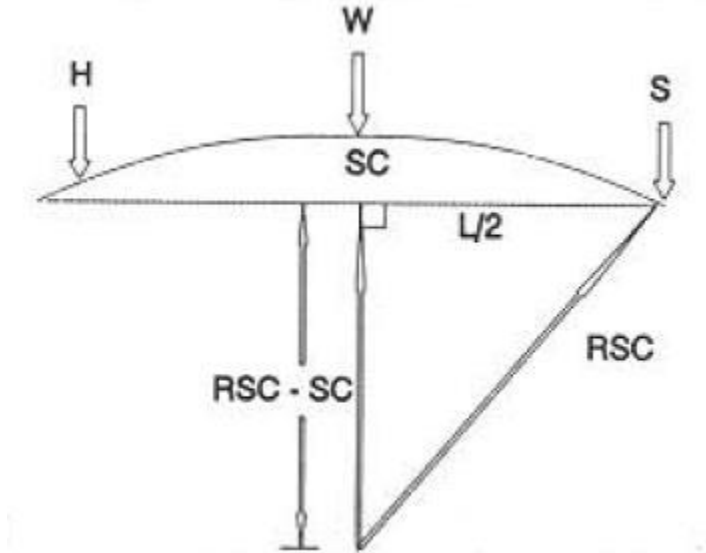


**Figure 1.6** Side Cut Radius RSC, Side Cut, Length of the ski

By the Pythagorean theorem

$$(RSC - SC)^2 + \left(\frac{L}{2}\right)^2 = RSC^2 - 2 * RSC * SC + SC^2 + \frac{L^2}{4} = RSC^2$$

L is the length between H and S. solving the equation

$$RSC = \frac{L^2}{8SC} + \frac{SC}{2}$$

$SC/2 \ll L^2/8SC$ , so it can be dropped.

SC represent in term of H, S and W becomes

$$SC = \frac{\frac{S+H}{2}W}{2} = \frac{S+H-2W}{2}$$

Combining the equations:

$$RSC = \frac{L^2}{8\left(\frac{S+H-2W}{2}\right)} = \frac{L^2}{2(S+H-2W)}$$

The radius of turn RT is given by the cosine of Edge angle  $\theta$  multiplied the Radius of Side Cut just found (considering a planar surface)

$$RT = RSC * \cos\theta = \frac{L^2 * \cos\theta}{2(A+H-2W)}$$

So, the radius of turns do not correspond to the side cut radius.





## 2. Ski characterization devices

### *Ski load distribution analysis during a static simulation of skiing activity*

An accurate knowledge of ski structural and mechanical properties is very important for engineers and users. A key point for the comprehension of these properties is the pressure distribution at the edge. The Edge Load Profile (ELP), a diagram representing the load distribution along an effective length of the ski, is a complex study to perform, but an accurate development of different shape for different skis provides a tool for ski qualification and design improvement.

Researcher and ski manufacturer developed different types of benches and several activities were carried out for measuring the static edge pressure profile when a ski is pressed against the bench with different angles and loads.

In this chapter the bench used in Padova for testing the ski during a bending, (the Slytech bench), the Chemnitz bench and the Nordica bench are presented. In Chapter 3 the elastic compensation structure are introduced and described, and in Chapter 4 the results are presented.

### **2.1 MTS 858 Mini Bionix**

The *MTS 858 Mini Bionix II* machine of the Department of Industrial Engineering of University of Padua has been used to test the foams . This machine is used to perform axial traction/compression tests or fatigue tests. It has a piston, located in the upper part, to which is fixed a jaw, and a second jaw fixed at the bottom to a load cell.

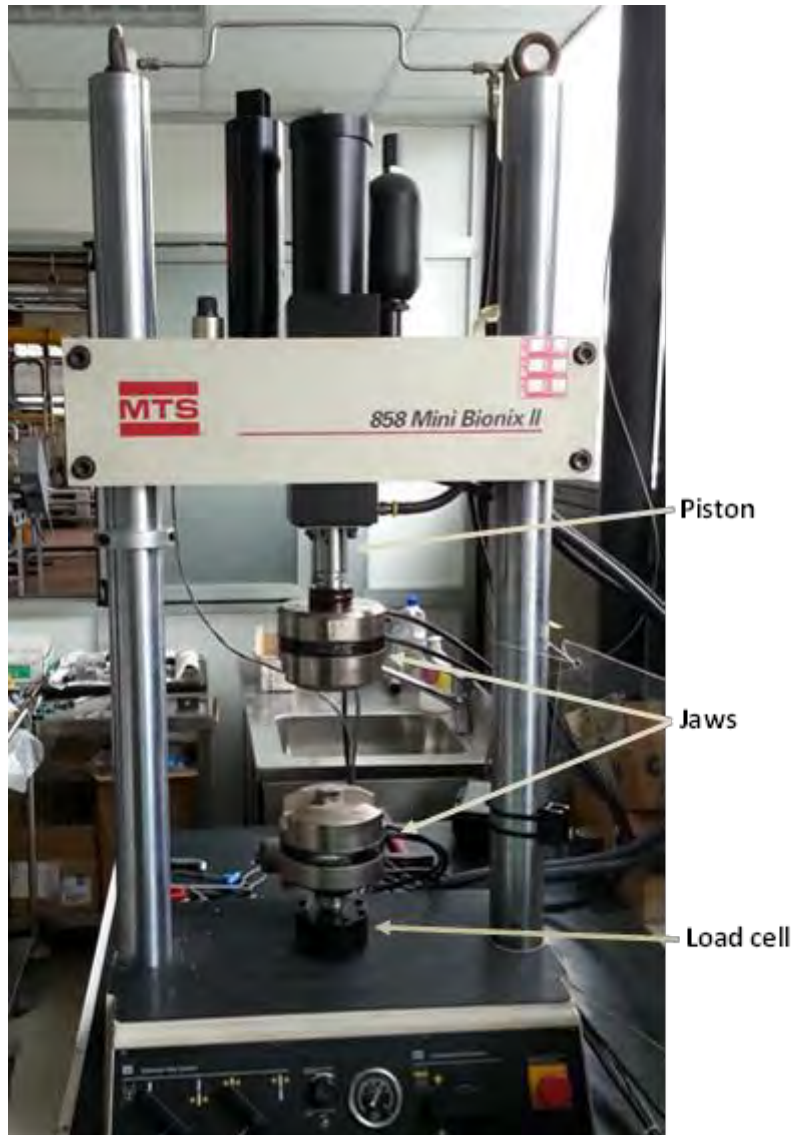


**Figure 2.1** MiniBionix II test machine of the Department of Industrial Engineering of University of Padova

The technical data of the *MTS 858 Mini Bionix II* machine are:

- Maximum dynamic force: 15kN
- Maximum static force: 31 kN
- Maximum pressure: 21 MPa
- Range of temperature:  $-40 \div 177$  °C
- Stroke ranges:  $\pm 50$  mm
- Type of movement: displacement, force and deformation.

With this system the punctual ski stiffness and the vibration damping has been studied.

The ski is fixed with the false boot to a steel support bar. All the system is clamped in the wax of the Minibionix machine.

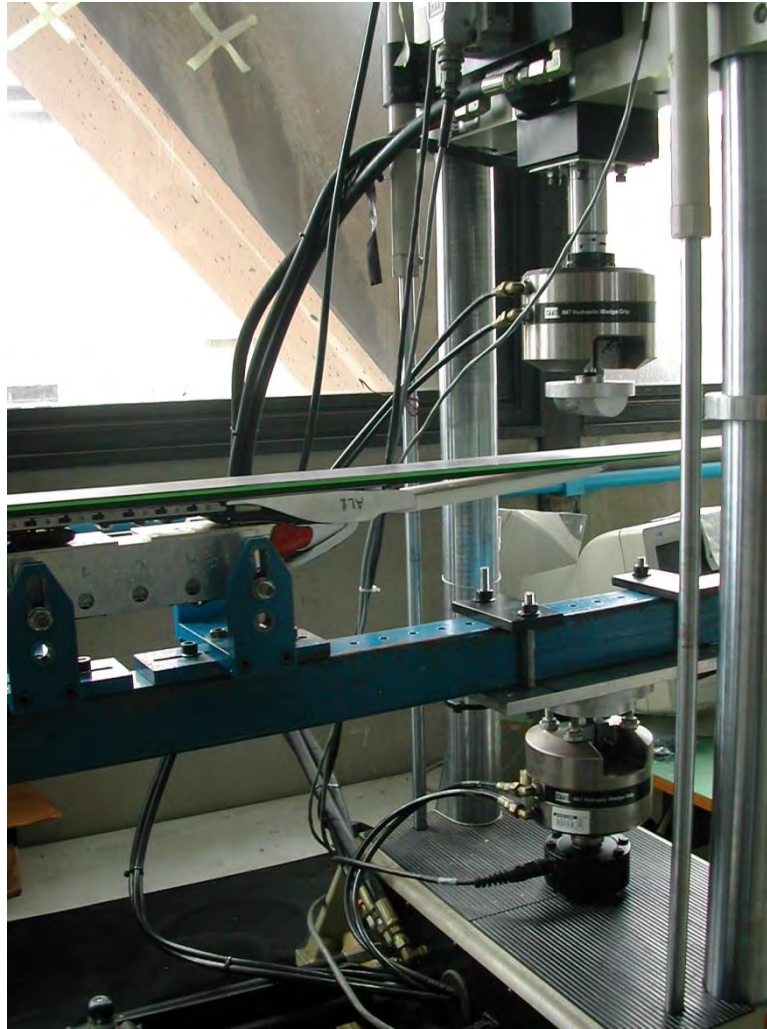


*Figure 2.2 Minibionix fixation system for vibration damping characterization*

The system do not simulate the reality, but the characterization permits the different elastic compensation structure comparison. A prefixed displacement is imposed, in correspondence of the arm ends, so the load transferred to the load cell is recorded.

## **2.2 Chemnitz bench**

The “Ski Deflection Profile“ bench that has been developed in Chemnitz University, by professor Stephan Odenwald, provides a tool for understanding the displacements generated to the ski during a static load applied.



**Figure 2.3** Chemnitz bench

Principal parts of this workbench are:

- 16 Sliders, spaced at 120 mm along the ski axes, enabled to slide only vertically along low friction guides. The slider has a maximum deflection of 19 mm. They are made by Polyethylen PE 1000 Reg black.
- 2 springs per slider that support it. Two different configurations are possible, with soft spring, with elastic modulus of 0.81 N/mm each, and hard springs, with a doubled modulus of 1.642 N/mm each spring.
- An hall magnet sensor per slider, that measure the displacement when a load gets on a slider.
- The load is applied by a linear electromechanical actuator with axis adjustable in a vertical plane, that gives up to 2000 N. The edging angles can be varied at steps of 10°, ranging from 0° to +45°.
- The ski is connected to the actuator by a dummy aluminum sole, shaped as the ISO boot sole. Three positions of application of the load are possible, spaced of 50 mm from the boot geometric midpoint. The position placed at +50 mm from the boot midpoint has been used for the test.



**Figure 2.4** Polyethylen sliders, guided and springs details

The load is applied to the ski at a certain velocity and angle. The ski press against the sliders until the prefixed load is reached. The load is maintained for three seconds, while the acquisition system register the displacement at 250 Hz.

**2.2.1 Test method**

As before, different loads are applied for different angles, but in this case the angles tested are less than Slytech tested and with a lower load, in particular with the harder springs configuration the loads applied are:

Angle	Load
0°	350 N
20°	500 N
30°	600 N

Increasing the angle some slide event could affect the test. The load applied is less than Slytech bench because with an higher load the slider under the binding could move more than the maximum 19 mm of stroke.

**2.2.2 Test output**

The bench output that comes from the test is a distribution of displacements along the ski, with steps of 120 mm. The original output was figured as the Slider Displacement Profile

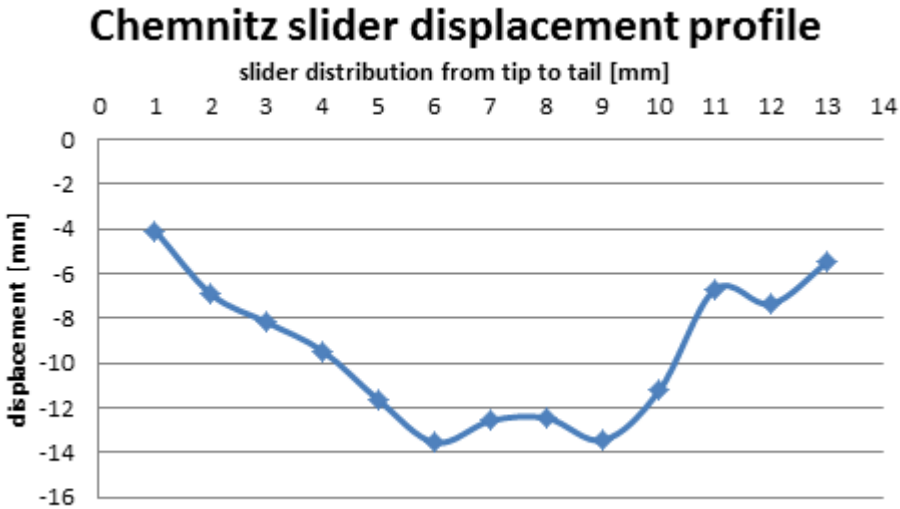
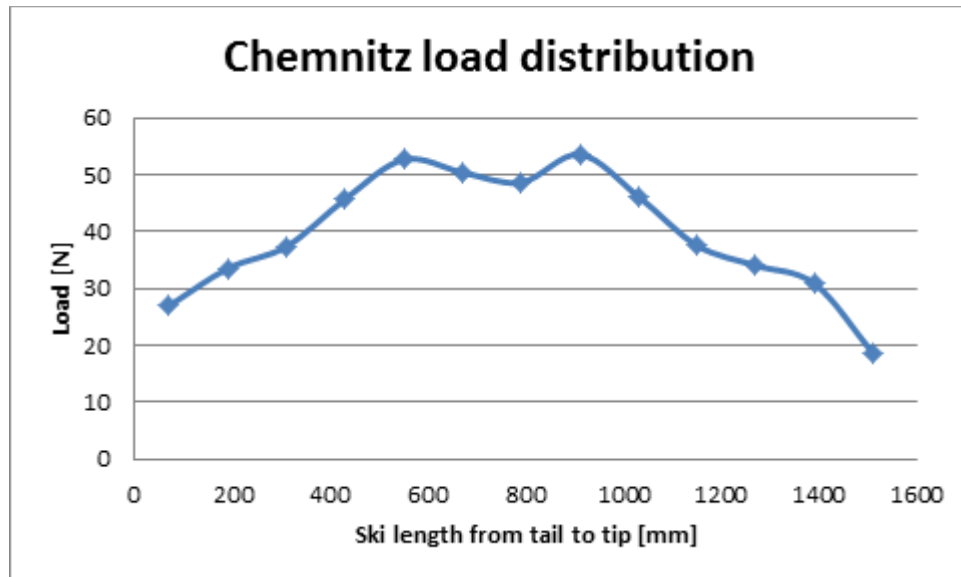


Figure 2.5 Chemnitz displacement profile from tip to tail

Then, trying to make the results more uniform, the displacement has been transformed in applied forces (N) by multiplying the spring elastic constant. So, the output result is a diagram that represents the load distribution along the ski.



**Figure 2.6** Chemnitz load profile from tail to tip

Along the ski, from tail to tip, the displacement, caused by the application of a load to the false boot, is influenced by the rigidity of the ski. In a rigid ski a longer ski portion length contributes to absorb the load. In this case also the most forward and rearward cells touched by the ski deformed significantly: this results can be seen with a “camber” ski construction. On the other hand, a “rocker” ski leave the last sliders undeformed, that means no load applied. As expected the ski has a lower effective length during skiing, especially with low tilt angle.

### 2.3 Flex bench of Tecnica Group laboratory

The flexion bench in Nordica laboratory allows to calculate the EJ product that is the stiffness of each position of the ski. EJ is the product of Young modulus E (N/mm<sup>2</sup>), which represents how much the material has to be loaded to have a unitary deformation, and moment of inertia around the bending axis of a general section of the ski. This bench is provided of two floating clamps composed by two cylindrical beams: one where the ski is leaned, the second beam is leaned on ski and look locally the ski. Two auto-centering clamps lock the ski transversal motion during the test. The procedure of clamping follow the normative ISO 5901 on flexion of ski, with this exception: the bond on shovel is imposed at 200mm from tip and not at 280mm.



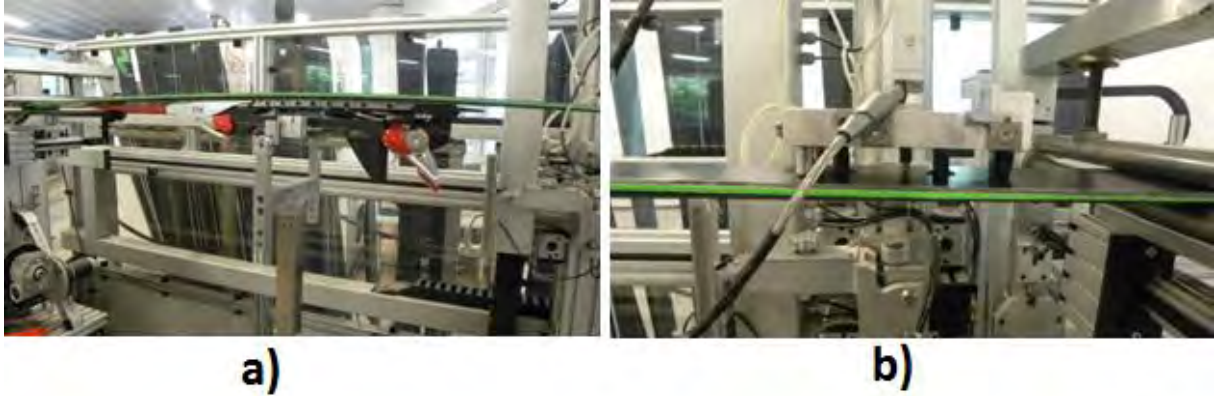


**Figure 2.7** Example of Nordica Bench during flex test and b) LDVT sensor applied on ski lower surface

Once the nominal length of the ski is set, the test starts with an LVDT measurement sensor contacting the ski base each 50 millimeters steps, while a cylinder applies a constant force of 350 N for each measurement. At each step the machine repeats the same motions, starting from the tail and aiming to the tip of the ski, taking in account also the sensor platform geometry. The results of the measurement is a curve in Cartesian plane, where x-axis is the position of LVDT, and y-axis is the EJ product [Nmm<sup>3</sup>/micron] named rigidity of the ski.

EJ is the constant number who connects bending moment and curvature in the equation of elastic line: from the theory about elastic line, (who represent the deformed shape of a structure) the relation between distributed load and bending moment is:

$$-q = \frac{d^2 M_f}{dx^2}$$

Assuming the hypothesis that ski is a beam supported on the two extremities: q is a constant distribution of load on ski upper surface, calculated like a ratio between force applied by the actuator and effective bending length. x is the length variable.

Bending moment equation:

$$M(x) = \frac{qL}{2}x - q\frac{x^2}{2} = -\frac{d^2\eta}{dx^2}EJ$$

Solving the differential equation, with the imposition of the boundary conditions ( $\eta=0$  at  $z=0$ ;  $d\eta/dz=0$  at  $z=1/2$ ), the elastic line equation becomes:

$$\eta EJ = \frac{qL^3}{24}x - \frac{qL}{12}x^3 + \frac{q}{12}x^4$$

It's difficult estimate the product EJ from this equation without knowing displacements. The sensor on ski measure the local deflection of ski (curvature): from theory of elastic line the relation between curvature of ski and bending moment is:

$$\frac{d^2\eta(z)}{dx^2} = -\frac{M_f}{EJ(x)}$$

So it's possible to build, using the software, a curve of EJ for all the elongation of ski length in variable Z.

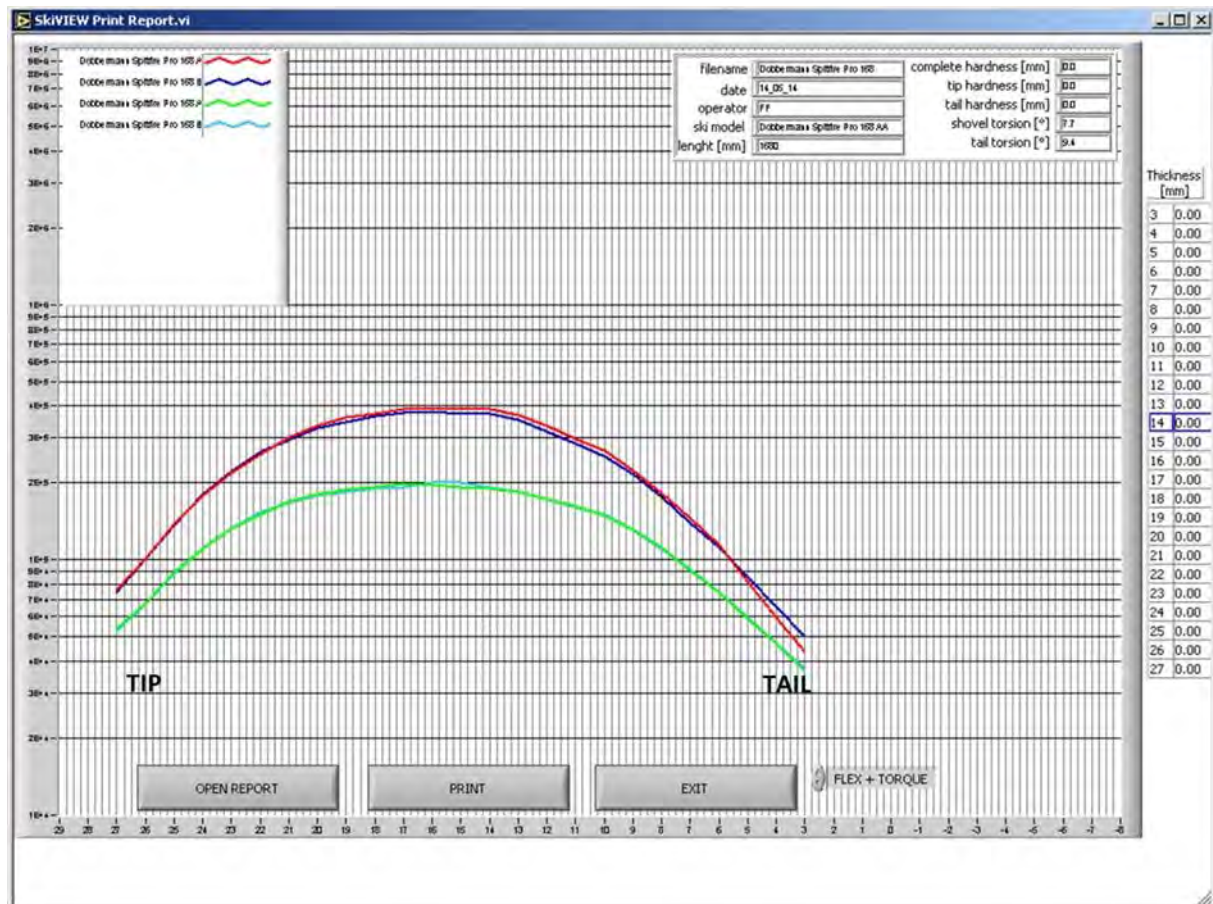


Figure 2.8 Output from data analysis for flex (red and blue lines) and torque test (green lines), Doberman Spitfire skis 168.

## 2.4 Torsion bench of Tecnica Group laboratory

The torsional rigidity is the resistance of a ski to twisting. The ski torsional rigidity comes from its construction and mainly core materials. A more rigid ski performs well on hard snow, whereas a less rigid ski will be easier to handle in soft snow.

It was possible to measure this parameter with the same bench of the flex test. In Nordica laboratory the test is performed without binding because of the different clamp system. The test supply a clamping system in the center part of the ski, while the tip part is fixed in a portion of the machine that provide a moment applied of 17,5 Nm that makes twist the ski at different angles, depending on the ski torsional stiffness. The LVDT measurement sensor is fixed on later portion of platform sensor, and register the displacement. From the PC elaboration data the graph that comes from is reported in Figure 2.8 with the flex results for the same skis.





**Figure 2.9** *Ski without binding system with the elastic compensation superstructure*

## 2.5 Slytech bench

Slytech Workbench is a specific lab equipment to test ski that gives a static simulation of a ski during the curve. Probably this equipment permits to obtain the more realistic ski simulations. Principal components of this workbench are:

- 21 uniaxial planar load cells, fixed to a rigid frame.
- A linear actuator with axis adjustable in a vertical plane, used to load any type of ski on an array of load cells: the edging angles can be varied at steps of  $10^\circ$ , ranging from  $0^\circ$  to  $\pm 70^\circ$ . On each cell, the contact takes place between the ski sole and the stiff neoprene surface supported by each load cell.
- An aluminum dummy boot sole to connect the ski to the previous actuator. This sole presents 5 positions of application of the load spaced of 50 mm from the boot midpoint: position placed at +50 mm from the boot midpoint was used in the tests.
- Data acquisition system connected to a PC.

A representation of the Slytech workbench and its components are presented in Figure 2.10.

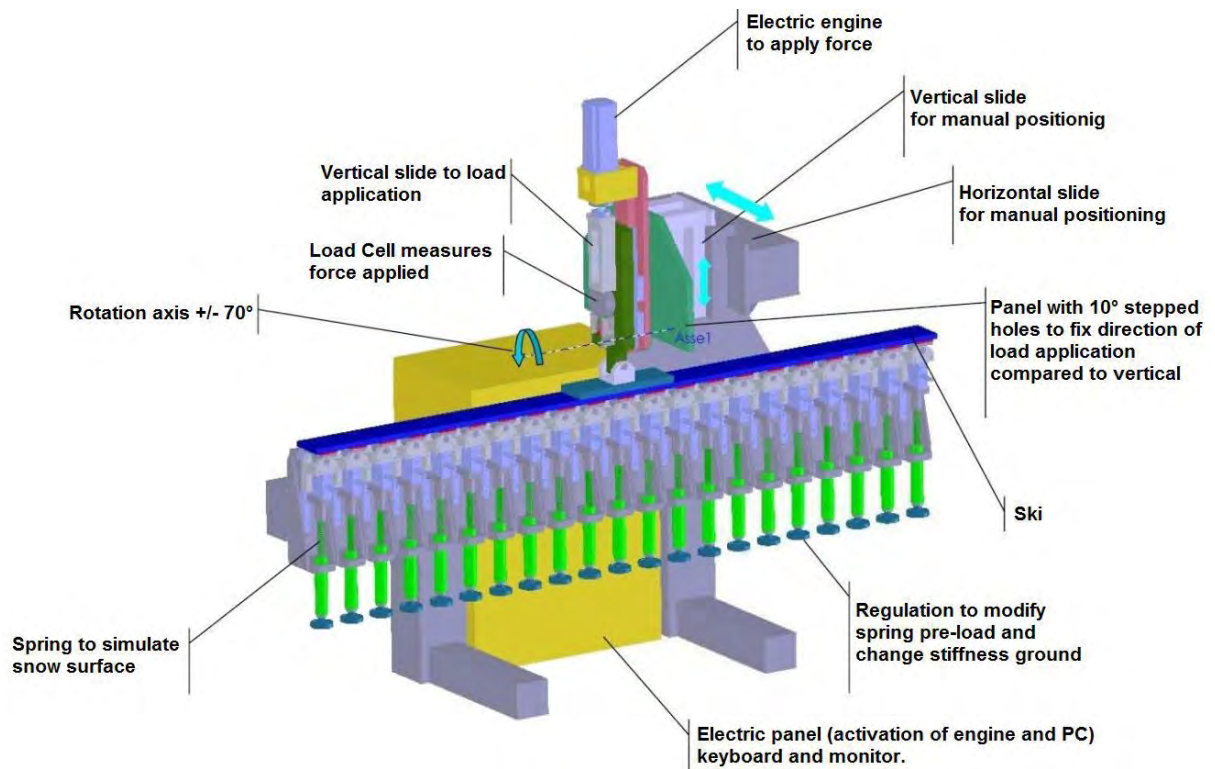


Figure 2.10 3D model of Slytech bench

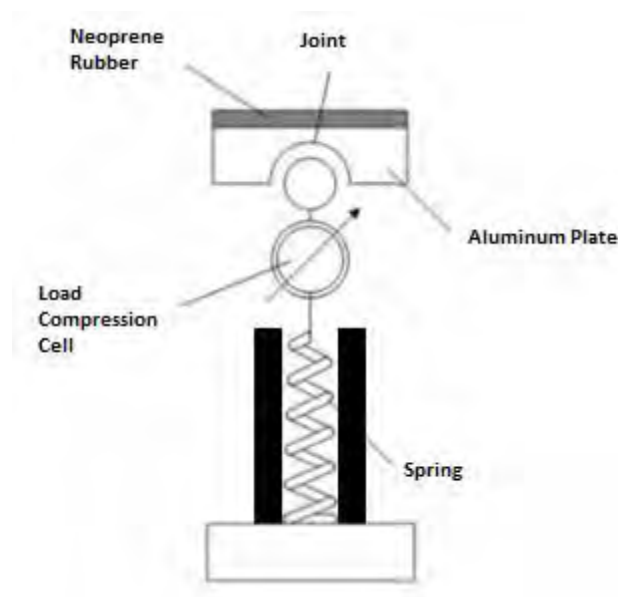
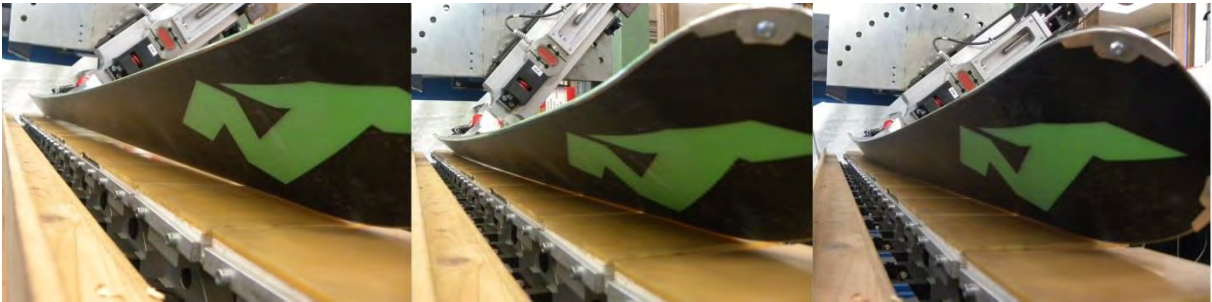


Figure 2.11 Simplify 2D model of load cell system

A single cell is made by a hinged aluminum plate with following dimension (LxWxT 103,5x100x8 mm); underneath it there is a joint that allows transferring the vertical force at one of the 21 compression load cell. Plates are regularly spaced of 2mm from each other.

Springs placed under load cell simulate the different snow stiffness; they can be locked to reproduce surfaces very stiff surface, that simulate the hard snow. Joint that links load cell with the aluminum plate allows rotation around axis orthogonal to longitudinal length of the ski. On the surface of each aluminum plate a polyvinylchloride (PVC) plate is placed, on which is glued a layer of neoprene rubber, a gum where ski can transfer its load. The rubber layer permits to grip the steel edge and deform the ski, bending it, simulating a curved turn; in Figure 2.12 the sequence is pictured.



**Figure 2.12** Sequence during Slytech bench test

Neoprene has the property that is deformable for long repeated cycle without permanent print or deformation. Another peculiarity is the lesser grip of neoprene with surface, in this case the metallic edge of a ski. Very low grip is a point of improving workbench performances. How it's observable in the following picture, this workbench allows simulating different inclination of the ski on the plates and this correspond to different edging angle during a curve.

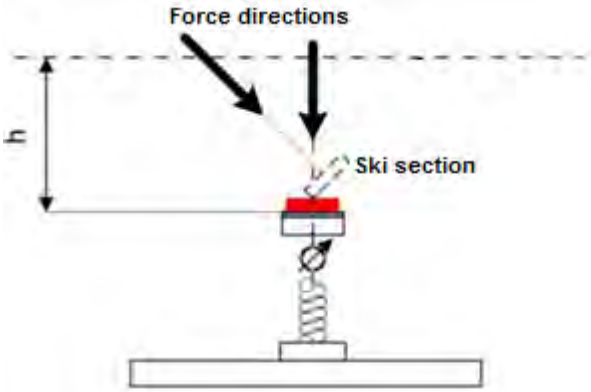


**Figure 2.13** Example of force direction on ground

During a ski test, each cell measures a load value and it is recorded by the computerized system, so in real time the load distribution on the cell is displayed on a graph, given an immediate idea of the characteristics of the ski. Each test can be stored in a database on the

PC memory of the workbench itself to make possible the comparison between each performed tests.

The stiffness of every spring could be change rotating the screw under the same spring. The normal bench disposition is rigid, so with all screws closed.

### 2.5.1 Test Methods

The edge loading test consists on applying an increasing load from 500 N to 1400 N with increasing edge angles, as reported on the table:

**Table 2-1** For each angle a corresponding load is applied

Angle [°]	Load [N]
0	500
10	600
20	700
30	850
40	1000
50	1200
60	1400

Load is applied in correspondence of the cell n°11 by the actuator that is powered by an electric motor unit with an holding torque of 6 Nm. A load cell is installed under the vertical cylinder, and has the function of controlling the load implemented on the software (retroaction system).

The output data from each load cell are recorded by a software on a .txt file and then converted in graphs using Office Excel. To each test a .txt file is associated.

Loads measured at the i-th cell are plotted along the ski length to obtain the Edge Load Profiles (ELP): the load cell position could be normalized to the ski length to compare skis with different length. For each edging angle the bench provides different ELP for any type of ski. These difference are coming out from ski length, sidecut, construction and binding plate position and properties.

An example of the diagram that comes from the test is reported in Figure 2.14:

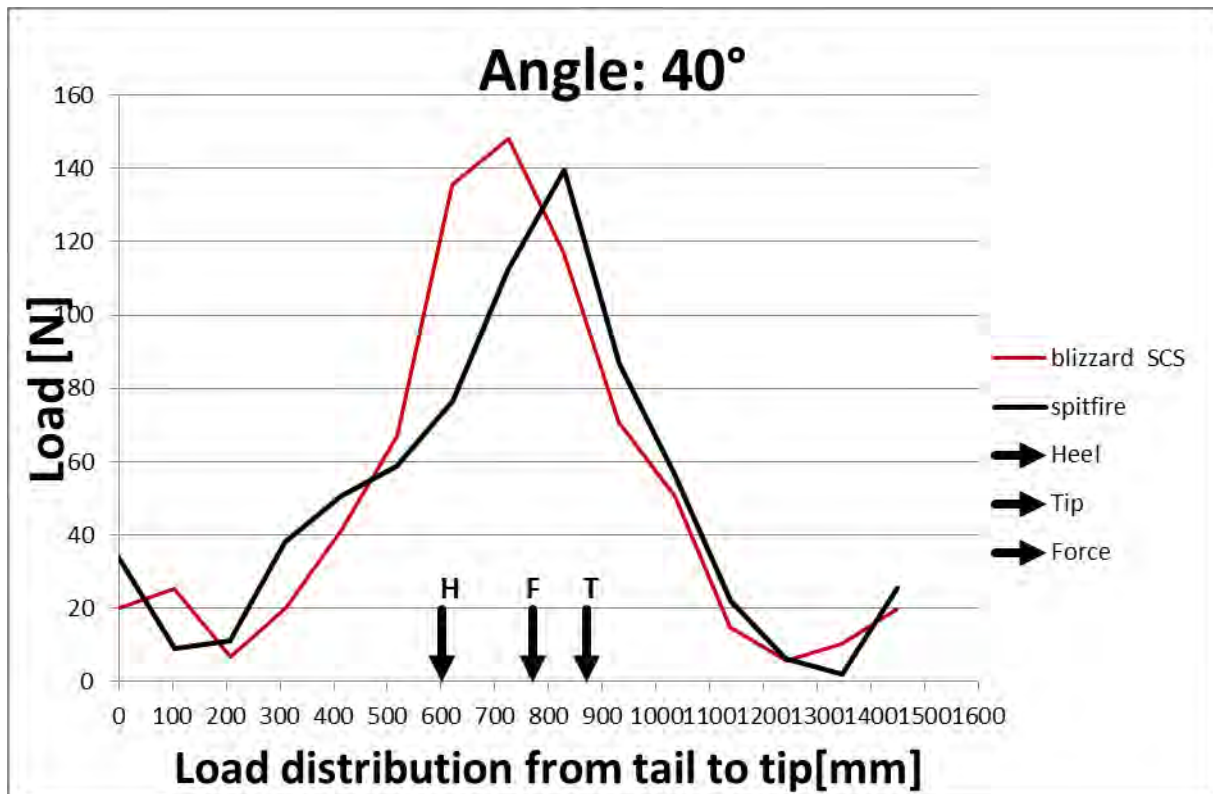


Figure 2.14 Example of ski load distribution output for two different skis

Each point of the curve is an output of the respective load cell. They are interpolated with a spline line.

The principal peak in the center decreases with higher angles, tail and tip peaks increase with angles and the plateau in front of the bindings increases also with angle; this permits ski to have a great contact area with the snow during skiing at high curvatures. This plateau could be changed and increased modifying the ski internal structure, or changing bindings position, or coupling the ski with external superstructures of elastic compensation, as the aim of this part of the thesis.

### 2.5.2 Test output

From the higher number of tests, conducted also from colleges (Eng. Federico Signoretto and Riccardo Baldan), performed on the bench, some conclusions about Edge Load Profile are below summarized:

- the Edge Load Profile is a repeatable curve that can be measured as the peculiar “footprint” of each ski on the snow;
- the Edge Load Profiles of different skis should be correlated with their field test ranking (“good”, “average” or “bad” scoring) in order to identify the target Edge Load Profiles that have to be preferred for each market segment or for various snow conditions;

- the Edge Load Profiles have to be seen as one of the engineering parameters to be evaluated for an integrated approach to ski functional design;
- the measured Load Profile will be helpful in the validation of numerical analysis of the ski-snow interface.
- Edge load profile of the same ski with an added superstructures shows how rigid became the ski and how the superstructure stiffness influences the shovel deflection.



### 3. Elastic compensation superstructure, “arm”

A typical load distribution along the ski reveal a huge pick of force on the center part of the ski, where the binding is connected with the ski. The rest of the force is transferred from the toe and tail part of the ski, but this is only a small amount of the total force transferred and the rest of the ski is almost completely unloaded.

The ski deformation is comparable to an arc of a circle during a curve for “commercial” ski, as reported in figure with the line C, Figure 3.1.

It is reasonable support that the initial access to the curve and then, along the same, the adherence to the ground, the side seal, the stability and smoothness of the ski, would take decisive advantage from a conformation that, in the front portion of the ski , is much more similar to an ellipse arc, line E in the same figure.

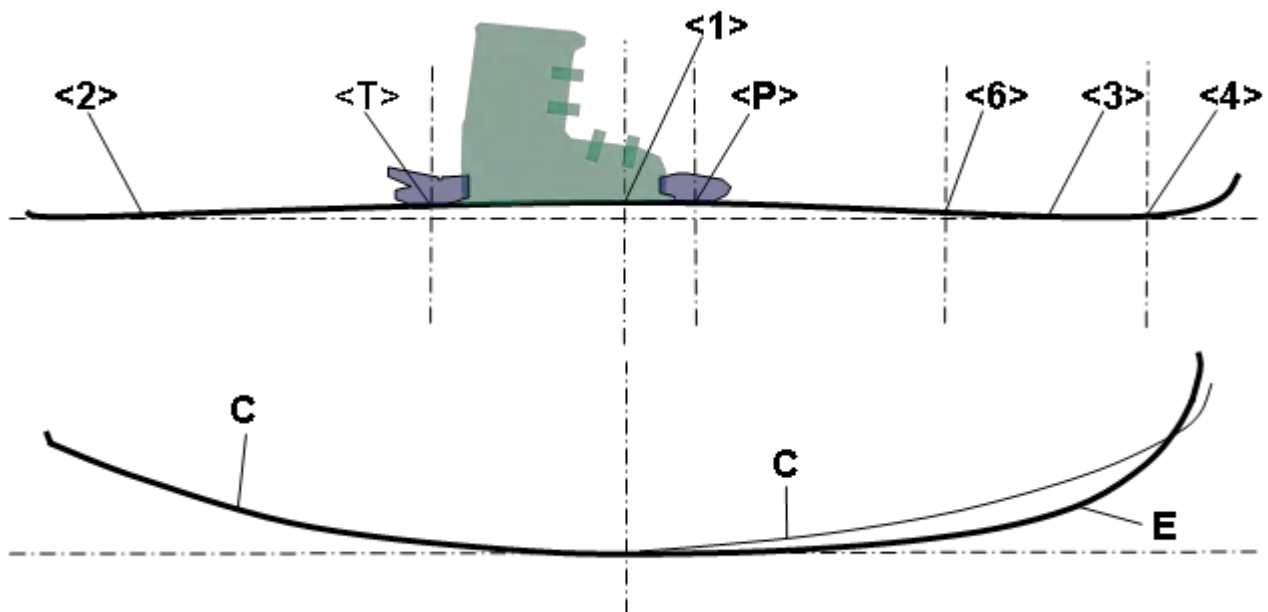
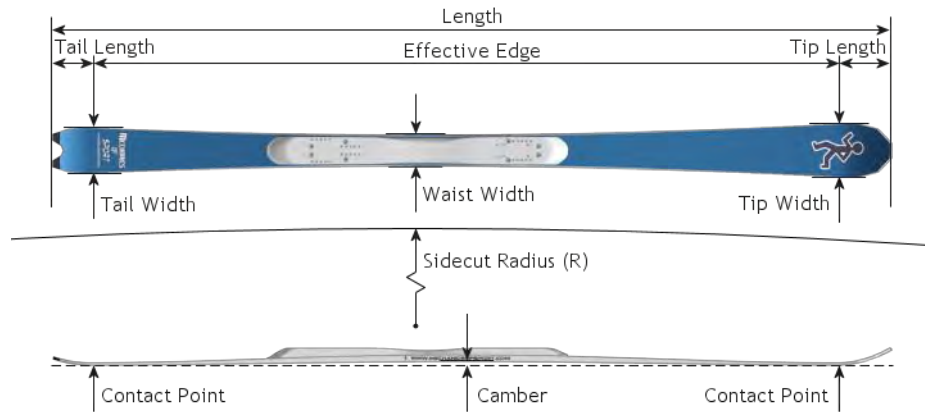


Figure 3.1 Loaded ski deformation

#### 3.1 Definition of the different part of the ski

In Figure 3.2 the different part of the ski are presented,



**Figure 3.2** Ski geometries

When a ski lay down onto a flat surface, a camber geometry is observable.

Camber is an amount of space in the ski where the center rises higher than the contact points in the tip and tail. This is generally not classified or measured in ski construction, but has profound effect on a skis performance. Camber is the pre-loaded factor in the ski.

Side-cut is the difference in width between the tip and the tail in relation to the waist. Generally, the narrower the waist width in relation to that of the tip and tail, the smaller the radius of turn, the sharper and quicker the turn will be. Conversely, the smaller the difference, the larger the turn will be. The side-cut geometries are reported in some part of the ski: as an examples 119-73-102 are the tip waist and tail width express in mm respectively.

### 3.2 Patents

One of the first patent introduced by professor Quaggiotti V. was called “Sci Bi-Pattino”. It provided a double skater along the axe of the ski, an arm from the tip part of the first skater until the middle point of the front one joining together the ski. In the Figure 3.3 some prototypes developed during his research are shown.



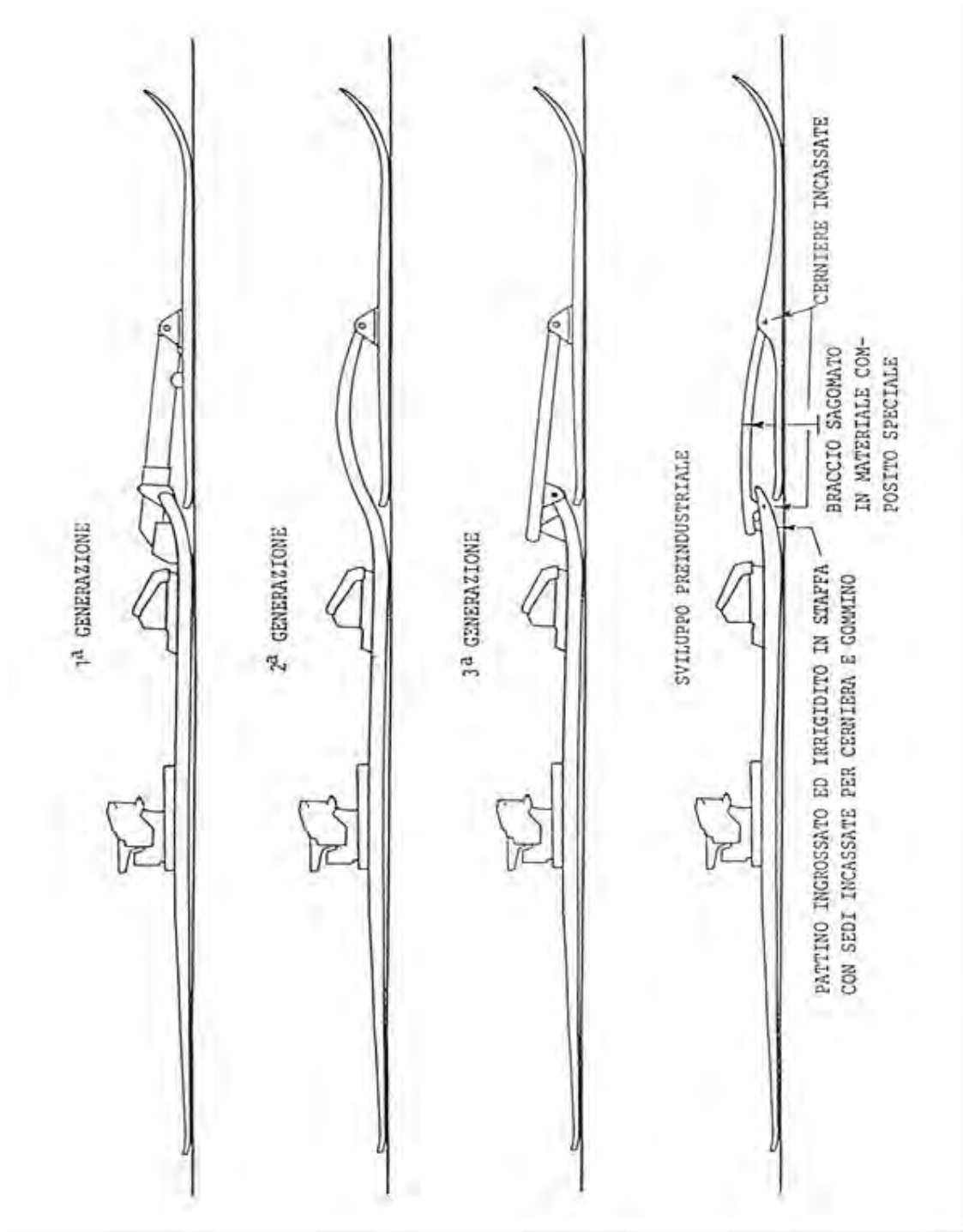


**Figure 3.3** Some schematic examples of the models developed for "Sci Bi-Pattino"

Some contradictions that came out during the experimentations, as the excessive load applied at the joint, difficulties during aligning and intrinsic discontinuity with the ground, put the basis for a second patent. The concept is the same, but in this case the ski remains with the typical mono-structure, with an innovative "elastic compensation over-structure".

The added structure, integrated with the bindings system, called "arm", ends in the front part of the ski, between the boot toe and tip. As shown in the Figure 3.5 the effects are double: the

ski is pre-loaded, so the distribution of the force transferred from a skier are distribute over three points, and reacts when the ski is bent allowing to assume the ellipsoid form represent in Figure 3.1, line E.

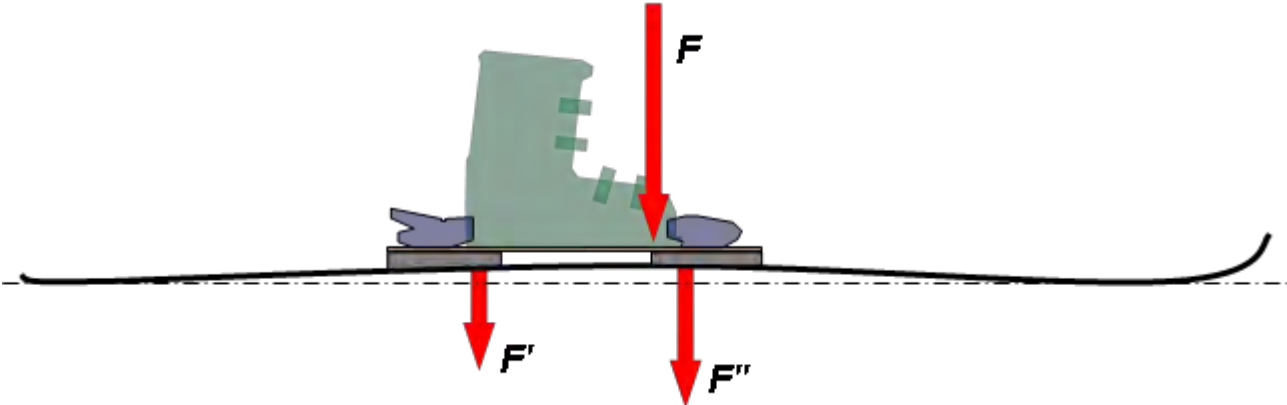


Figure 3.4 Normal distribution of force transferred by skier

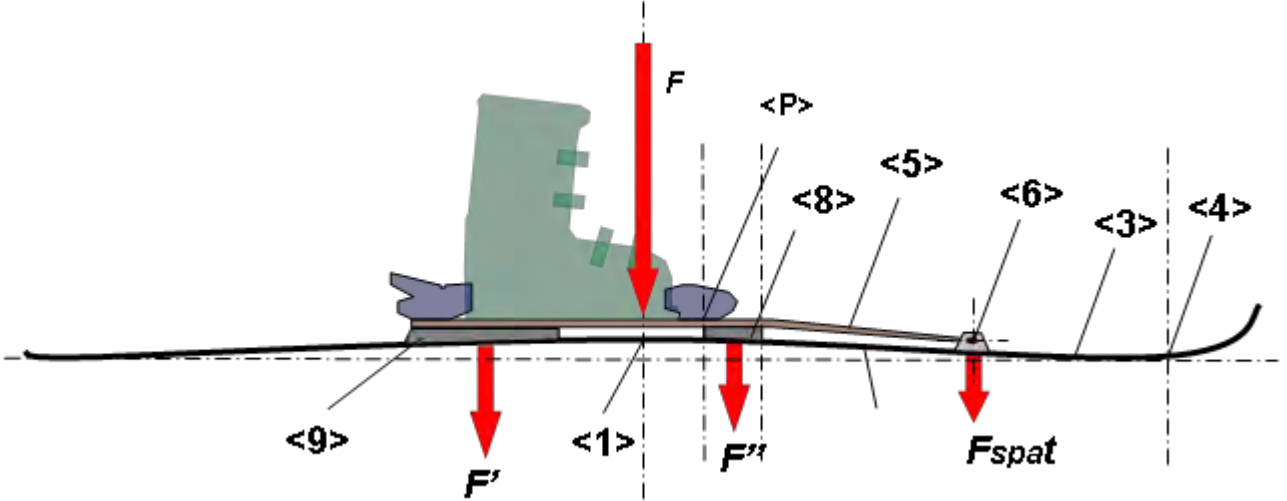


Figure 3.5 New load distribution due to the elastic compensation structure

The elastic compensation structure and the joint is one of the most innovative part of the patent, all the details are reported in Appendix.

The first model was developed during the 2004-2005 is reported in Figure 3.6.



Figure 3.6 Nordica GS Word Cup with the innovative elastic compensation structure

During the years more innovations have been introduced, especially for what concerned with arm characteristic, joining system and materials used. In the next paragraph the latest developments made so far with the collaboration with Nordica are presented.

### 3.3 Prototypes

Thanks to the precious collaboration with Nordica, Tecnica Group, four different types of “arm” have been developed until now. The arms were developed to have different stiffness values, therefore a different influence on ski deformation under load, and different behavior of load distribution.

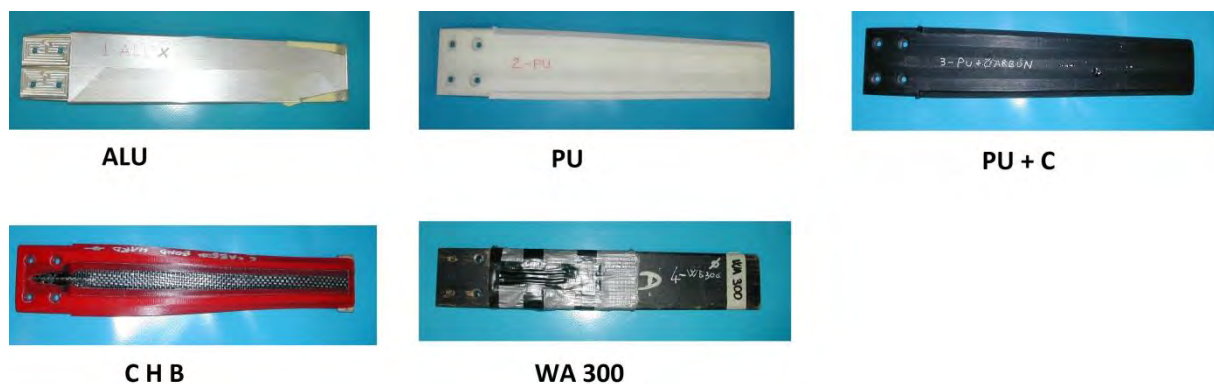
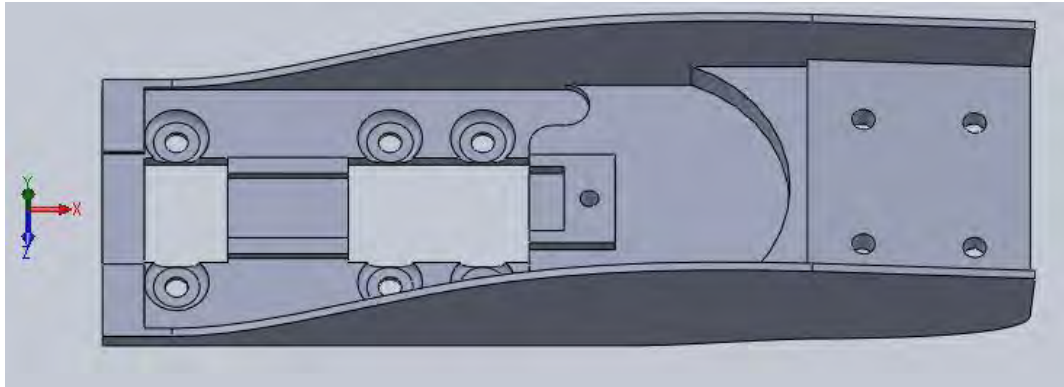


Figure 3.7 Prototype arms realized

The arms are identified with the material that they are made with: the ALU arm is made of aluminum alloy, series 7075-T6, PU by polyurethane, PU + C polyurethane and two layers of carbon, C H B stands for carbon hard bond that refers to the process used as explained better later and WA300 refers to oak wood. All of the arms have a total length of 300 mm, and 5 mm are for the fixation system to the aluminum plate.

The wood arms, realized in a previous study, are distinguished by the letter A and B because the microstructure of the wood is not controllable and could change the properties of the arm. Furthermore, two wood arms with a length of 350 mm were developed, but they are not considered here.

All of them are designed to have the same joining system, fixing the arm to the aluminum support designed and developed by Eng. Signoretto Federico.



**Figure 3.8** *Model of aluminum support*

This support has the ability of being integrated with the race Marker plate adopted for the test by removing a plastic minor component.

With the hypothesis of a unique piece of aluminum, an aluminum arm has been studied by numerical simulation, and then manufactured.

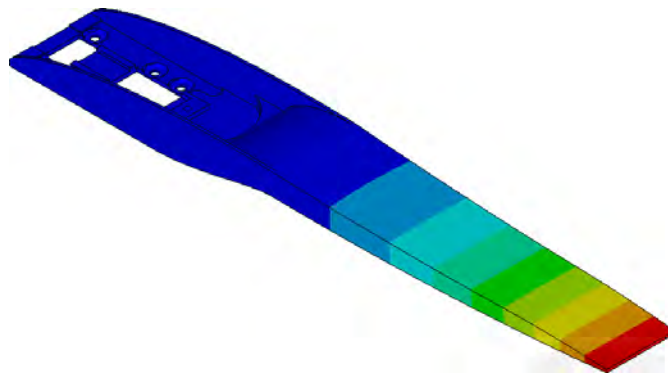


**Figure 3.9** *Example of Y displacements plot analysis*

The aluminum support has an average thickness of 2 mm, with some reinforcement where necessary. The mass of the support is 200 g. The different arms are made with different shape, material and production techniques.

The following table summarizes the arms that are going to be tested:

**Table 3-1 Arms Legend**

ID arm	Material	Cross section	Esthetic color	Mass [g]
ALU	Aluminum alloy, 7075	C-shape	Silver	184
PU	polyurethane	X-shape	White	185
PU+C	Polyurethane and carbon	X-shape	Black	141
C H B	Polyurethane and carbon composites	Curve-shape	Red	177
WA300	Wood	Full rectangular	Black paint	189
WB350	Wood	Full rectangular	Black paint	257

In the next section one by one the arms, the main characteristic and differences that identify the product are described. After, paragraph 4 are shown the result of the tests that comes from the analysis data of benches explained before.

### 3.3.1 ALU



**Figure 3.10** ALU, aluminum arm

Designed and developed by Eng. Signoretto Federico the aluminum arm comes from a finite element analysis. It is realized from a full rectangular shape of aluminum by milling machining.

The aluminum alloy used is a series 7000 Aluminum alloy, with zinc as the primary alloying element. It is strong, with a strength comparable to many steels, and has good fatigue strength and average machinability, but has less resistance to corrosion than many other Al alloys.

7075 aluminum alloy's composition roughly includes 5.6–6.1% zinc, 2.1–2.5% magnesium and 1.2–1.6% copper. The Table 3-2 reports a detailed list of elements included in Aluminum alloy 7075.

**Table 3-2** 7075 Aluminum alloy elements

Alloy	%Si	%Fe	%Cu	%Mn	%Mg	%Cr	%Zn	%Ti
7075	0.40	0.50	1.2 2.0	0.30	2.1 2.9	0.18 0.28	5.1 6.1	0.20

The temper designation follows the cast or wrought designation number with a dash, a letter, and potentially a one to three digit number.

T6 temper 7075 has an ultimate tensile strength of 510–572 MPa and yield strength of at least 434–503 MPa. It has a failure elongation of 5–11%. The T6 temper is usually achieved by homogenizing the cast 7075 at 450°C for several hours, and then aging at 120°C for 24 hours. This yields the peak strength of the 7075 alloy. The strength is derived mainly from finely dispersed eta and eta' precipitates both within grains and along grain boundaries.

The C-shape arm realized perfectly fit with the aluminum support and goes to touch the ski in its front part. The total length of the arm is 300 mm and it was based on the results of previous studies. The contact with the ski is made with a rubber insert, so the ski is not damaged during the performances.

Generally, the rubber insert may influence the pre-load that the arms get to the ski. This will be considered later on.

### 3.3.2 PU



**Figure 3.11** PU, polyurethane arm

The white arm is made only with polyurethane, with no reinforcement of other material. The news is represented by the shape, defined as X-shape when analyzed in the cross-section. This allows to obtain an higher inertia moment, so more stiff in bending.

The chemistry of urethanes makes use of the reactions of organic isocyanates with compounds containing active hydrogens. When poly-functional isocyanates and intermediates containing at least two active hydrogens per mole are reacted at proper ratios, a polymer results that can produce rigid or flexible foams, elastomers, coatings, adhesives, and sealants. An isocyanate group reacts with the hydroxyl groups of a polyol to form the repeating urethane linkage, as shown in Reaction:

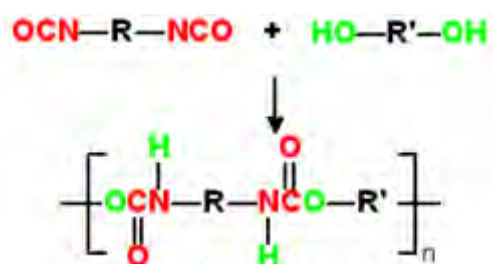


**Figure 3.12** Urethane linkage formation from isocyanate group and polyol reaction [wikipedia]

The PU used to realize the arm is identify as SG 95 A/LP. The technical data sheet is reported in the Appendix, here some main properties are shown:

- 82 D Hardness Shore D at 23°C
- 2192 MPa flexural modulus
- 54 MPa tensile strength
- 72°C heat deflection temperature
- Shrinkage of 0.2%

The arm is obtain by injection of liquid polyurethane inside a silicon mould; the process is called vacuum Casting.

### ***Vacuum Casting Process***



**Figure 3.13** *Silicon mould*

The arm is developed by a 3D computer simulation. A first model is then realize by stereo-lithography technology that permits to obtain a full shaped model object, mechanically structural or not depending on the technology and material adopted. With the “master” is possible create the mould.

The surface quality and the dimensional accuracy of the “master” is a determining factor for the quality of vacuum casted components.

The master has been realized by *Tecnologia and Design*, Treviso, by using a stereo-lithography machine, Figure 3.14.



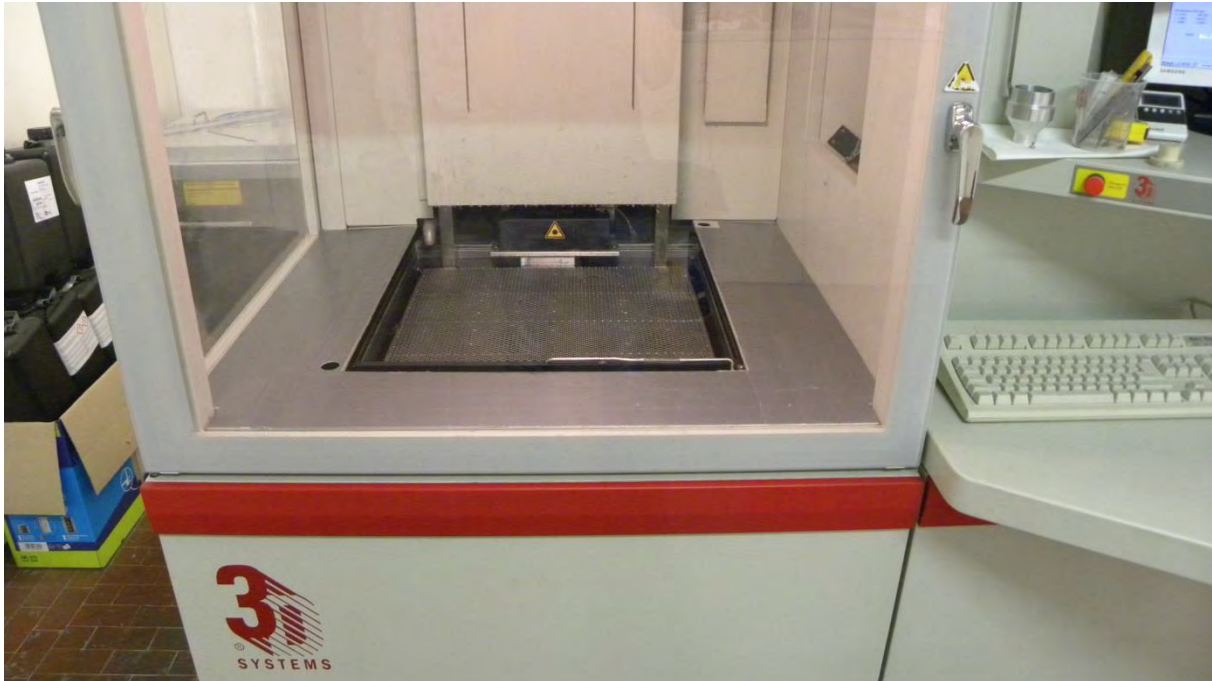


**Figure 3.14** Stereolithography machine, 3i SLA5000

This technology is the fastest possible way of creating detailed one-off components, ranging in size from small to exceptionally large.

The master model is carefully prepared to ensure a high quality finish to the surface and the definition of the parting planes, so a manual thorough master finish is necessary to eliminate the 0.15 mm layer steps.

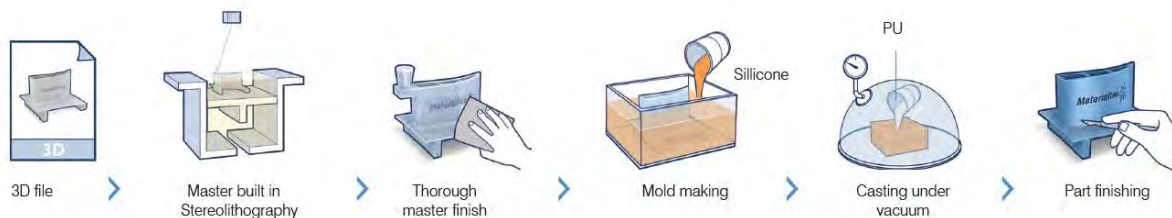


**Figure 3.15** Typical process prototype realization [<http://manufacturing.materialise.com>]

The arm model is suspended inside a box using a studied structure: the contact points will become the mould injection point and vents. Silicon precursor are mixed together, leave it to get free the gas within contained and the box is full fit with the mixture. After 24h the silicon mould is done. Out of the box it is manually opened with a cutter, with care of not damaging the cavity part, so the master is removed, leaving a cavity to make copies.

Two-component polyurethanes are typically used as copying material. This allows fast production of high quality parts. Generally, vacuum casting is a copying technique used for the production of small series (10 to 20) of functional plastic prototypes.

Once the mould is ready, a small series production can start. Silicon mould is pre-heated and put inside an autoclave. In the upper part of the machine, a weighted quantity polyurethane



precursors are mixed together for 15 min, the vacuum is created in autoclave. The vacuum permits to eliminate the humidity contained by precursors. Once mixed, the moisture is put inside the mould without applying any additive force. The injection point is fundamental to obtain a completely full shaped object. The exothermic reaction will not damage the silicon. At the end of the vulcanization time the object have to be extracted.

### 3.3.3 PU+C



**Figure 3.16** PU + C, polyurethane with carbon layers

The arm is made with the same polyurethane as before, with black pigments, and two sheets of 0°-90° carbon fiber mat. PU+C is realized with the same X-shape, by using the same mould, with the bottom and upper part in carbon. The shape remains the same and also the length.

The process is also the same, but one more operation is needed. Before putting the mould in autoclave, it's necessary to cut the carbon fiber as the arm size and fit it with silicon mould.

This process is going to damage more the mould, because of the operation of fitting the carbon layers and extracting the part.

### 3.3.4 CHB



**Figure 3.17** CHB, polyurethane with carbon visible layer

The shape of this arm is different, but the technology is similar yet. With stereo lithography the master is obtained, and create the mould as shown before. In this case the carbon reinforcement is represented by a composite carbon fiber. The composite has to be formed with the correct shape and maintained press to the mould during vacuum casting process. This permits to obtain a visible carbon face.

A future development for this is using a thermoplastic composite, with the same material of the arm, so no additive process are request to obtain a non-complex shape. The carbon layer will be put inside the mould without any preform and during injection the pressure will modelled the carbon and will create the bond.

### 3.4 Flex arm properties

All different arms were tested to measure the flex stiffness. Two different tests were developed, one at Nordica laboratory (identify as “Nordica” in the pictures), the other in Padua Department (“DII”).

#### 3.4.1 Nordica arm stiffness test

The arm is rigidly fix to a specific steel support, considered as infinitely rigid, and locked with the same system used in the skis, that means four iron screws. The load has been applied 150 mm from the end of the support. A dynamometer moved at 100 mm/min registering the force and displacement during the load application. During the test a computer acquisition system registers the displacement every 5 kg applied. The test reach the maximum of 200 N for the PU, PU+C and CHB arms, and 400 N with ALU and WOOD arms, due to the higher stiffness of the these.



Figure 3.18 Stiffness arm characterization

#### 3.4.2 Nordica test Results

The results of the test conducted in Nordica are summarized in Figure 3.19.

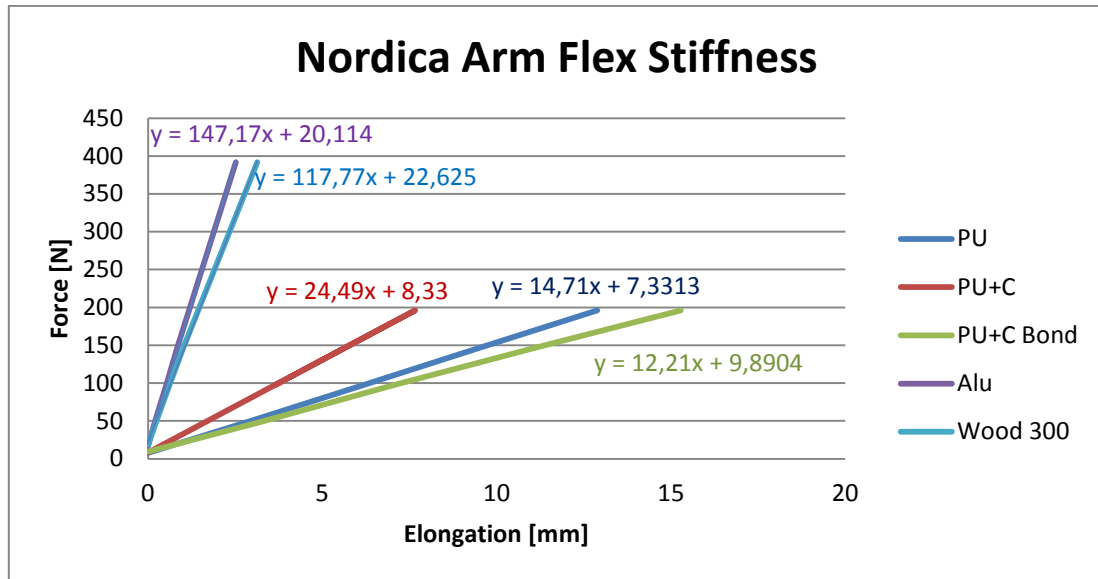


Figure 3.19 Flex stiffness determination

The results shows in order from the more rigid arm to more soft are: ALU and WOOD very similar, PU+C, PU and C H B. so, with this characterization it seems that the shape has a significant influence to the properties. This is generally correct but some consideration are necessary.

Table 3-3 Nordica Arm stiffness

Arm ID	K[N/mm]
ALU	147,17
WOOD	117,77
PU	14,71
PU+C	24,49
CHB	12,21

The table reassume the arm stiffness found during Nordica test with the rigid support

### 3.4.3 DII arm stiffness test

At DII laboratory the test has been conducted not with a rigid support, but with the arm installed on the ski. So, not only the arm stiffness can be found, but also the stiffness of the all system. The Minibionix machine has been used for the test, as presented in chapter 2.



**Figure 3.20** *MTS machine configuration during arm stiffness characterization in DII*

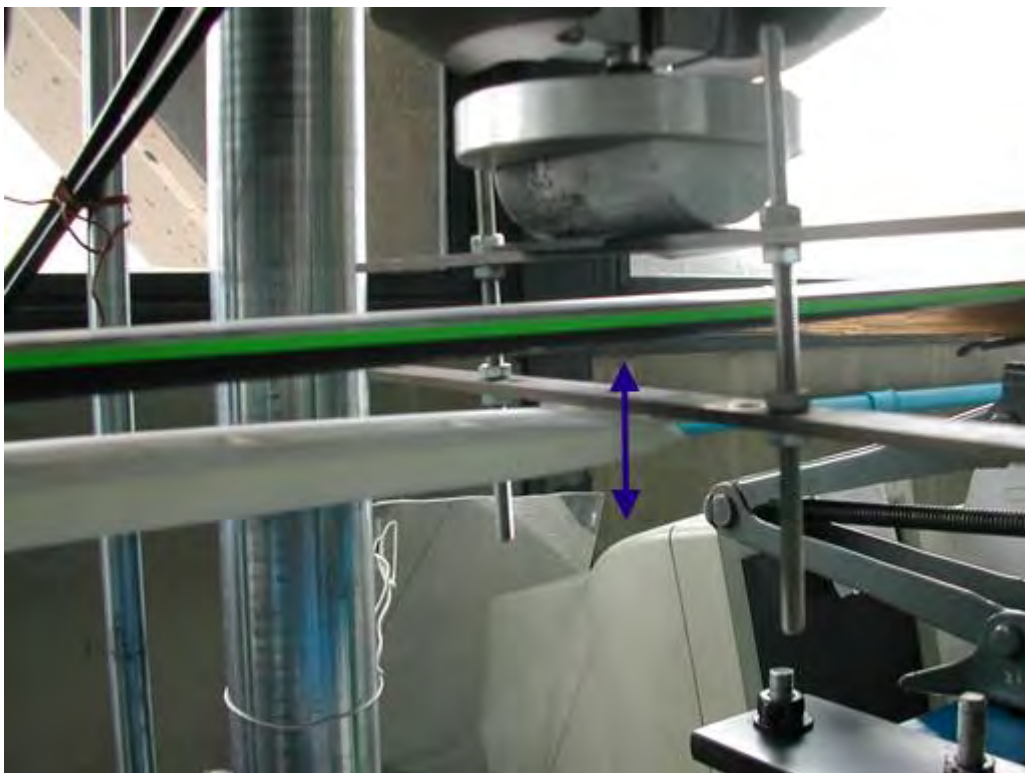


**Figure 3.21** *Details of the system used to characterize only the arm stiffness*

The ski is fixed as shown in figure to a blue bar that is clamped in clamp. A displacement of the upper cylinder is imposed at 12 mm, statically and dynamically. During the test the load

cell acquisition registered the load transferred to the cell. The displacement is applied at the tip of the arm, so at 250 mm from the fixation system to the aluminum support.

With this system the measurement of the ski and arm contribution is possible and has been tested, as reported in the results.

A displacement profile during the time has been programmed with the Minibionix machine, as reported in the Figure 3.22.

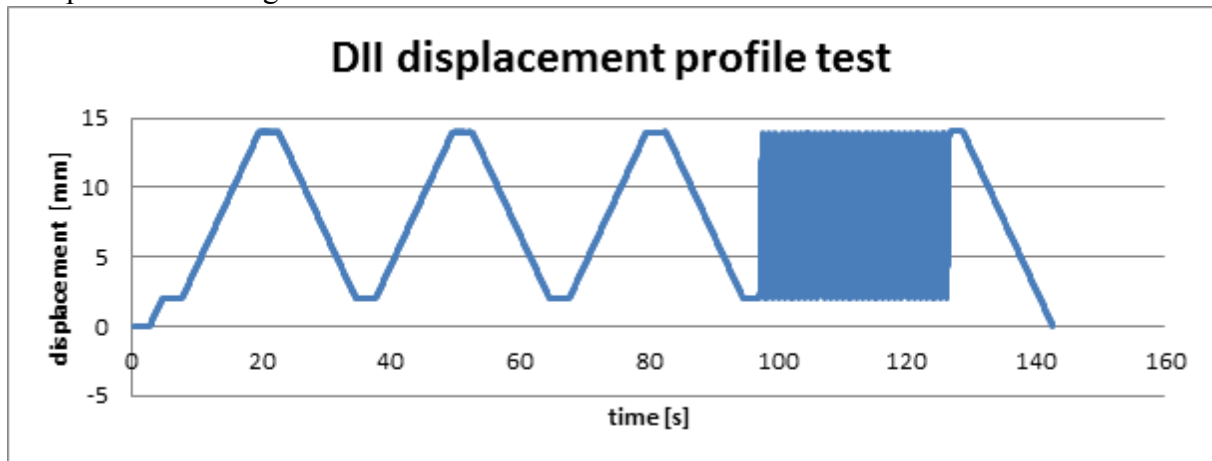


Figure 3.22 Displacement profile imposed test

The procedure involves:

- 2 mm of preload;
- Three static cycles, at 1 mm/sec speed rate, with a relative displacement of 12 mm;
- 30 dynamic cycles, 1 Hz, 12 mm relative displacement;

This procedure has been followed for arm only and also in the ski + arm configuration.

#### 3.4.4 DII test results

In order to find the stiffness parameter, the third static cycle and a median of the last three dynamic cycles has been chosen for the analysis.

For all the arms the Force-Displacement loop has been created, and so the stiffness is found as the slope of linear regression approximation. Here an example of the procedure adopted is reported.



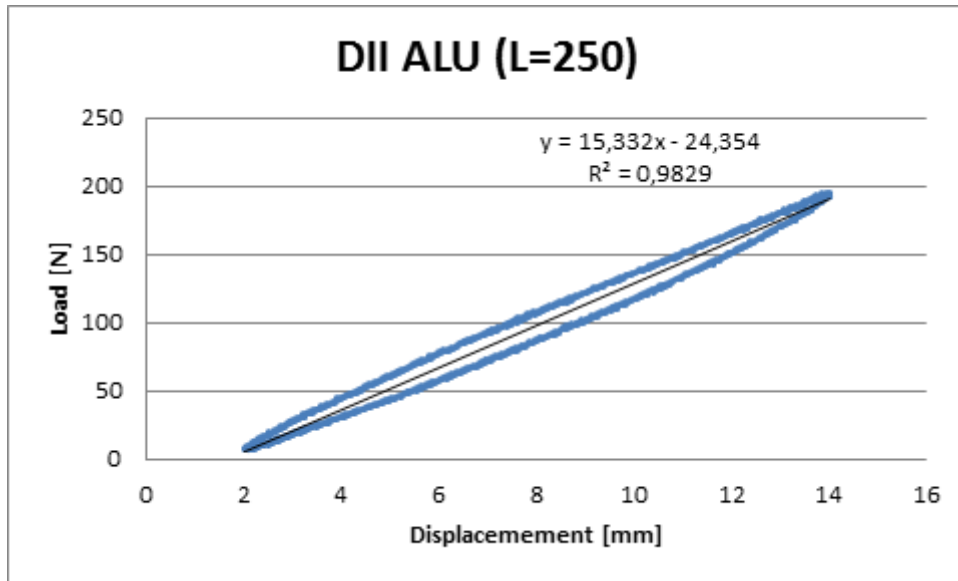


**Figure 3.23** *N over mm loop for the ALU arm*

Summarizing, in the following table there are the stiffness found for the system (ski+arm) and only the arm.

**Table 3-4** *Arm and ski+arm stiffness*

	K [N/mm]	K [N/mm]		K [N/mm]	K [N/mm]
	Static	Dynamic		Static	Dynamic
Ski + ALU	15,33	15,76	ALU	11,55	11,55
Ski + WOOD	15,35	15,71	WOOD	8,65	8,89
Ski + PU+C	13,6	13,89	PU+C	6,39	6,43
Ski + PU	12,27	12,52	PU	3,46	3,60
Ski + CHB	12,31	12,57	CHB	2,59	2,69

### 3.4.5 Comparisons

In the next diagram, the stiffness found with the different method are compared. The colors used are intentionally the same of the arms.

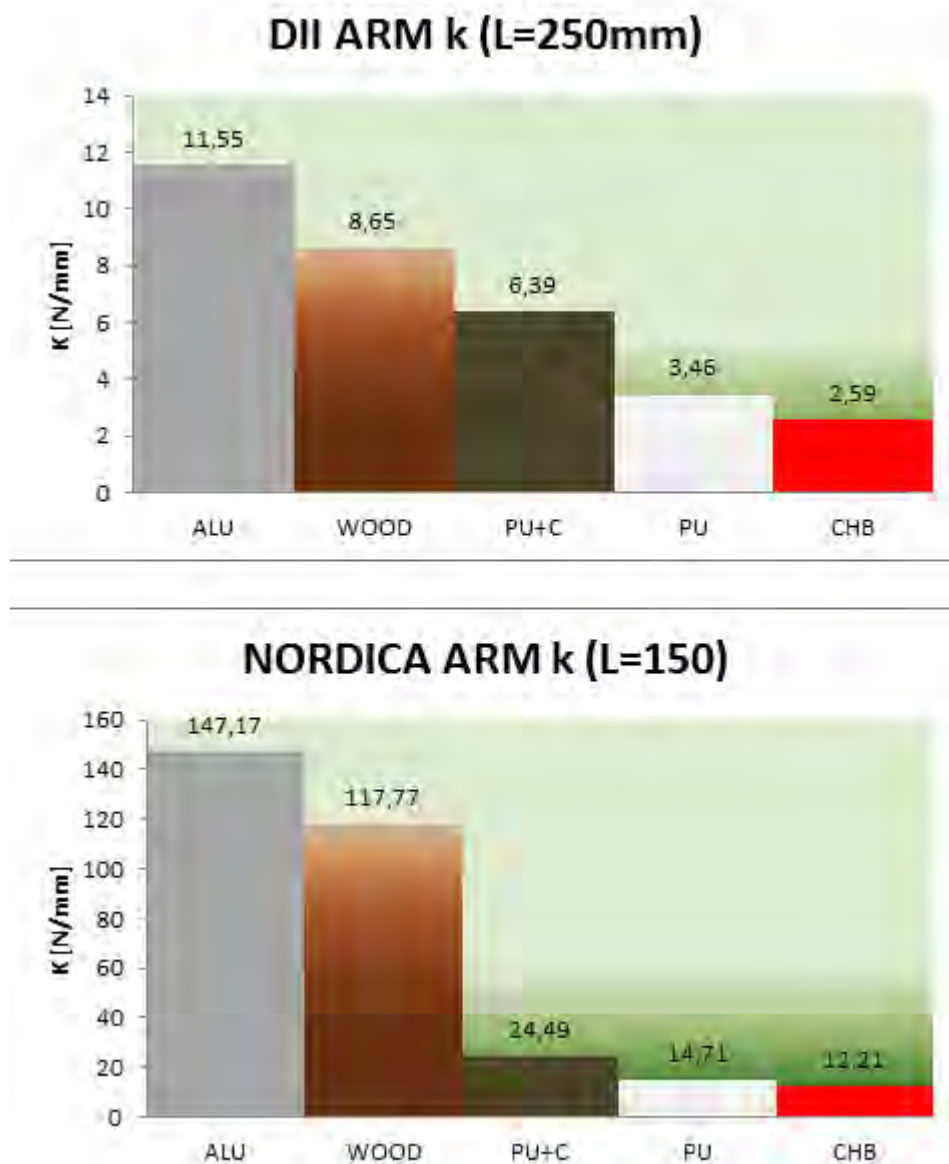


**Figure 3.24** Comparisons of stiffness arm found in hte different laborary, the first picture refers to Padua dipartment, the second to Nordica bench.

It can be noticed that the results of Nordica and DII differs by a factor of 10, but the same trend is maintained. This apparent discordance is explained in the discussion of the results that follows.

Also the comparison between the arm stiffness and the system Ski+arm is analyzed.

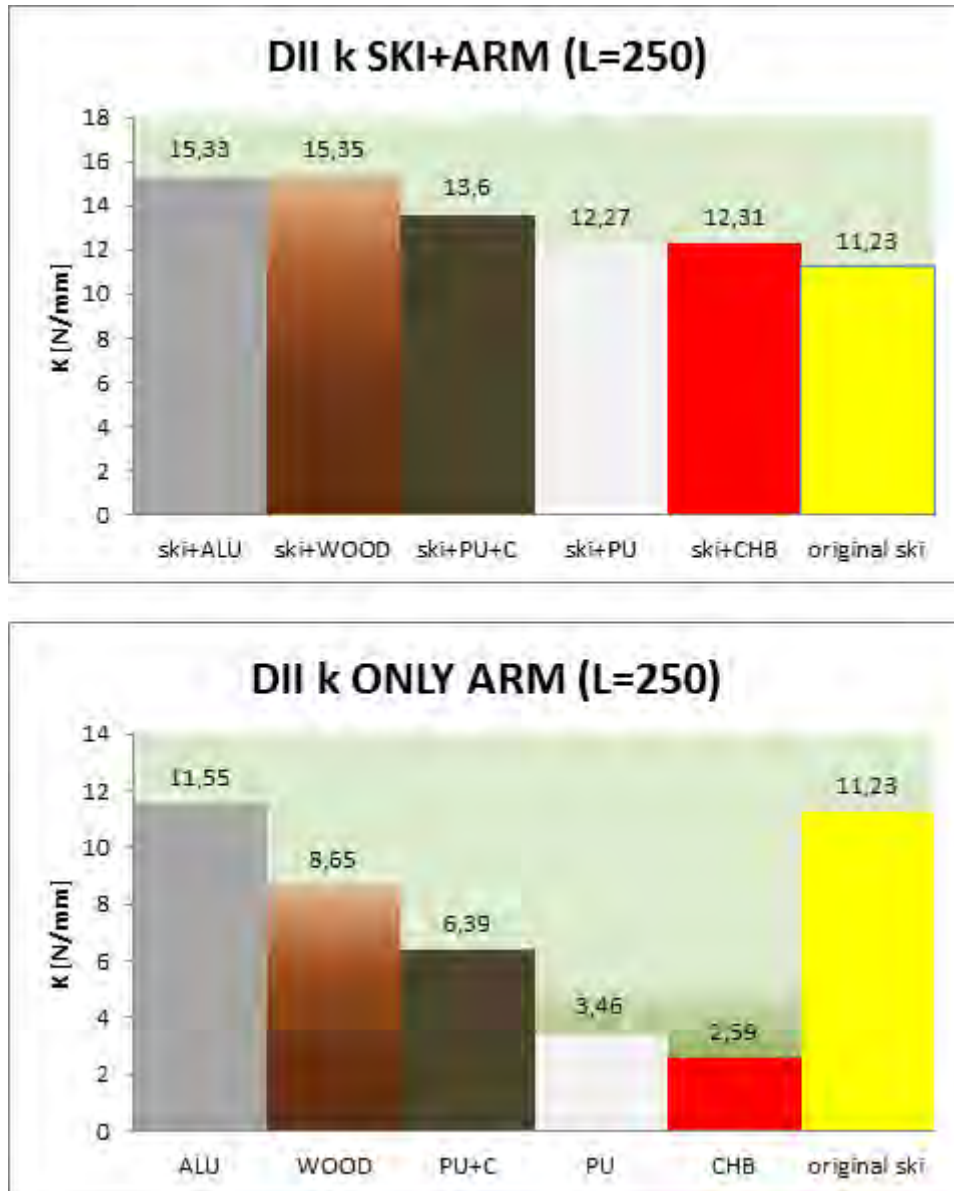


Figure 3.25 Padua comparisons between the stiffness found for the system ski + arm and only the arm

Unfortunately it is not possible to find an easy correlation between the  $K_{\text{ski+arm}}$  and  $K_{\text{arm}}$ .

### 3.4.6 Comments to the results

The huge difference between the stiffness found with the two methods could be explained with the different fixation system. In fact, in Nordica laboratory only the arm fixed to a rigid support was tested. In DII laboratory the arm fixed to the ski has been taken into account, all fixed in a bar that is fixed to the cell that register the load. So, all the system can move during the application of the displacement. This contributes to give a lower load with the same displacement if compared with a rigid support. But this configuration it's closer to reality, even if it is not representing the ski deformation during a curve.



It can be noticed that the ALU arm stiffness it's almost the same of the shovel stiffness found for the original ski. But this do not corresponded with a double stiffness value for the ski + arm configuration. Instead, the ski + WOOD and ski +ALU configurations have the same stiffness values, 15,35 and 15,35 N/mm<sup>2</sup> respectively, even if the contribution of the arms alone are different, . WOOD 8,65 N/mm<sup>2</sup> and ALU 11,55 N/mm<sup>2</sup>.

In addition, the point where the load is applied has to be taken into account. In Nordica it was at almost 2/3 of the length, rather in DII the arm was tested at the tip of it. Also this fact contributes to reduce the value of the stiffness.

Secondly, the load in the two test it has been applied with opposite direction. DII as the arm works during skiing, on the contrary in Nordica.

### 3.5 Vibration damping

At Padua Department it was possible to perform also a vibration damping test.

The vibration of ski during a race can influence negatively the performance, affecting the stability of the skier. The faster the skier goes, the sooner the ski begins to lose contact with the snow surface as repetitive impacts can cause vibrations. Frequently, this vibration is severe enough to affect the rider's control and balance.

The three key aspects considering the vibration damping are amplitude, frequency, and decay. Amplitude is the magnitude of each oscillation. In skiing this is usually measured as the acceleration at which the bent ski returns to its neutral position. Amplitude is sometimes measured as the height that the oscillating ski tip reaches since this is easier to picture, although it is less meaningful. Frequency is the number of oscillations per second. Finally, decay is a measurement of the portion of amplitude that is lost each oscillation. Increasing the decay is the only way to make anything –including a ski– more damped.

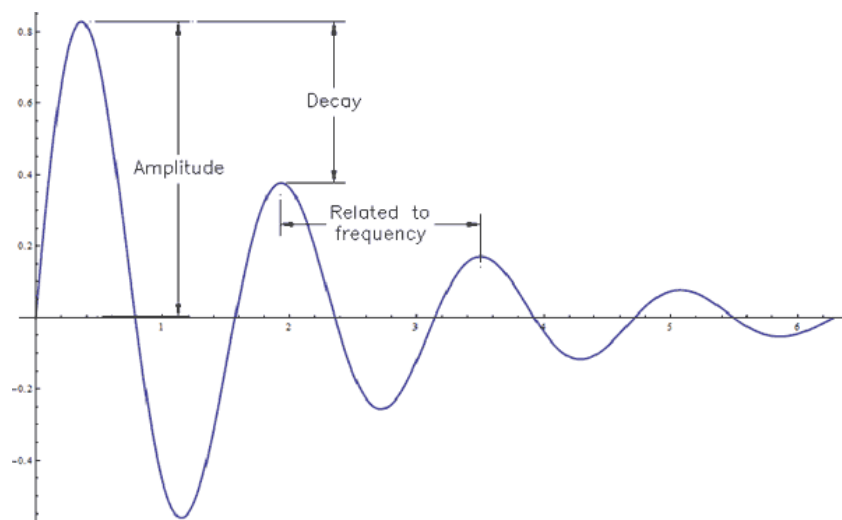


**Figure 3.26** *Vibration damping important quantities*

The logarithmic decrement parameter provides information on the amplitude rate reduction of free vibrations. Through its knowledge it is possible to determine the damping coefficient of 1 degree of freedom system. It is estimated in the free response, described in the time domain, and is defined as the natural logarithm ration between any two consecutive amplitudes. Generally,  $x_1$  and  $x_2$  are two consecutive amplitude measured at a distance of a damped period  $T$ ,  $\zeta$  is the damping ratio and  $\omega$  the pulsation:

$$x_1 = x(t) = e^{-\xi\omega t}(B_1 \cos \omega_d t + B_2 \sin \omega_d t) = Ae^{-\xi\omega t}$$

$$x_2 = x(t + T) = Ae^{-\xi\omega(t+T)}$$

$$\frac{x_1}{x_2} = e^{-\xi\omega T}$$

The logarithmic decrement is defined with the relation:

$$\delta = \ln\left(\frac{x_1}{x_2}\right) = \xi\omega T$$

Therefore, to calculate the damping ratio via the logarithmic decrement, the free response of the system in the time domain has to be known experimentally. Only by this way it is possible to determine the values of displacement  $x_1$  and  $x_2$  spaced by a period damped.

It is common with experiment practice to consider the displacements  $x_1$  and  $x_2$  for  $n$  damped periods, to obviate any errors in period measurements and better approximate the damping to the model.

### 3.5.1 Procedure

The test used the same Minibionix machine introduced previously, maintaining the fixation system used during the arm stiffness characterization. The test is characterized by an error introduced with the fixation system. In fact, all the system during the test were oscillating. This factor is the same in all tests, so the data can be representative for the comparisons that are explained.

The ski is fixed with the false boot to a steel support bar. All the system is clamped in the clamp of the Minibionix machine.

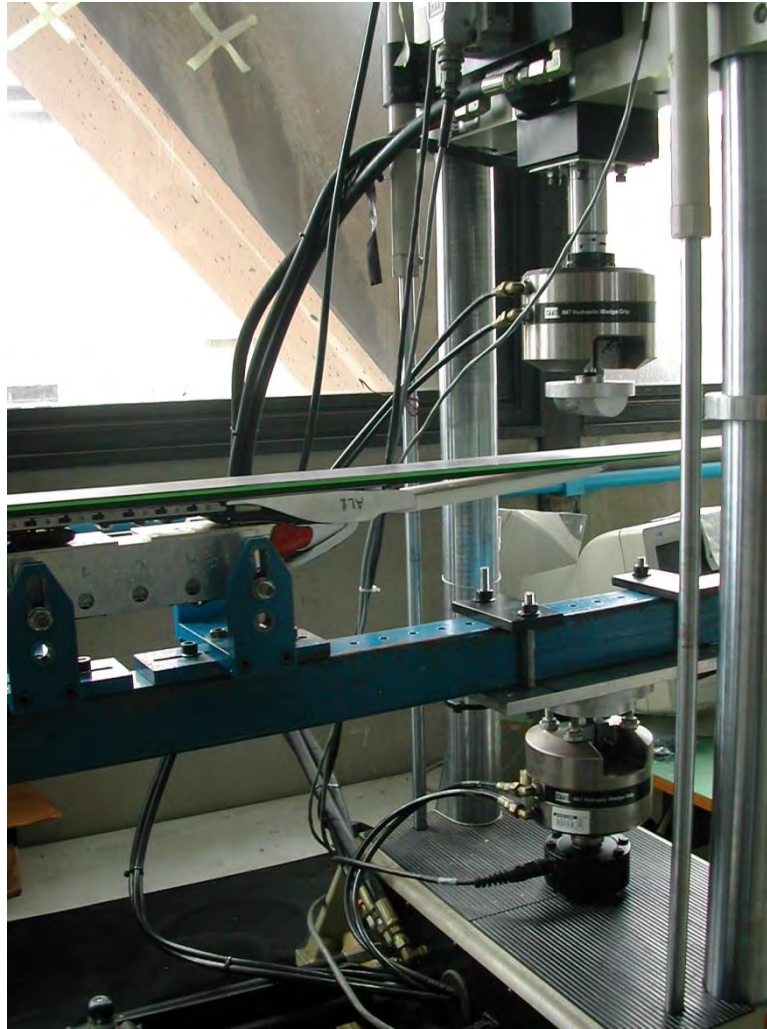


**Figure 3.27** *Minibionix fixation system for vibration damping characterization*

The procedure used involves only the acquisition of load during the time, at 0.00097656 sec time between points.

Manually the ski tip is bent and realized. The ski, and all the system starts to vibrate and until it reaches the stability. The load cell registers the load variation in time. The .txt file is then exported in Excel and analyzed.

The load variation during the time is plotted, using a scattered plots with only markers:

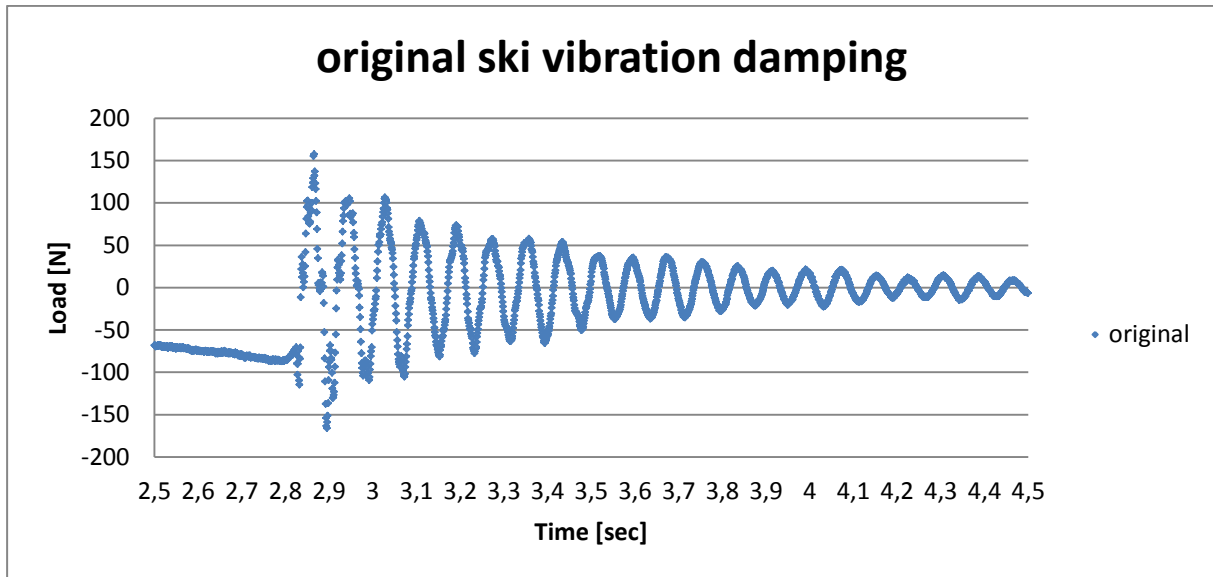


**Figure 3.28** Vabration damping test for the original ski

Then, the maximum peaks are extracted and plotted in a different graph, where it is possible to create an exponential interpolation line, Figure 3.29.

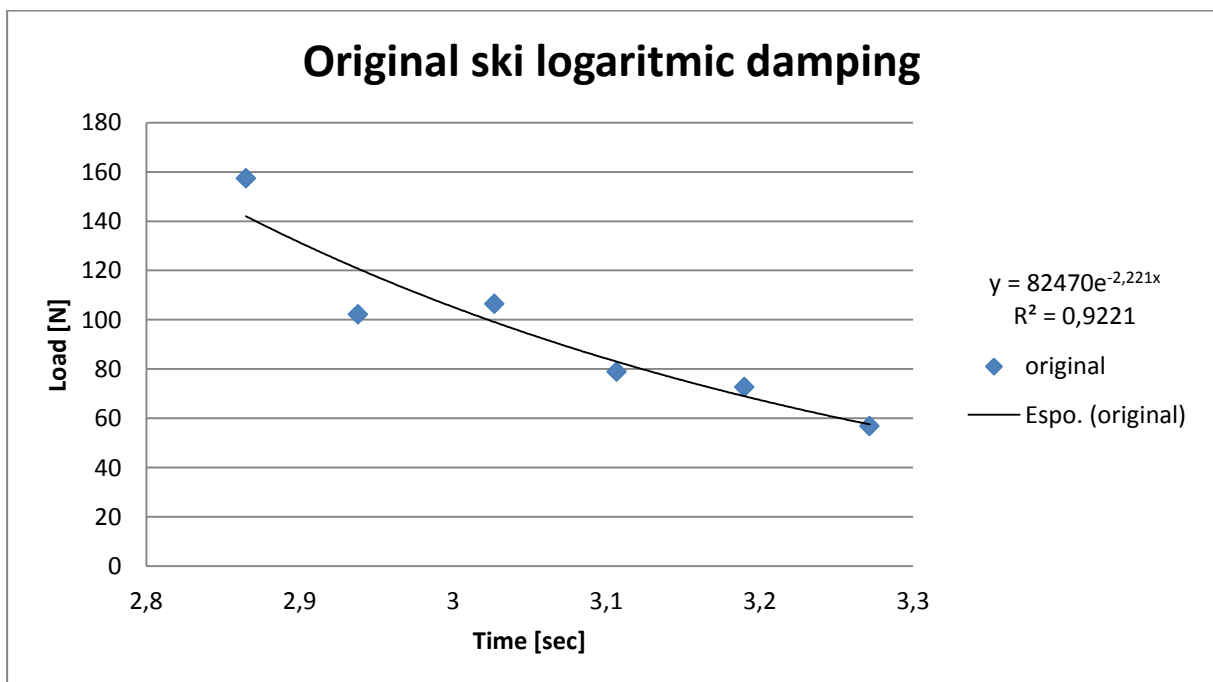


**Figure 3.29** Maximum values exatred from the oscillation damping

With this system all the constants and variables needed to find the logarithmic decrement parameter are explicit.

The following table summarized the exponential interpolation function found for each configuration and the logarithmic decrement parameter associated

**Table 3-5** Exponential function, mean period and logarithmic decrement parameter found for each ski configuration

Ski	Exponential function	Mean period	Logarithmic decrement parameter $\delta$
Original	$y = 82470e^{-2,221x}$	0.0811	0.1802
WOOD	$y = 2E+11e^{-5,207x}$	0.0700	0.3646
PU + C	$y = 3E+06e^{-3,754x}$	0.0750	0.2815
CHB	$y = 5E+06e^{-3,392x}$	0.0775	0.2629
ALU	$y = 4E+06e^{-3,312x}$	0.0713	0.2442
PU	$y = 989393e^{-3,085x}$	0.07552	0.2330

In the table the ski configuration with decreasing effect are represented. The more influence structure is represents by the WOOD arm, with also the shorter mean period damped. Follows the structure PU+C, CHB, ALU and PU. All the arms contributes positively, that means when the system is externally perturbed the normal configuration is reached in a short period than the original ski only.



## 4. Work bench result influenced by arm prototypes

### 4.1 Dobermann Spitfire Edge load profile

The ski load distribution has been studied with the Edge Load Profile Slytech bench. The examined ski is a Doberman Spitfire 168, with in total five different types of “elastic compensation arms”, usually called “arms”.



Figure 4.1 Dobermann Spitfire ski, Nordica.

The bindings adopted were Marker 16 correctly adjusted at 12 DIN. All the arms tested are summarized in the next table:

Table 4-1 Tested arms

ID Arm	Description	Arm mass (g)
ALU	Aluminum alloy	184
PU	White PU	185
PU+C	Black PU with carbon sheets	141
C H B	Carbon hard bond (red)	177
WB300	Wood arm, length 300	189

Arm mass means the weight of the arm and the four screws necessary to fix it.

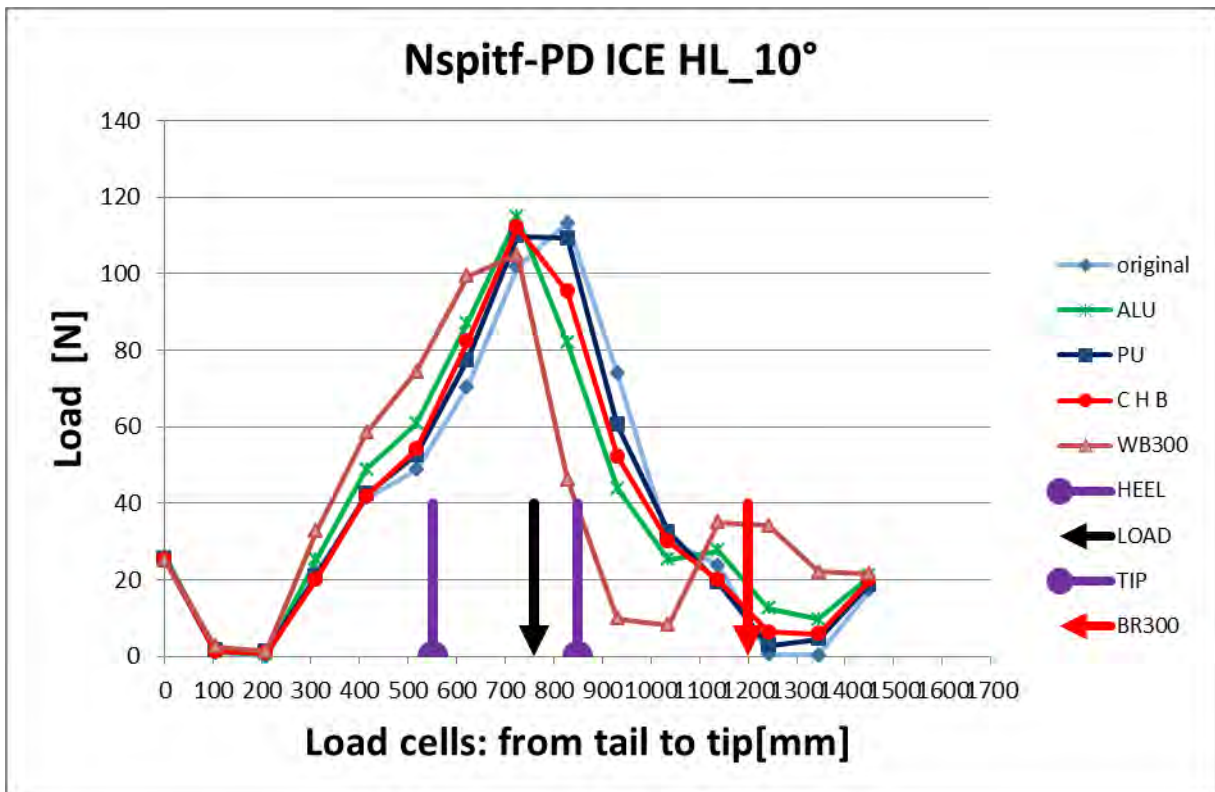
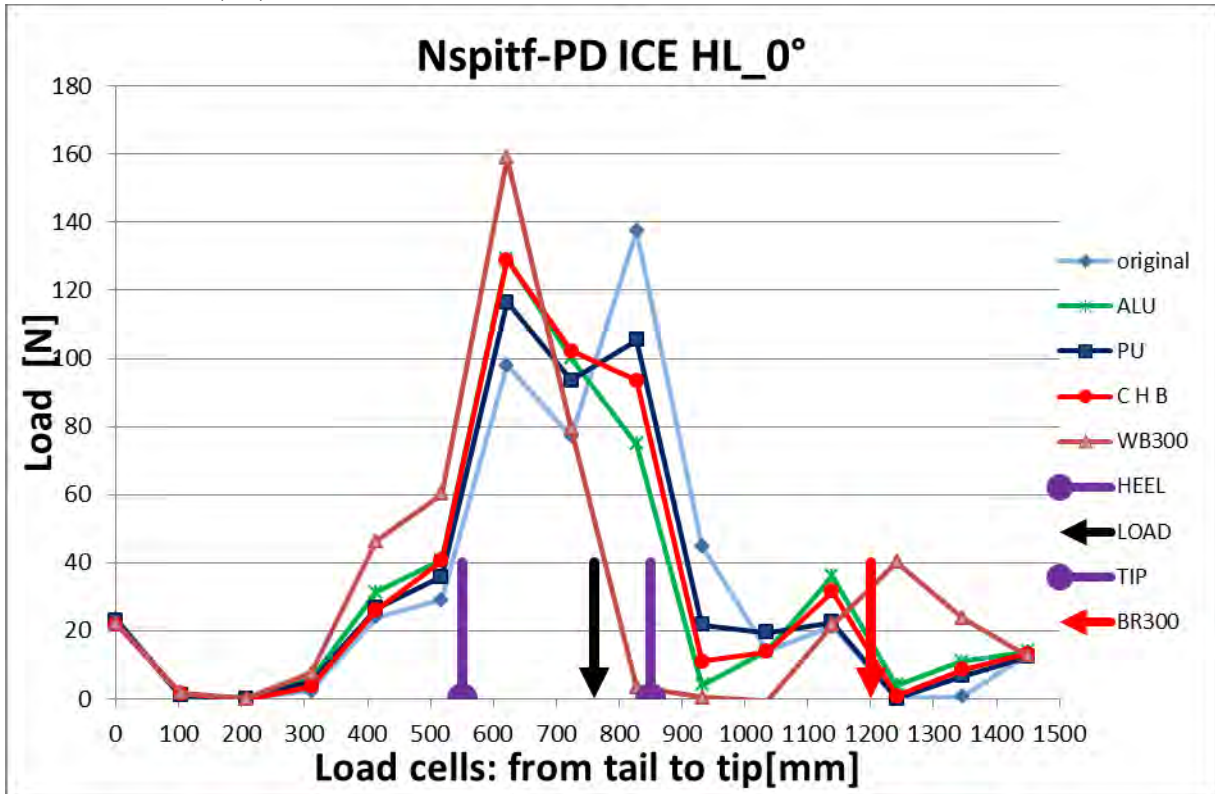
### 4.2 Slytech bench results

The test with the Slytech bench is conducted following the procedure:

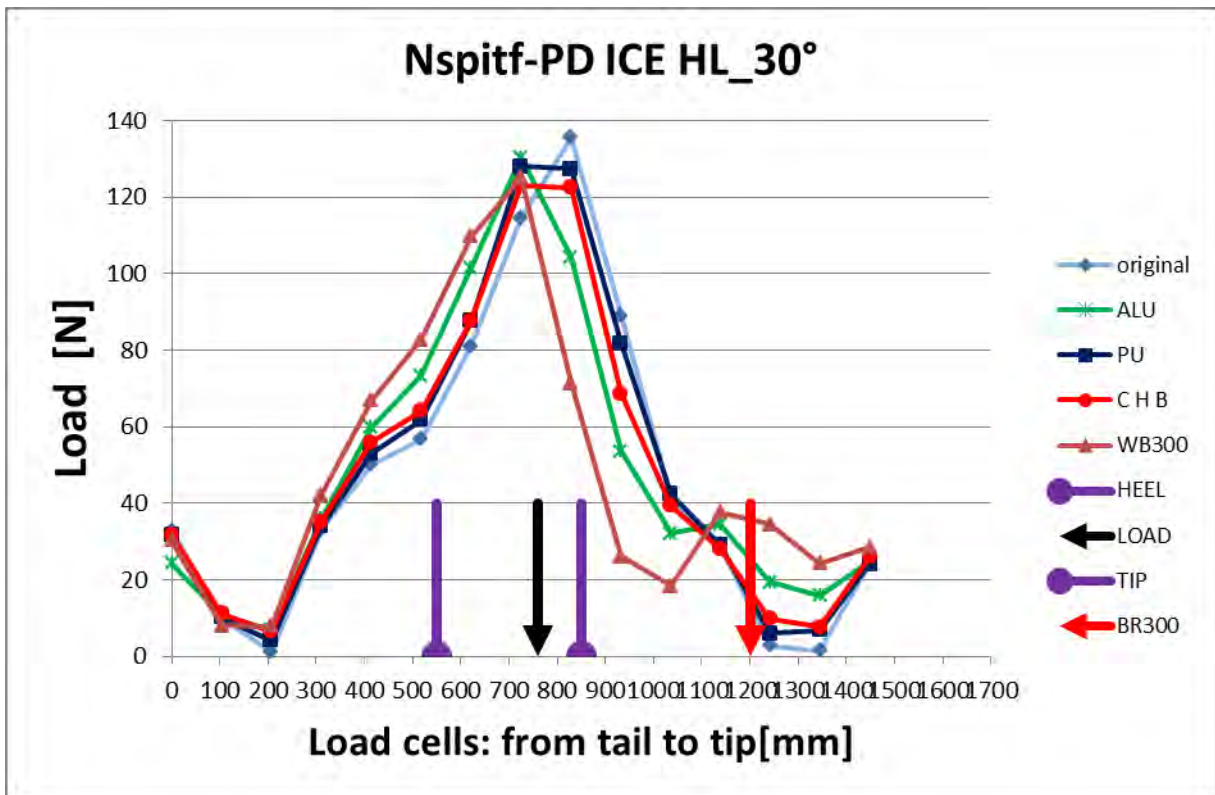
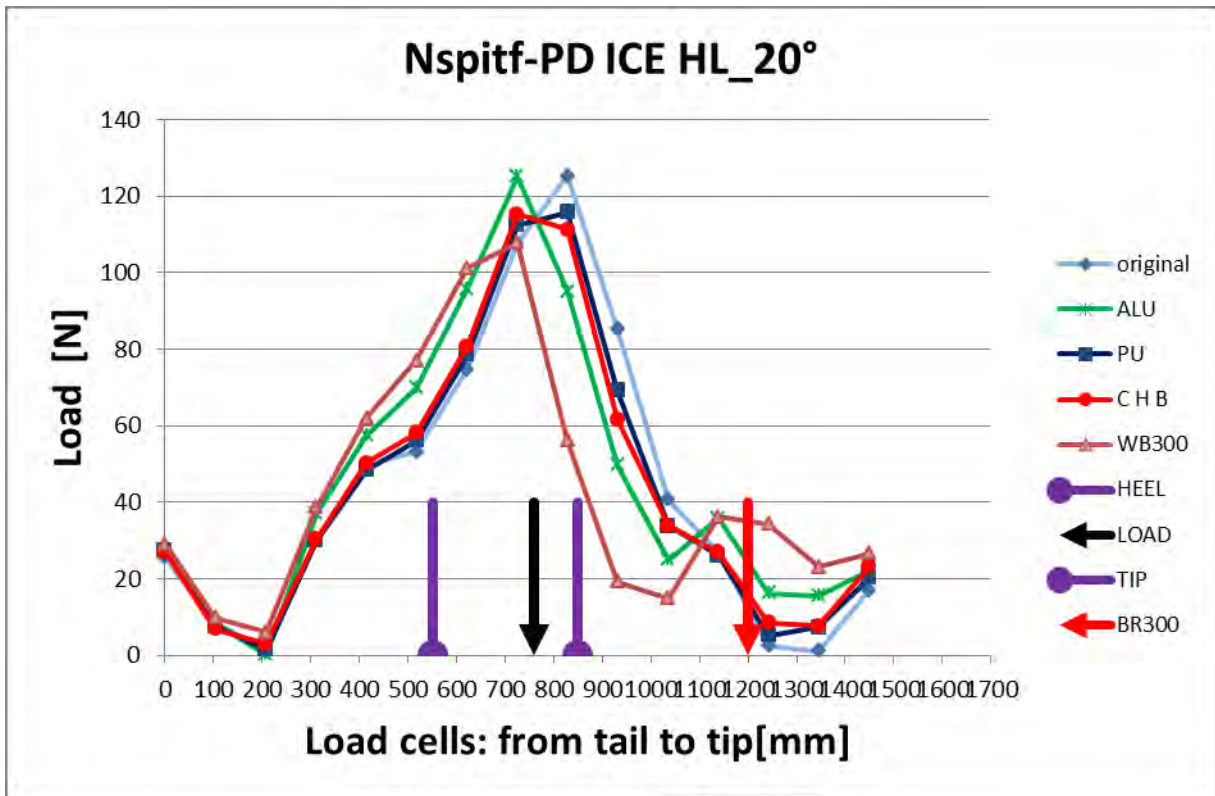
- Fix the false foot to the binding system
- Auto offset of the bench
- Test at different edging angles at different loads (Table 2-1)

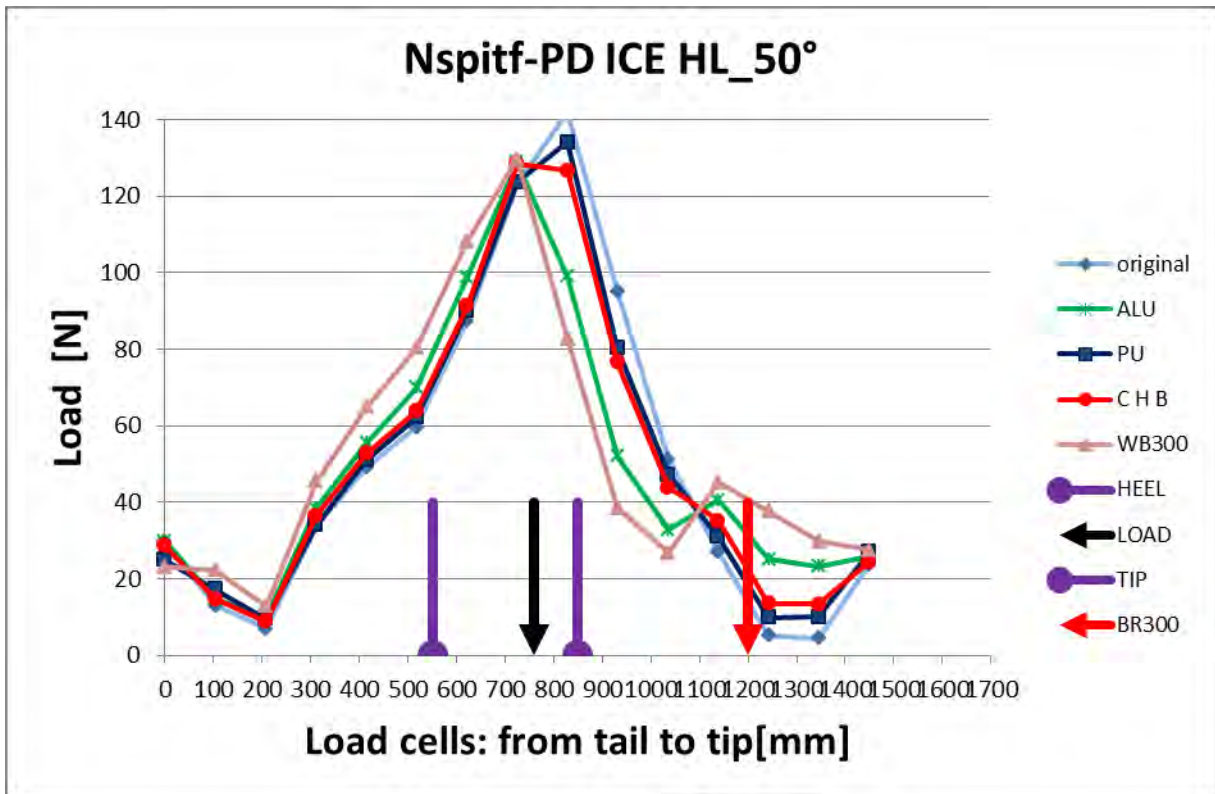
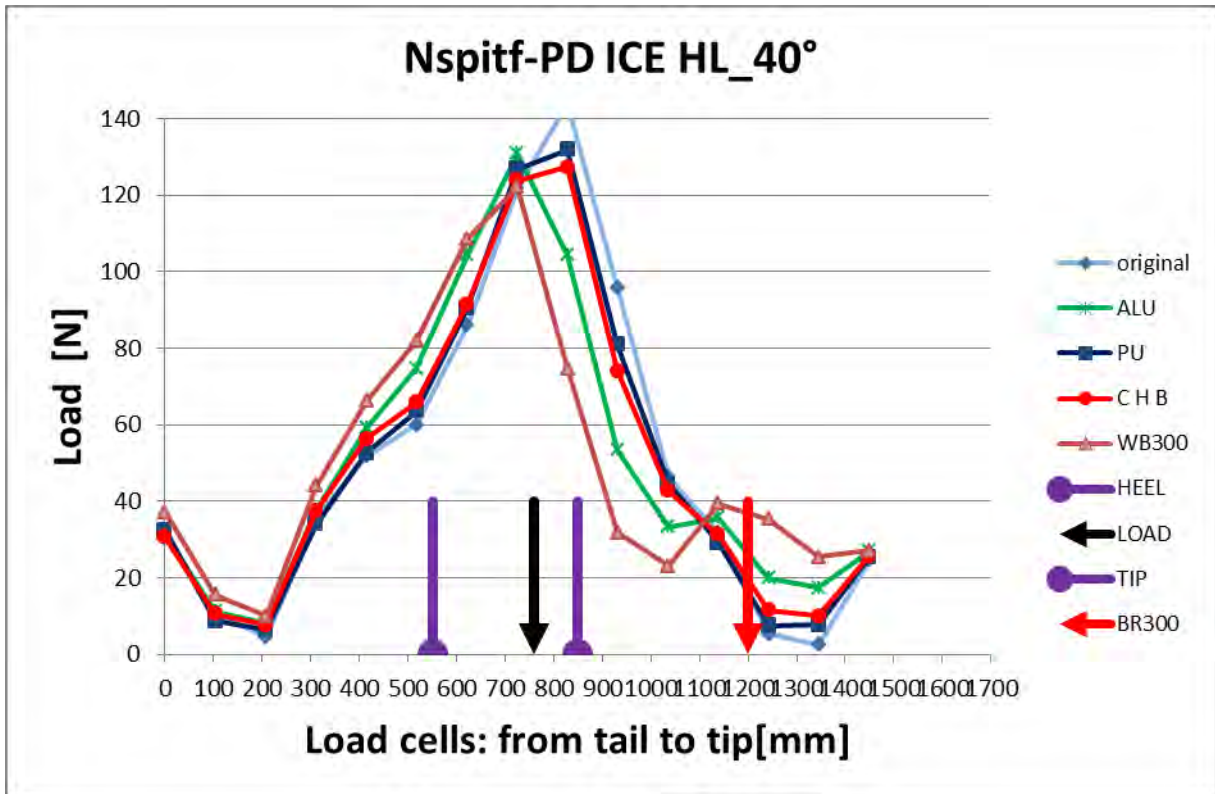
The following diagrams represent the edge load profile (ELP) for different angles for all the configurations. The title of the graph means: *Nspitf* stays for the ski Nordica Spitfire, *PD* the bench used in Padua Department, so the Slytech bench, *ICE* and *HL* the type of snow

simulated, ice, with High Load applied. This last two identification are introduce to discern *PD* and Chemnitz (*CH*) workbenches. In Padua, infect, the snow condition that can be simulated are: *ICE*, hard snow (*HD*) and medium (*ME*); with *CH* bench, a mild snow (*MI*) and a soft snow (*SF*).









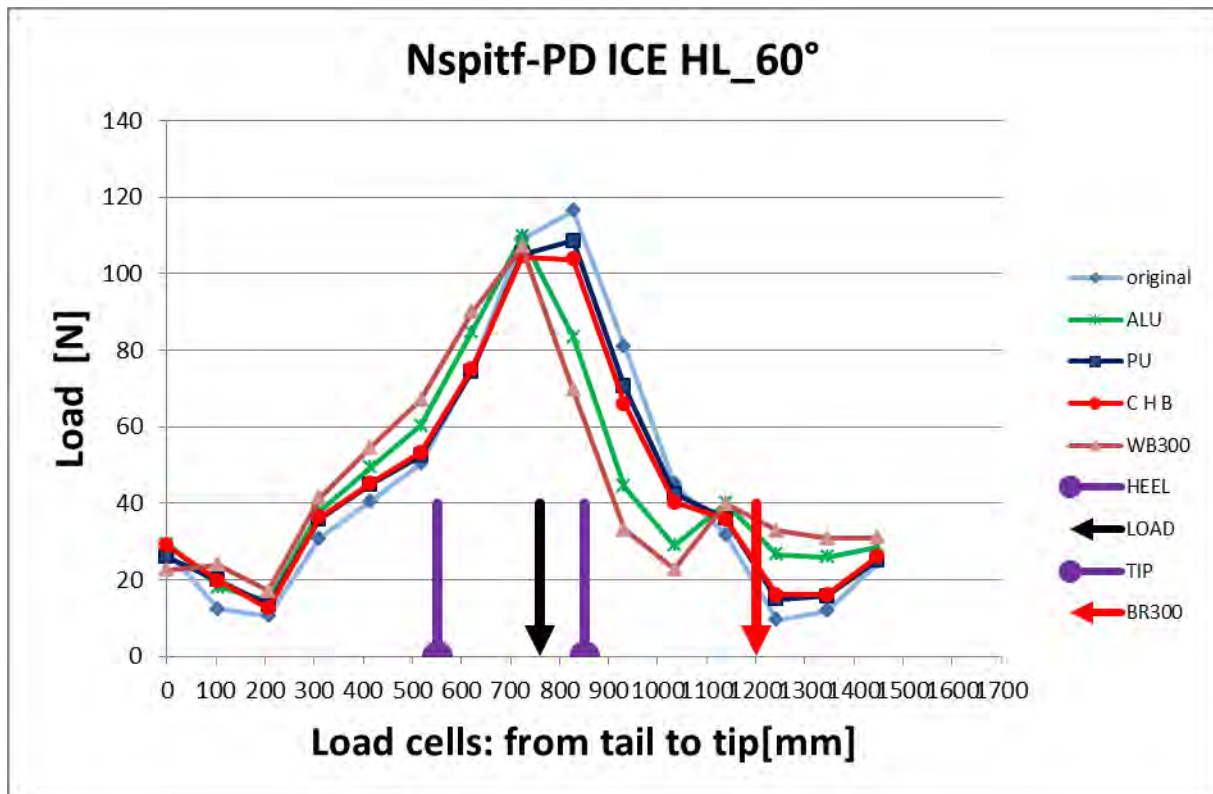


Figure 4.2 Ski load distribution for Sitfire Dobermann with different arms

#### 4.2.1 Comments to the results

In general, four different types of shovel load distribution can be observed:

- Original ski. The curve of the original ski presents a deep load drop in the shovel, with the minimum value being slightly higher than zero only from 40° onwards.
- The effect of “Plastic arms”. (PU, and C H B): these arms have a similar effect at the different edging angles, but giving only a mild load increase to the front part of ski.
- The arms named ALU gives a more effective load distribution to the shovel of the ski.
- The effect of WB300 arm is different: it seems to shift back the load profile, inducing the highest load peaks in the tip portion of the shovel but leaving a certain load drop in the rear part of the shovel.

These results represents a qualitative response from the bench. As said before, the aim of the elastic compensation structure has to redistribute the load along the ski, eliminating the valley on the front part.

The Edge Load Profiles obtained with Slytech bench, for the ski + arm configurations shows that the shovel is better loaded . This is because the ski increases his stiffness and changes his behavior.

From these results one could conclude that that the presence of PU and CHB structure compensation doesn’t significantly change the load distribution. The effect it’s visible at each

angle but it not so significant. On the contrary, the ALU and Wood effect is more evident and could be distinguished from the previous one. Qualitatively, ALU and WOOD can be taken as reference for a new future design.

### 4.3 Results from Chemnitz bench

Even though the Chemnitz bench works in a different manner than the Slytech one, some comparisons could be made.

As explained in Chapter 2.2 , the ski is pressed against a series of sliders that deform under the load independently. From the displacement acquisition, knowing the spring elastic constant, the local deflection distribution of the ski it's found. The graph represents the forces over the length of the ski on a bed of springs.

In this case, only few angles are tested, with the corresponding load applied:

**Table 4-2** *Angles and Loads applied with Chemnitz bench*

Angle	Load
0°	350 N
20°	500 N
30°	600 N

Each test is repeated five times, and the results are shown as a mean of these bench tests. A first comparison between the same ski at different angle is made. The tested ski is always the Nordica Spitfire Pro, in this case with the original configuration, that means with only the aluminum support, without over-structure. The title of the picture identify the ski, CH stays for Chemnitz bench that simulate a MI mild snow applying a LL low load, compared with Slytech.

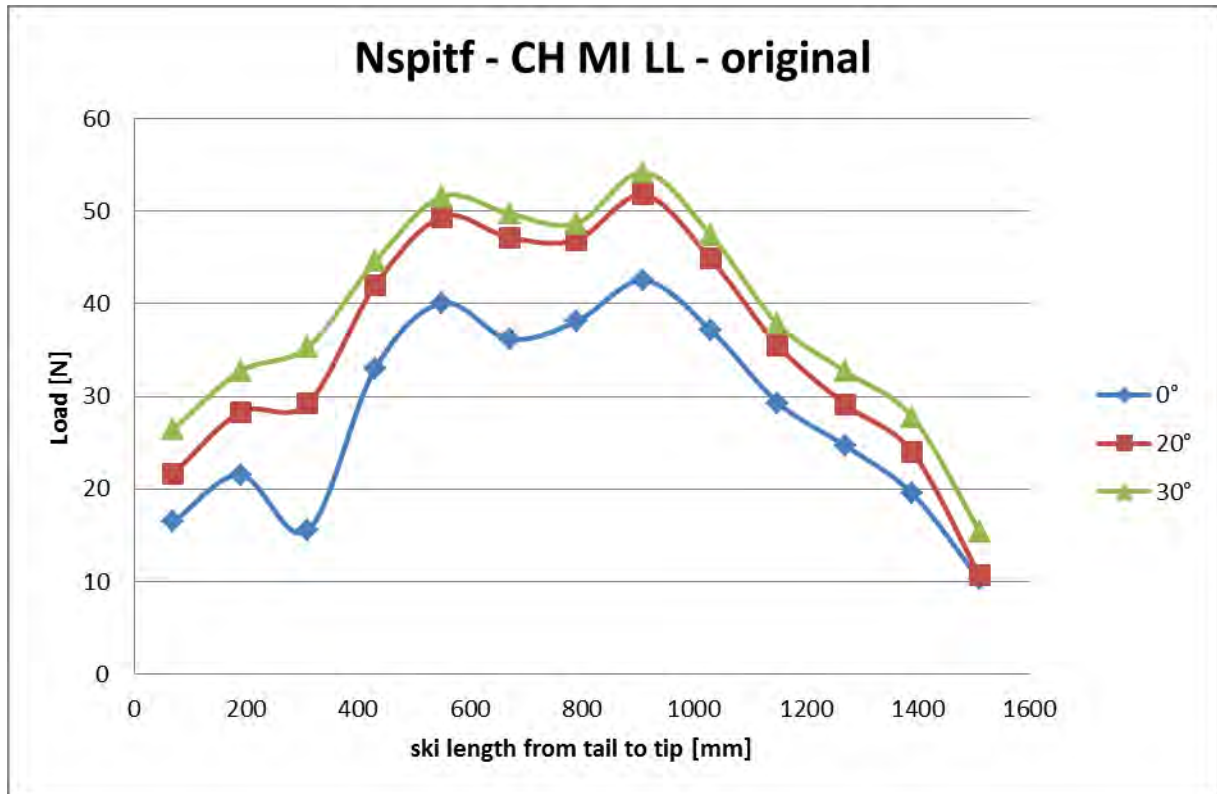


Figure 4.3 Chemitz load profile, original ski configuration for 0°, 20° and 30°

Some considerations are possible:

- The bench is sensible enough to discretize the curves at different angle with different load applied.
- On the tail part of the ski, a larger variations of the plots can be noticed. This corresponds to cell number 12 of the bench. It could be explained with the fact that this slider particularly had some friction even during the test, caused by the temperature. In fact, the holes created in the polyethylene sliders perfectly fit with the guided at 25°C, and during the test the temperature was lower. Nevertheless, the results are significant, because the tail zone it's considered as relevant in this study.
- The two main peaks correspond to the binding toe and heel.
- Moving towards the tip of the ski, a decreasing curve with different slopes can be noticed. This particular shape is common for “low camber” ski. The expression used means that the ski has a quasi-normal geometry, and the camber is not so pronounced.

However, during this elaboration the focus is posed for the effect of the elastic compensation over-structure. The arms effect in ski load distribution at 0° and 30° are presented in the next Figures.



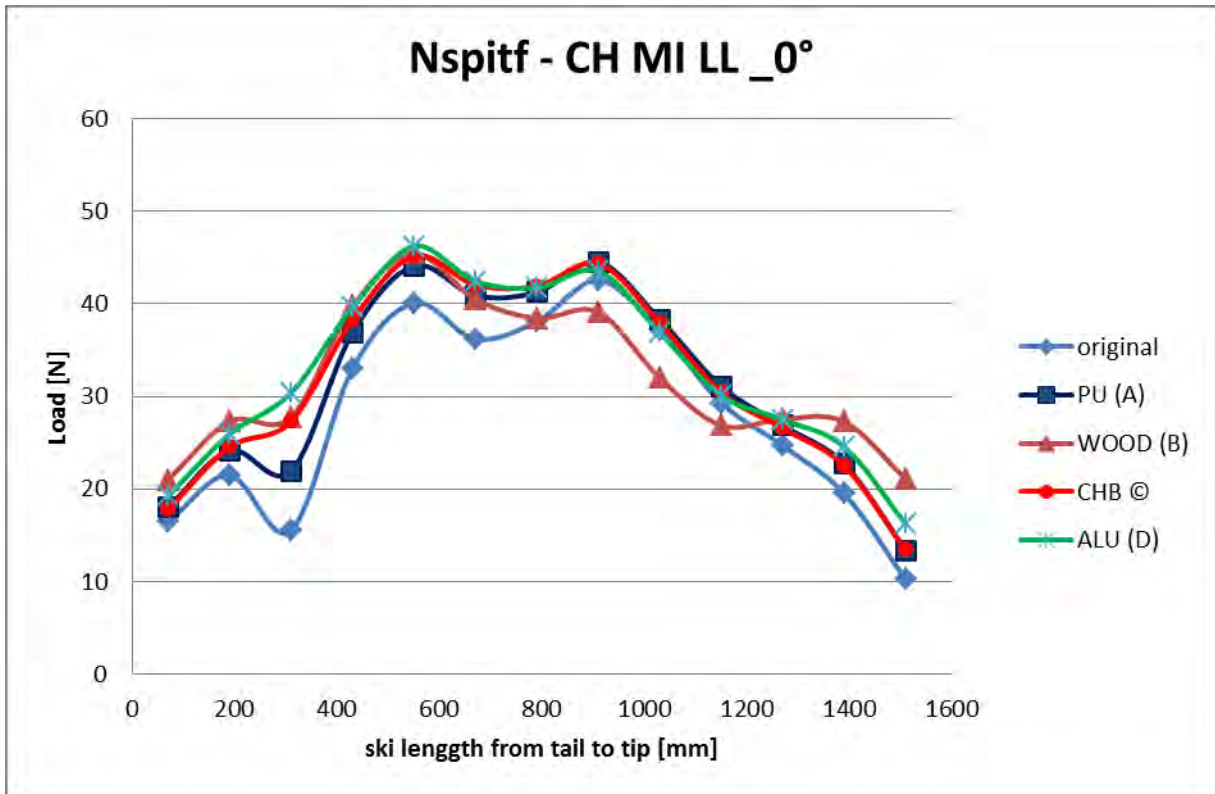


Figure 4.4 Chemnitz load profile for all configurations at 0°

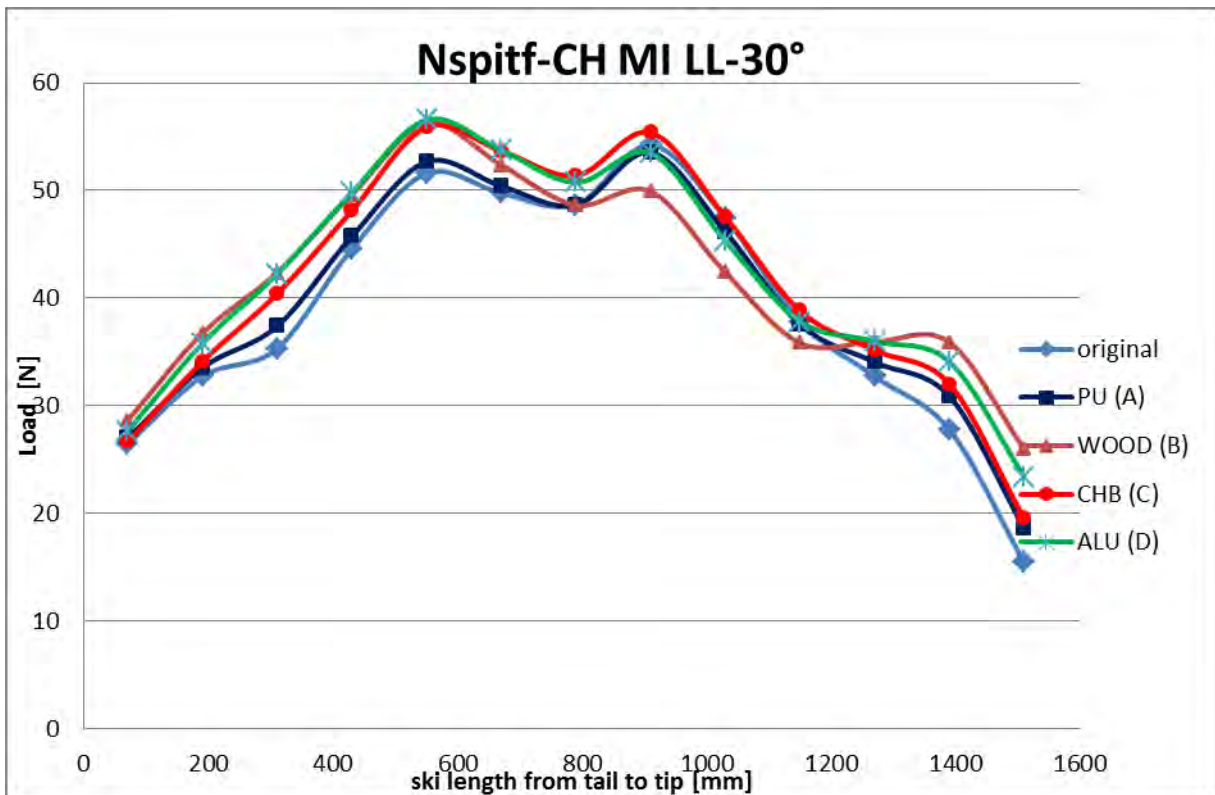


Figure 4.5 Chemnitz load profile for all configurations at 30°

In both the configurations the Wood arm plays an important role: it shifts the maximum peak towards the heel part of the binding and redistributes the load on the shovel. It can be noticed that moving to the tip portion the curves is not always decreasing but shows a positive derivate trend. This configuration corresponds more with a “full camber” geometry ski. This means that the camber geometry is relevant and have an higher influence on the ski stiffness. Then, the ALU, CHB and PU had an effect always less significant. At the end of the Chapter some bench comparison are presented.

### 4.4 Results from Nordica flex bench

In Tecnica Group the bench used to characterize the ski flex does not take into account the simulation of a curved turn, but investigates only the ski rigidity EJ parameter (or GJ for torsion).

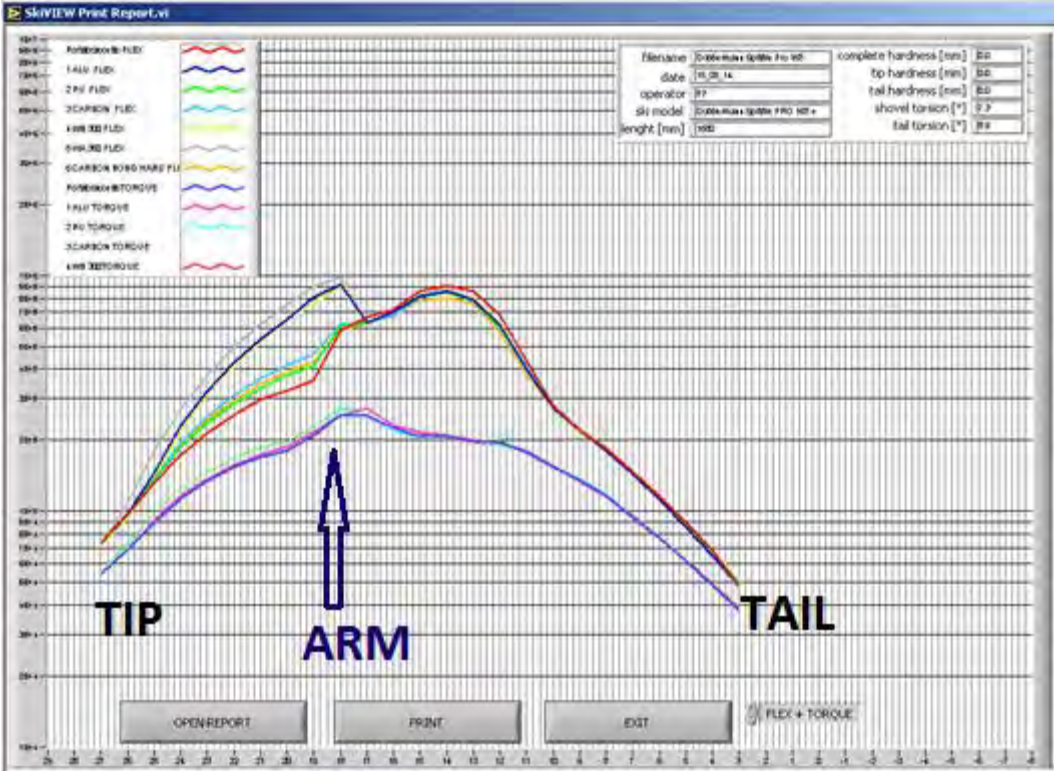


Figure 4.6 Output for flex test (group of upper lines) and torsion test (the others)

From tip to tail in this case, the values of EJ are displaced every 50 mm, as explained before (Chapter 2.2 ). The output shows flex rigidity and torque for all the combinations.

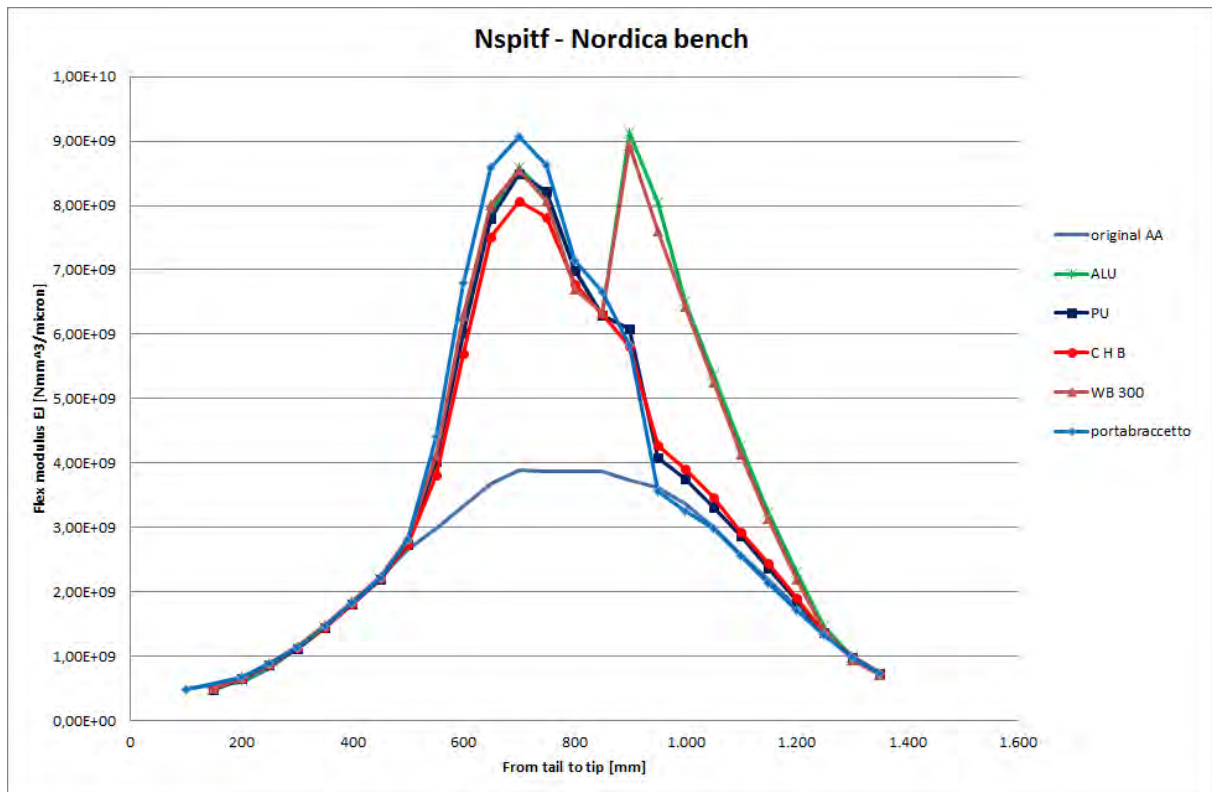


Figure 4.7 Nordica reworked data bench output.

First of all, not all the ski length can be tested because of mechanical obstruction.

The output rigidity of the ski represents how much the ski opposes to the deflection under a load. Considering the shovel zone, the maximum growth of rigidity is given from Aluminum and wood WB300 superstructures, that have a very similar effect. The other arms have a smoother and comparable effect. Doubled values of rigidity are justified by aluminum support and arm effect. In particular, the comparison between original ski, without aluminum support, blue line with no markers, and the ski with the aluminum support, blue line with rhombus markers, shows the great influence of the support in ski rigidity. The arms effects can be seen more in shovel part.

Wood and aluminum arms makes a completely different profile of rigidity.

PU and C H B arms have an increasing effect respectively. This is coherent with the Slytech bench and Chemnitz bench results.

Therefore some comparisons between the benches are possible.

#### 4.5 Padua – Chemnitz benches comparisons

A significant comparison between these two benches can be done just for the 30° edging, because with Slytech bench lower angles are less significant and it is not possible to test higher angles with the Chemnitz bench.



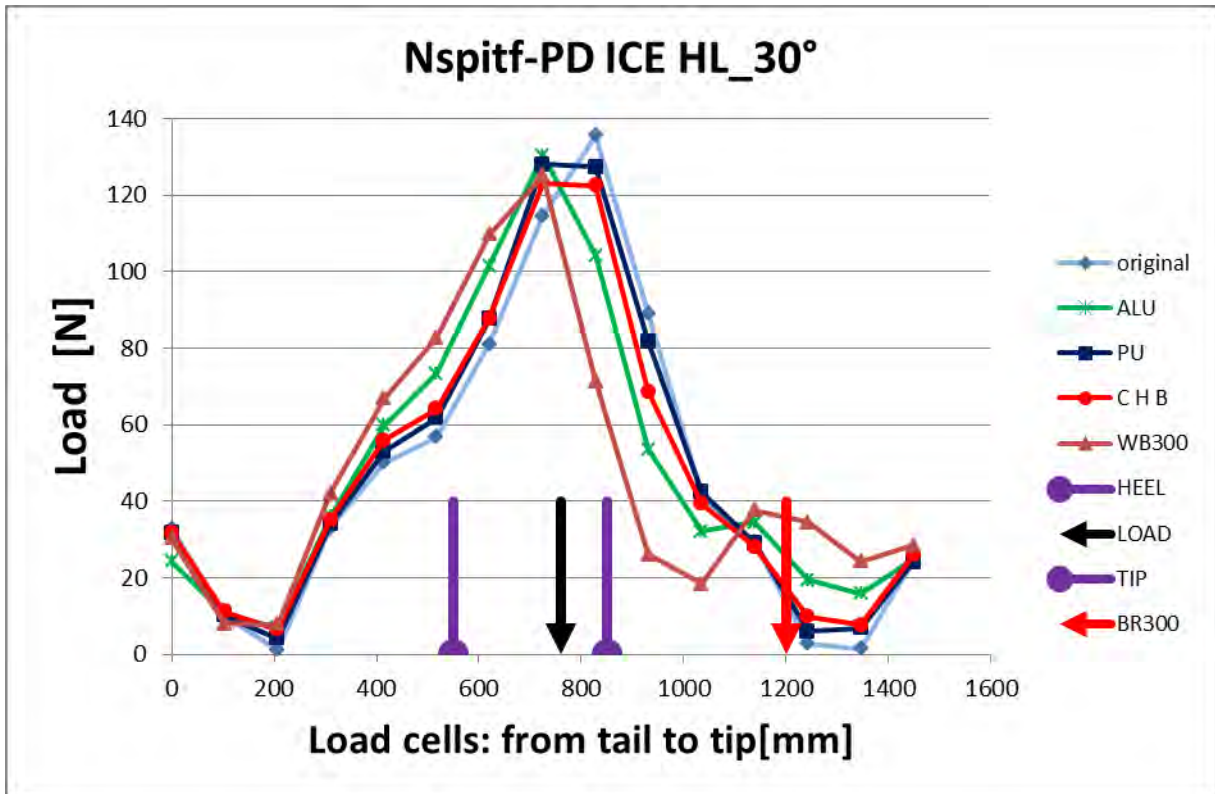


Figure 4.8 Padua Load Distribution Profile at 30°

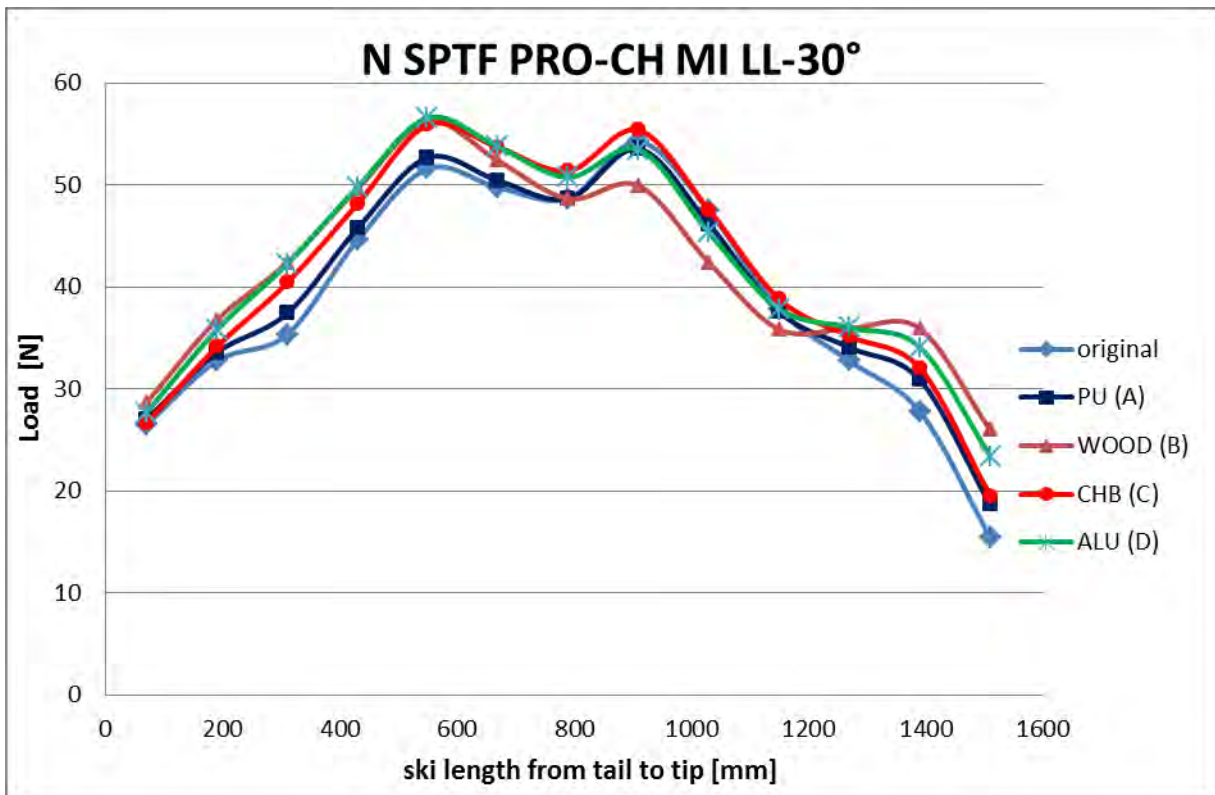


Figure 4.9 Chemnitz Load Distribution Profile at 30°

Even though the Newton values are completely different the trend of the curves interestingly matches: the WOOD arm, the second stiffer arm, contributes more in load distribution. With the Slytech profile it can be noticed how the shovel supports an high amount of load. These fact correspond to a higher rigidity of the ski, that permits to deform the ski in different way. Watching to the Chemnitz bench profile , the ALU curves presents a different trend, that means a different displacement profile of the ski under loads.

### 4.6 Chemnitz – Nordica benches comparisons

The comparisons between the Chemnitz and Nordica benches have to be conducted taking the 0° for the Chemnitz bench. Must be remembered that, in Nordica bench the ski is free to deform, as like a three point bending test, and the plotted value is the rigidity of the ski, measures with the EJ product.

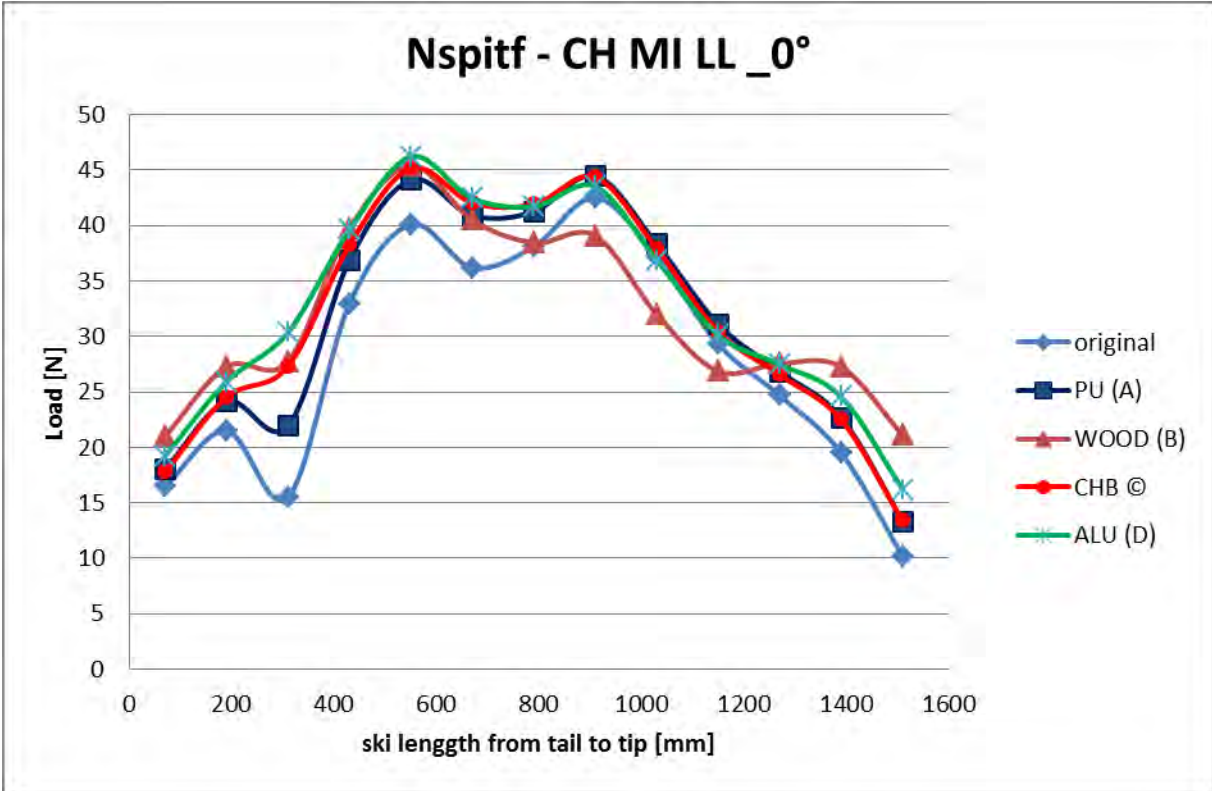
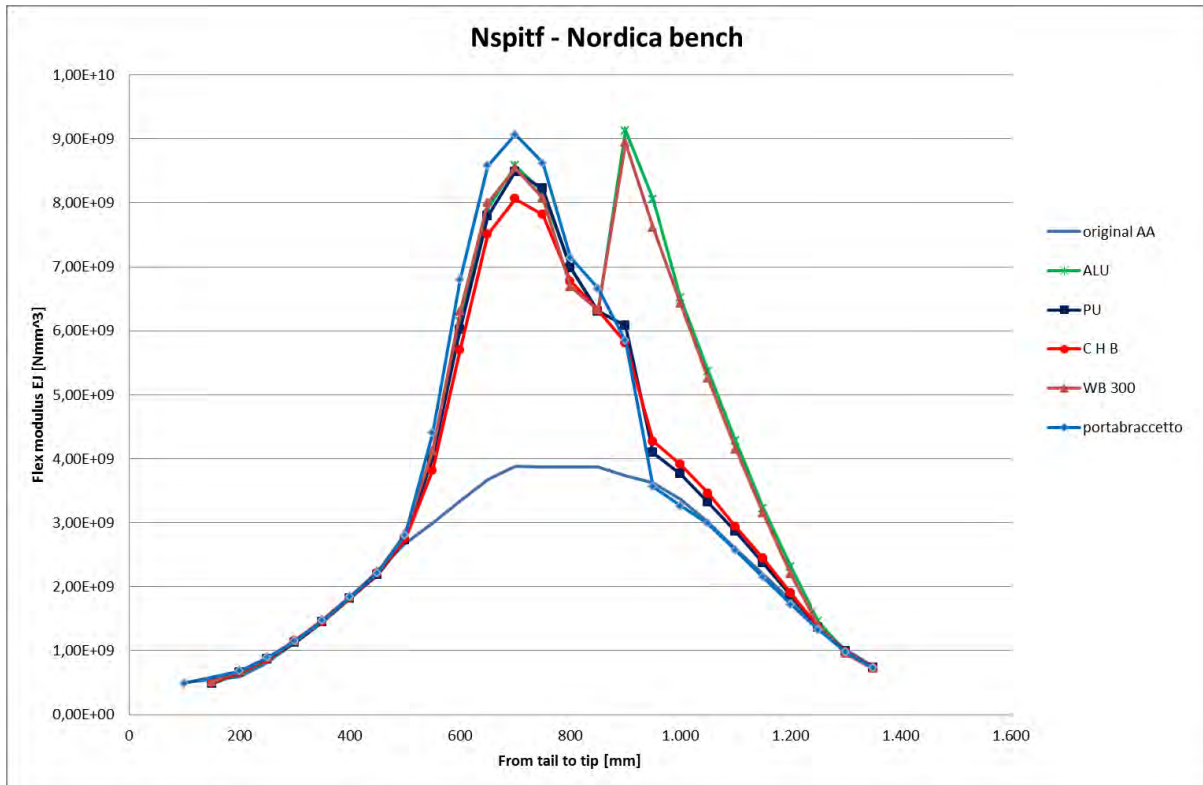


Figure 4.10 Chemnitz Load Distribution Profile at 0°



**Figure 4.11** Flex rigidity profile from Nordica Bench

Once more, in Nordica bench it can be noticed how much the aluminum support influences the ski rigidity parameter.

Also in this case, the curves maintained the same trend, showing particular influenced for the ALU and WOOD, and the smoother effect of PU and CHB.

#### 4.7 Comments

First of all, we focus the attention at the apparent incoherence between the rigidity values for the arm and the profile influence respectively.

In fact, the CHB tested in Padua and in Nordica reveals the lower stiffness, that should be correspond to the lower influence in ski load distribution and ski rigidity. But this is not verified: the CHB arm influenced the profile distribution more than the PU. Some representative graph are reported here to summarize.

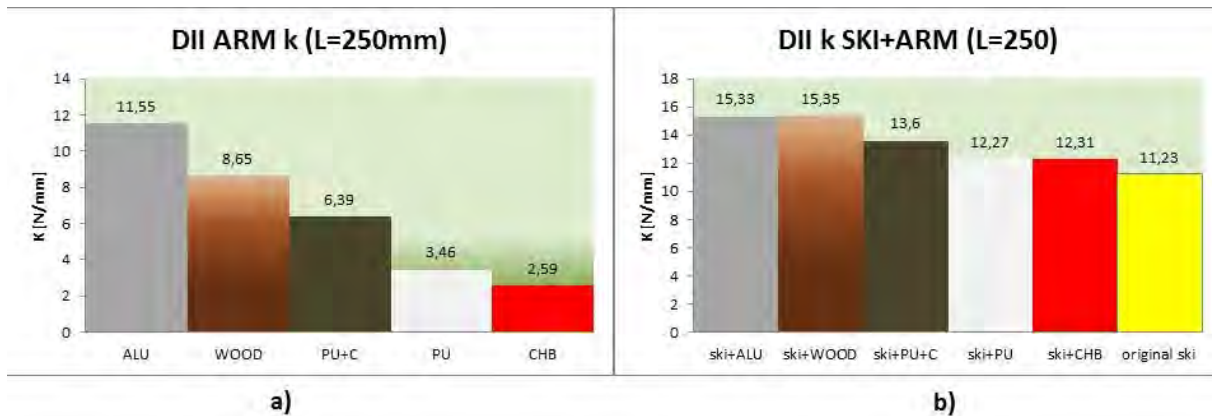


**Figure 4.12** Stiffness comparison: a) arms stiffness; b) ski + arms stiffness

As we can see from Figure 4.12, the CHB arm is less stiff than the PU arm, but it influences more the load profile and the total ski stiffness. This apparent inconsistency could be explained with the different geometry of the arms. Even though the PU is more rigid, it doesn't touch the ski when fixed on it. Some rubber insert are necessary to create the contact immediately. Instead, CHB touches immediately the ski when mounted on it, with an high preload, non-investigated yet.

The same considerations could be done with ALU and WOOD. Also in this case the WOOD, less stiff, influences more the load profiles.

Moreover, in the Appendix some graph that shows the rubber influence in ski load profile distribution are presented, for the ALU arm tested at Padua University.

## 4.8 Feedback from skiers

According to an ideal distribution of loads there should be no unloaded areas along the ski edge in a turn. The superstructure has this effect, but each ski has to be provided with a "specific" arm, engineered in order to modify the load distribution profile. Until now, there is not a sound evidence to support this hypothesis.

Aim of this work was to support the research with in-field test, in order to validate the influence of the elastic compensation structure. To obtain this response, an evaluation form was created and submitted to testers. By this method it's possible to understand if differences in the load profile can have influences on skiing performance, and more, which is the best method to characterize the ski experimentally, reproducing the curves that correspond to a better feeling during skiing.

The subjective evaluation form explanation is reported below. Summarizing, the numeric evaluation attributes 4 for a bad influence, 10 for an excellent influence. The form investigates five fundamental behaviors of the ski. The table below represents the form that skier have to fill in for each configuration.

## SKI – EVALUATION PARAMETERS

### 1 – EDGE SWITCHING QUICKNESS:

*evaluate the quickness in switching from one edge to the other.*

**10 – excellent:** the ski releases very easily the old edge and moves very quickly to the new one

**8 – good:** the ski releases easily the old edge and moves quickly to the new one

**6 – sufficient:** the ski releases hardly the old edge and moves slowly to the new one

**4 – poor:** the ski remains bond to the old edge and moves very slowly to the new one

### 2 – EDGE CATCHING QUICKNESS:

*evaluate the ski shovel readiness and intensity in catching the edge and initiating the turn.*

**10 – excellent:** very fast and intense grip at the beginning of the turn

**8 – good:** fast and good grip at the beginning of the turn

**6 – sufficient:** slow and moderate grip at the beginning of the turn

**4 – poor:** very slow and poor grip at the beginning of the turn.

### 3 – CARVING PRECISION :

*evaluate the precision of the ski in following the desired turning radius without skidding*

**10 – excellent:** very high precision – no skidding at all

**8 – good:** good precision – no evident skidding

**6 – sufficient:** sufficient precision – the skidding can be controlled

**4 – poor:** poor precision – the skidding is evident and can hardly be controlled

### 4 – REACTIVENESS AT THE END OF THE TURN:

*evaluate the capacity of the ski in “pushing” the athlete out of the turn*

**10 – excellent :** ski exits the turn with maximum “push”.

**8 – good:** ski exits the turn with good “push”.

**6 – sufficient:** ski exits the turn with enough “push”.

**4 – poor:** ski exits the turn with no “push”.

### 5 – VIBRATION DAMPING:

*evaluate the capacity of the ski in damping the vibrations during straight skiing or edge change*

**10 – excellent:** the ski does not present any perceivable vibration.

**8 – good:** the ski presents some perceivable vibrations.


**6 – sufficient:** the ski presents evident vibrations.

4 – **poor**: the ski presents high vibrations affecting his performances.

**TYPE OF SNOW**

- 1 – winter snow icy
- 2- winter snow transformed
- 3- winter snow humid
- 4- spring snow icy
- 5- spring snow slushy

**Table 4-3** *Subjected evaluation form*

DATE: _____		
Subject:	SURNAME _____ NAME _____	
	AGE _____ HEIGHT(m) _____ MASS (kg) _____	
	SKILL LEVEL _____	
	TYPE OF SNOW _____ hour: __ : __	

SKI TYPE OF TEST	<span style="color: red;">4 (poor)</span> <span style="color: red;">6 (sufficient)</span> <span style="color: red;">8 (good)</span> <span style="color: red;">10 (excellent)</span>							
	FREE				POLES			
	4	5	6	7	8	9	10	
1. EDGE SWITCHING QUICKNESS:								
2. EDGE CATCHING QUICKNESS:								
3. CARVING PRECISION								
4. REACTIVENESS AT THE END OF THE TURN								
5. VIBRATION DAMPING:								

The tested arms were covered with a neutral color, so the skiers were not able to distinguish it. With this system the different color, material and shape of the arm do not influence the skiers during the evaluation. A neutral identification it has been adopted, with alphabetic letters:

**Table 4-4** *Neutral arm classification*

Original ski	No arms
A	PU
B	WOOD
C	CHB
D	ALU

The test have involved three colleagues, good skiers but not professional tester, during two days spent in Hintertux glacier, Austria. The tests took place on the 8th and 9th of September.



The snow conditions changed a lot during the day, from 9 am to 13 pm; after the 13 o'clock it was not possible to ski anymore. The type of snow is evaluated as “spring snow slushy”.

### 4.8.1 Test procedure

The skiers tested all the configurations in sequence.

Skier A: he starts skiing at 9:45 and at 11 he had finished to test all the ski configuration. It was possible to perform only one run per ski configuration.

The test start with the original ski, and follows the sequence A B C D. This series permits to test ski that present significant different benches curves. In fact, as seen before, PU (A) and CHB (C) have a comparable effect, rather WOOD (B) and ALU (D) seems to produce the same influence. With this order the skier could have better felt the differences between the configurations. The same procedure is maintained for the skiers.

Skier B: he starts at 11 and stops at 13. Evaluated as the more significant skier, he repeats the test also the day after.

Skier C: she tests only the configuration original, A,B and C.

During the ski lift, after each run, an interview was taken that summarize the feeling with the ski tested. The interview results are explained in the results paragraph.

### 4.8.2 Form results

Once collected the data from the three skiers, an histogram with the mean and standard deviation of the evaluation for each filled space is created.

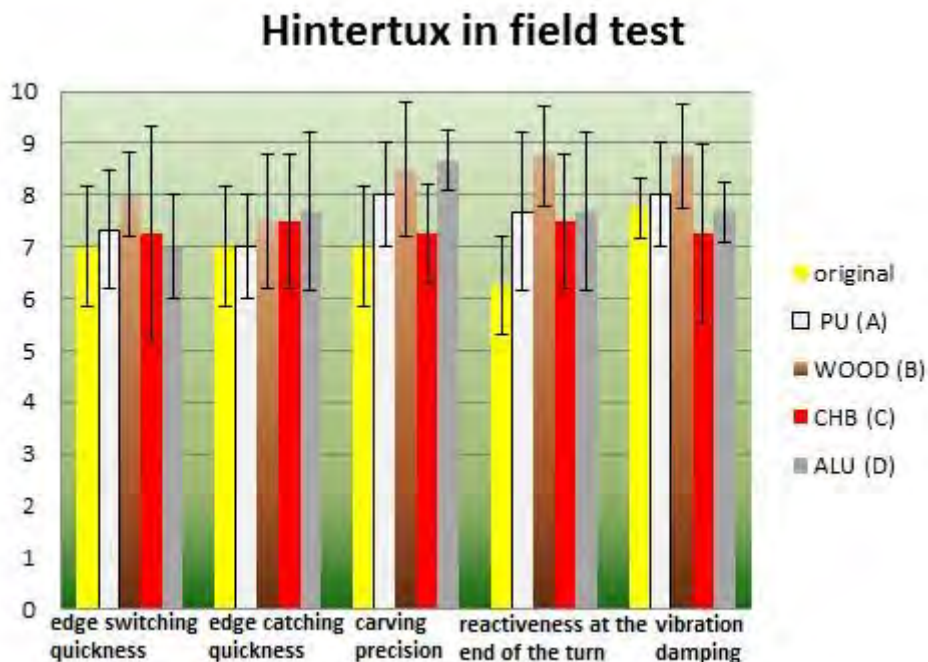


Figure 4.13 Results from in field test conducted in Hintertux

Even though the vibration damping column is complete, the weather and snow condition were not the best to explore this aspect.

On average the presence of the arm produces an higher score. But only arm B, wood arm, remains always one point upper that the original ski. All the others have less influence.

Generally the property improved is the “Reactiveness at the end of the turn” and the “Carving precision”. The switching quickness and edge catching quickness with the arms showed a lower effect: this could depend on the soft snow conditions, where the edge catching is not substantial.

### 4.8.3 Comments to the results

Despite the effort, until now, there are no sufficient tester to create a statistical database.

The tests were conducted during the summer, so the snow was evaluated as spring snow slushy. Overall, the feeling is positive.

Another in field test has been conducted in Stubai by five expert skiers, took place during the firsts weeks of July.

Only one form paper was filled, and is reported in the next histogram. Other verbal evaluation form were however in line with these results. During these tests the WOOD arm was not taken into consideration, so there are no comment about it.

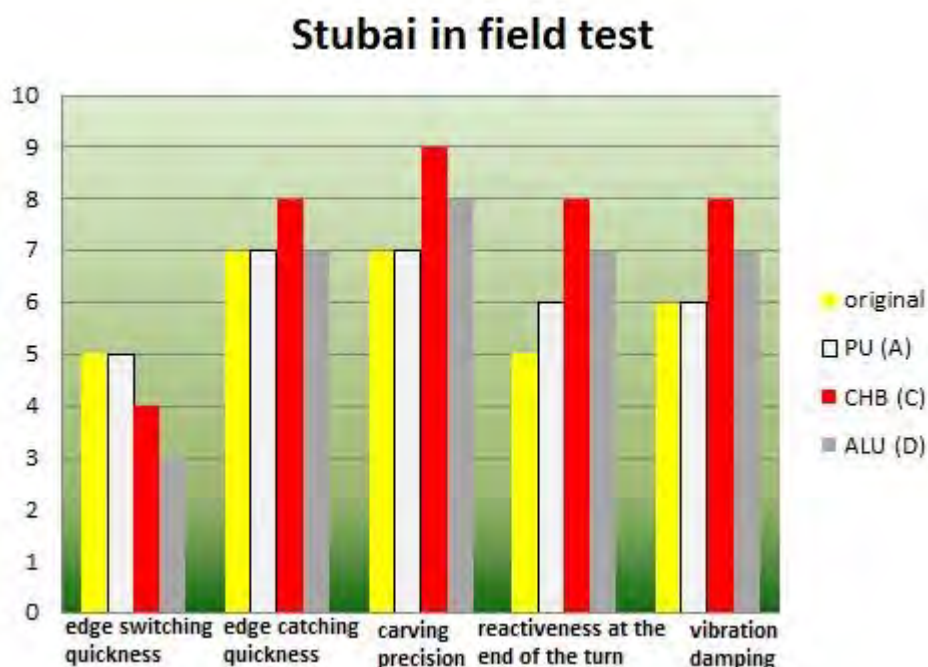


Figure 4.14 Stubay in field test results

Verbally the best quality feels is the carving precision, that is the ability of the ski to follow the desired turning radius without skidding, with no evident skidding. The best results were obtained by C H B arm, that is also esthetically the coolest one. Other properties that makes



this arm better than the other are the edge catching quickness, reactivity at the end of the turn and vibration damping. Summarizing, C H B have a fast catching edge and a good grip at the beginning of the turn, good precision following the desired turning radius, a good reactivity at the end of the turn, that push the athlete out of the turn efficiently and a good vibration damping.

The negative note for C H B and more ALU, is the edge switching quickness. The ski with the superstructure, generally remains bond to the old edge and moves very slowly to the new one. This fact could be explained with the additive mass introduced by the aluminum support, the race plated adopted and the weight of the arm.

The worst arm is ALU, called too stiff for the Dobermann Spitfire.

#### **4.8.4 Other comments**

Each skiers has a different feeling skiing, and can express it with different words. So, it's really difficult to catch what the skier feels and tries to explain. More tests and data analysis are necessary to evaluate the results statistically. This involves an expensive investment: includes more pair of the same ski, provided with the aluminum supports and duplicates arms with the same characteristic. Moreover, the tests have to be conducted during the winter season with perfect and known snow conditions.

Nevertheless, the testers expressed positive comments especially for the stability during a carved turn. It seems like that not only the central zone under the bindings react with the snow, but all the ski do it. It's like a "longer ski" under the boot.

The negative note are: total weight of the ski, reactivity. The ski tested mounted a race binding, and the weight introduced with the aluminum support, arm, and fixation system, are translate with a ski that is more difficult to move.



# 5. Foam: a new device for ski load distribution acquisition

## 5.1 Introduction

The principal purpose of this part of the work is to test some foam materials that could simulate the snow's behaviour in a skiing slope, in order to obtain the edge pressure distribution of an alpine ski in realistic conditions.

To obtain the Force applied over the penetration displacement curves comparable with the snow curves provided by Federolf's experiments [*Finite element simulation of a carving snow ski*. Peter Andreas Federolf, 2005], each material was subjected to a crushing test, at different angles and with a prefixed penetration depth (15 mm), using the central part of a ski (100x65 mm), opportunely fixed to the piston of the test machine. After the characterization, the foams that better simulated the three types of snow, hard, average and soft, were placed in contact with the surface of the Edge Pressure Bench and the "footprint" of the ski was acquired by laser scanning.

Usually in literature the snow characterization is powered by the interest to simulate numerically the ski-snow interaction. Here, the attention is focus on the experimental evaluation of the edge pressure distribution along an alpine ski. This permits to substitute, or better, integrate the previous system used, the Slytech bench.

## 5.2 Materials and methods

The snow properties that were taken into account came from the Federolf's experiments, that provides the representative Force-displacement curves for different kind of snow.

Using these curves, we tried to find a foam that could simulate the snow behavior, following the same trend. The foam panel finally selected for the scope is a polyurethane expanded foam used in thermal and acoustic insulations.

In what follows a general introduction to snow mechanical properties, and to the machines that were used to characterize the foam behavior is reported.

### 5.2.1 General mechanical properties of snow

The snow does not only support the skier. All the forces which enable the skier to turn, originate at the ski-snow interface.

Snow is one of the most multifaceted materials known. It consists predominantly of ice and air, but also contains liquid water and water vapour. It constantly undergoes a metamorphism process. The mechanical properties of snow change over a very large scale.

The development of carving as a new technique of skiing has changed the physical processes involved in the ski-snow interaction. In the conventional skiing technique the turning forces are mainly generated by skidding over the snow's surface. The shape and bending properties of carving skis, however, are adjusted to typical turn radii. Thus skidding becomes obsolete. The ski still penetrates the snow's surface due to the mechanical load of the skier, but to generate the turning forces of ideally carved turns no additional skidding is necessary.

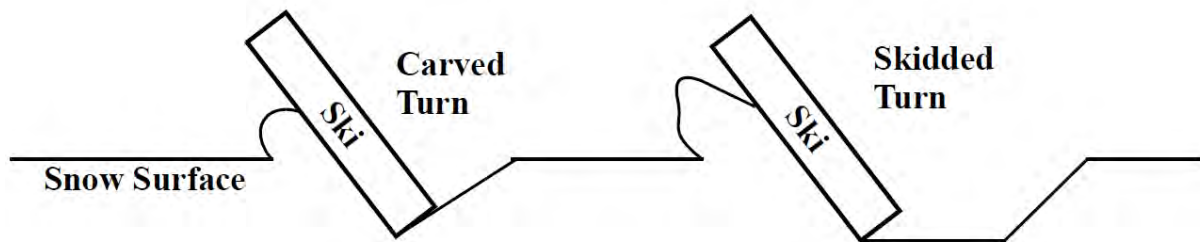


Figure 5.1 Different types of ski-snow interaction in carved and skidding turns

The carving technique is characterized by minimized skidding during a turn. The ski merely cuts into the snow surface to a depth which allows the snow to support the load of the ski.

The more suitable parameters that have to be considered when investigating the ski-snow interaction are:

- the snow mean resistance pressure to the penetrating object;
- the penetration depth;
- the penetration speed.

The mean resistance pressure of snow on a penetrating plate or piston, however, has been studied in a number of laboratory experiments. The most comprehensive study was published 1979 by Fukue, in *Mechanical Performance of Snow Under Loading*. He concluded that during the deformation different processes occur depending on the penetration speed. At 0.097 mm/s ductile compression of the snow under the penetrating plate was observed. For a penetration speed of 0.98 mm/s the snow is deformed in brittle compression, in which a bulb of compressed snow forms under the plate.

During Federolf's experiments in order to characterize the ski-snow interaction, two new test devices were built. The first device, called "Agervis", deforms the snow at a constant rate. The second device, called "Fast Snowdeformer", was designed to measure impact of the penetration speed on the mean resistance pressure to a penetrating piston.

He found that resistance force versus the penetration distance changes while changing the angle of the measurements. The angle at which changes happened was found to be 40°. When a ski passes over a snow surface the snow is first loaded and thus penetrated, but after the pressure maxima under the ski binding has passed, the snow is unloaded. If elastic energy has been stored in the snow it is then released as snow expands under the withdrawing plate. In this case the contact pressure does not drop instantly to zero, but decreases measurably. With the device Agenvis the snow pressure is also recorded as the penetrating plate is being withdrawn. Figure 5.2 shows such an example of an Agenvis measurement in a ski resort.

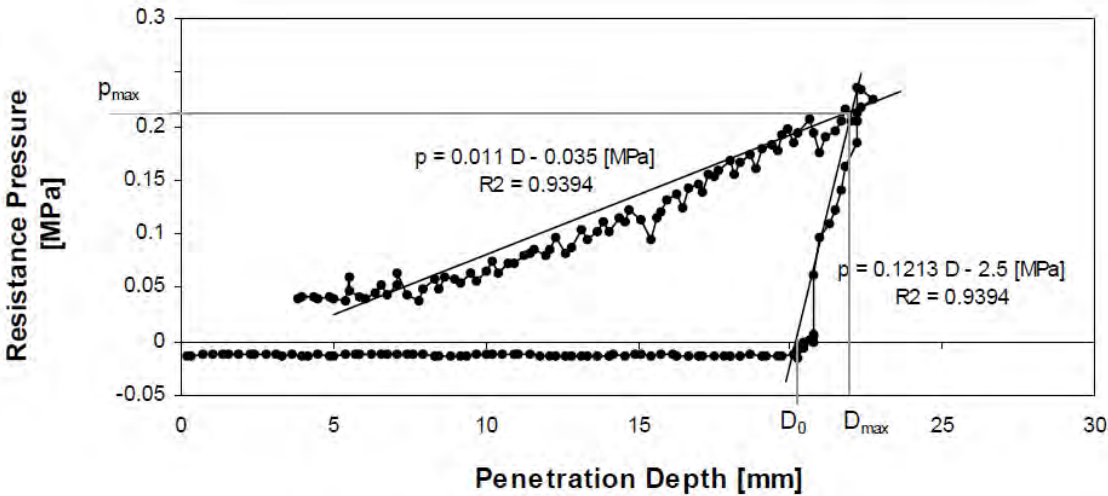


**Figure 5.2** Measurement of the mean pressure on the penetrating plate during penetration and withdraw. edging angle of 30°

In penetration tests with a plate which is inclined less than 40° the mean snow resistance pressure increases linearly in a good approximation. In penetration tests using edging angles above 40° the snow resistance initially increases rapidly, but is frequently reduced by pronounced fractures. The fracture events seem to be inexplicable and to occur randomly. The observed shear fractures occur at random during the penetration. Hence it is impossible to predict the exact mean pressure acting on the penetrating device for large edging angles. However, the general trend of the mean snow resistance pressure in the presence of shear fracture mechanisms can in many cases still be approximated by a linear regression, although the deviations from the regression line are generally much higher and in some measurements a linear trend is not visible at all. In Figure 5.3 are shown the mean resistant pressures as a function of penetration depth, acquired during in field test developed by Federolf.

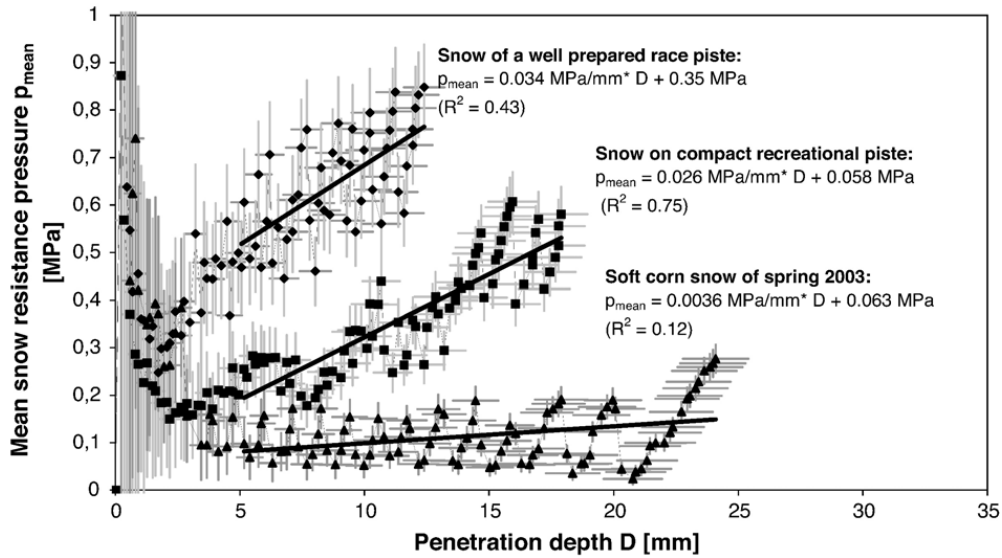


Figure 5.3 Mean resistance pressure as function of penetration depth for three different type of snow

In the Figure 5.4  $D$  denotes the penetration depth of the trace on the snow,  $d$  the penetration distance,  $b$  the width of the plate and  $\theta$  the edging angle.

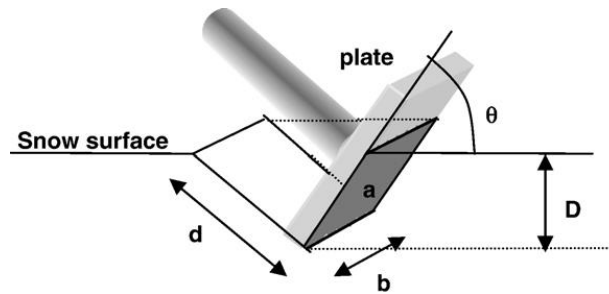


Figure 5.4 Schematic of the plate penetrating the snow.

The mean resistance pressure  $p_{snow}$  increases to a good approximation linearly with the penetration depth  $D$ :

$$p_{snow}^{mean} = AD + B$$

Typical values of the parameters  $A$  and  $B$  used to describe the mean snow resistance strength for typical conditions on the investigated ski pistes are summarized in Table 5-1. These values were obtained by classifying all of the tested groomed ski pistes into the three categories, soft snow, average snow and hard/icy snow and averaging over all measurement results.

**Table 5-1** Coefficients *A* and *B* found by Federolf that describe the snow behavior under load in the three different conditions.

	Coefficient A for edging angles $\leq 40^\circ$ [MPa/mm]	Coefficient A for edging angles $> 40^\circ$ [MPa/mm]	Coefficient B [MPa/mm]
<b>Soft snow</b>	0.005	0.002	0
<b>Average snow</b>	0.025	0.015	0.2
<b>Hard snow</b>	0.04	0.02	0.4

In his work, Federolf plotted the results in diagrams reporting the resistance pressure  $p$  in function of the effective penetration depth  $D$ , thus the following operations are necessary to convert the data obtained from MiniBionix machine

$$D = d \cos \theta$$

$$A_{contact} = bl = \frac{bD}{\sin \theta} = bd \cot \theta$$

$$p = \frac{F}{A_{contact}} = \frac{F}{bd \cot \theta}$$

Moreover, as in the works of L.M. Goldin and B. Zaffaina, the experimental data and the results obtained by Federolf were compared in a force-piston displacement graph, but the formulas found by Federolf were related to the penetration depth  $D$  and to the pressure  $p$ . Thus, to plot the snow curves, was necessary to convert the expression:

$$P = AD + B$$

to the following:

$$P = Ad \cos \theta + B$$

where  $A$  and  $B$  are constants of the fit line which are dependent from two variables (edging angle and type of snow) Table 5-1,  $d$  is the piston displacement and  $b$  is the length of the ski segment.

### 5.2.2 MTS 858 Mini Bionix

The *MTS 858 Mini Bionix II* machine of the Department of Industrial Engineering of University of Padua has been used to test the foams (Chapter 2.1).

The instrumentation used to test the foams consists of (see Figure 5.5):

- a support plate, attached to the lower jaw



- a tilt support, fixed to the support plate by some screw to allow a front/rear translation and a slight rotation around the jaw vertical axis
- a ski segment, fastened to the upper jaw with a hinge to allow self-alignment.

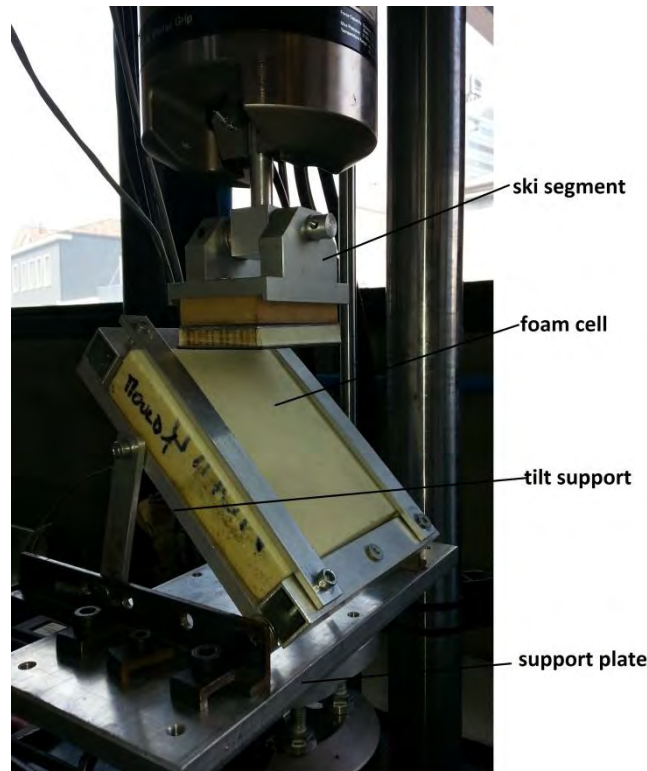


**Figure 5.5** *Minibionix devices*

With this system is possible to test the foams at different displacement speeds and different contact angles.

### **5.2.3** *Slytech edge load profile bench*

Slytech Bench is the same used for the previous characterization, the description is on Chapter 2.5 the outputs are the comparison necessary to validate the new method. Hence, a panel foam was fixed to the Slytech Bench over the cells used for load acquisition. Therefore, in the same time , it is possible to perform a normal test and to imprint the foam.

The panel foam is fixed and cut in correspondence of the interspace between the bench cells, to form a kind of “keyboard”. So each piece of foam is loaded and can transfer the load to cell below. Has to be taken in account that the bench cell register only the vertical component, so some additive data analysis are needed.

The foam “keyboard” is clamped to an aluminum C-profile and fixed to the bench, as shown in Figure 5.6, so it is possible to manage the foam for acquisitions



**Figure 5.6** *Imprinted foam keyboard fixed to Slytech bench*

During the test, as usually, the ski is loaded and pressed against the cells. In this case not all the possible degrees are tested, but only at 40° 50° 60°, due to the hardness of the foam and some space issues.

The laser acquisition are conducted with *Faro ScanArm V3* and *SmartScope ogp Flash CNC 300*.

#### **5.2.4 Faro ScanArm V3**

FaroArm is a portable coordinate measuring machine (CMM) that allows easy verification of product quality by performing 3D inspections, tool certifications, point cloud-to-CAD comparison, dimensional analysis, reverse engineering, and more. It is a seven axis measurement system with a FARO ScanArm V3 probe (with six degrees of freedom) connected at the end of the arm. It allows the measurement of single points with the hard probe and the scan of larger sections requiring larger volumes of data with the laser.



**Figure 5.7** *Faro ScanArm*

To ensure the maximum accuracy, in each joint are located temperature and overload sensors, which allow the arm to react to thermal variations and improper handling.

The laser scan guarantees an accuracy of  $\pm 35\mu\text{m}$  with a scan rate up to 19200 point per second.

The strength of Faro ScanArm for the scope is the portability, it can be transfer in loco of developed tests and with one acquisition all the length of the panel is scanned.

### **5.2.5 SmartScope ogp Flash CNC 300**

SmartScope® Flash™ CNC 300 is a large capacity video measuring system for dimensional verification of manufactured parts. It can be configured as a cost-effective multisensory system with optional through-the-lens (TTL) laser, touch probe, or micro-probe.

Three imprinted foam cells are scanned per time, not all the panel, for dimensional limitations.



**Figure 5.8** *SmartScope ogp Flash CNC 300*

Manual movements are performed to scan only the imprinted zone, and data analysis is more easy to conduce. Positive points of this system are: - the possibility to scan automatically single pre-set lines corresponding to the desired section and – a easier data analysis.

Both the imprints scanned with two different acquisition methods are meshed and then imported in Rhinoceros for the analysis.

### **5.3 Foam characterization**

The first tests performed were compressions at constant speed and under displacement control on the foams. The procedure used is as follows:

- Fixing the plate to the lower jaw and the ski segment to the upper one
- Mounting the specimen on the inclinable support
- Lowering the actuator up to a distance from the specimen of about 5 mm
- Zeroing the load cell signal
- Test execution, comprises of the following step:
  - Descent of the actuator until the achievement of the displacement imposed, with a speed of 30 mm/s, equal to the speed chosen by Federolf's. It has not been chosen a different speed because Federolf proved that the snow has not a viscoelastic behaviour.
  - Actuator's stationing in the reached position for 2 s.
  - Return of the actuator to the initial position at a lower speed respect the descent one.

The frequency of data acquisition was set to 100 Hz.

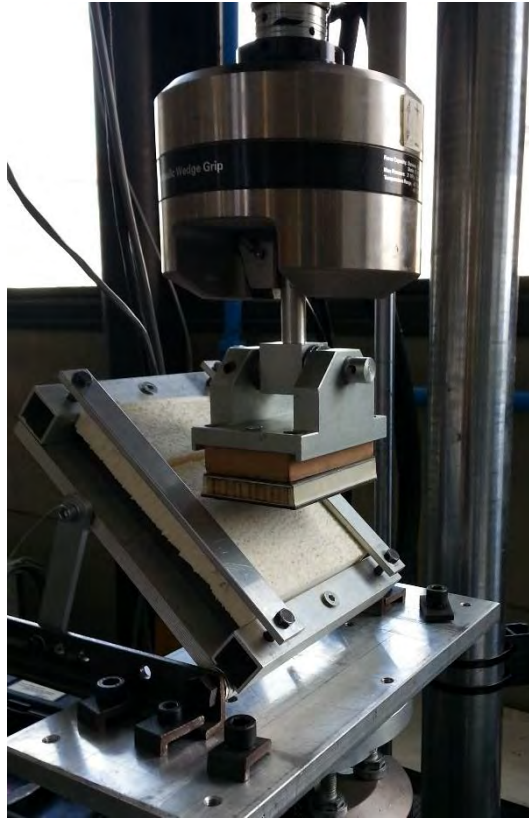


**Figure 5.9** Foam test characterization with Minibionix

### 5.3.1 Data analysis

As in previous works, a ground noise problem of the load cell has been observed. This is irrelevant since the measured quantity is about two or three orders of magnitude bigger respect the noise, but it is not eliminable by filtering because it is a white noise, Gaussian, uncorrelated, whit zero mean and also its spectrum covers all frequencies. After resetting the load cell signal the force recorded was not zero, but had peaks over  $\pm 2$  N, so it was decided to put a minimum threshold to the recorded force values.

Data acquired from the tests are the force  $F$  measured by the load cell and the piston displacement  $d$ , both acquired at the same frequency (100 Hz). *MiniBionix* machine saves them in files consisting of three column vectors reporting time, displacement and force data.

Data processing has required the following steps:

- Straightening of the force-displacement values because the machine give out negative values in a compression test
- Consider data over 3 N because of background noise is not eliminable
- Making a graph of recorded force  $F$  against penetration depth  $d$
- Elastic return (springback) calculation with the following procedure, Figure 5.10
  - Calculation of minimum force at which is considered finished the elastic return, during the return of the piston to the initial position:

$$F_{(springback\ end)} = 5\%F_{max}$$

- Research of the spring back end position corresponding to a registered force minor or equal to the spring back one
  - $F_{\text{(springback end)}} \rightarrow d_{\text{(springback end)}}$
- Calculation of the percentage spring back:

$$r_{\%} = \left( \frac{d_{\text{max}} - d_{\text{springback end}}}{d_{\text{max}}} \right) \cdot 100$$

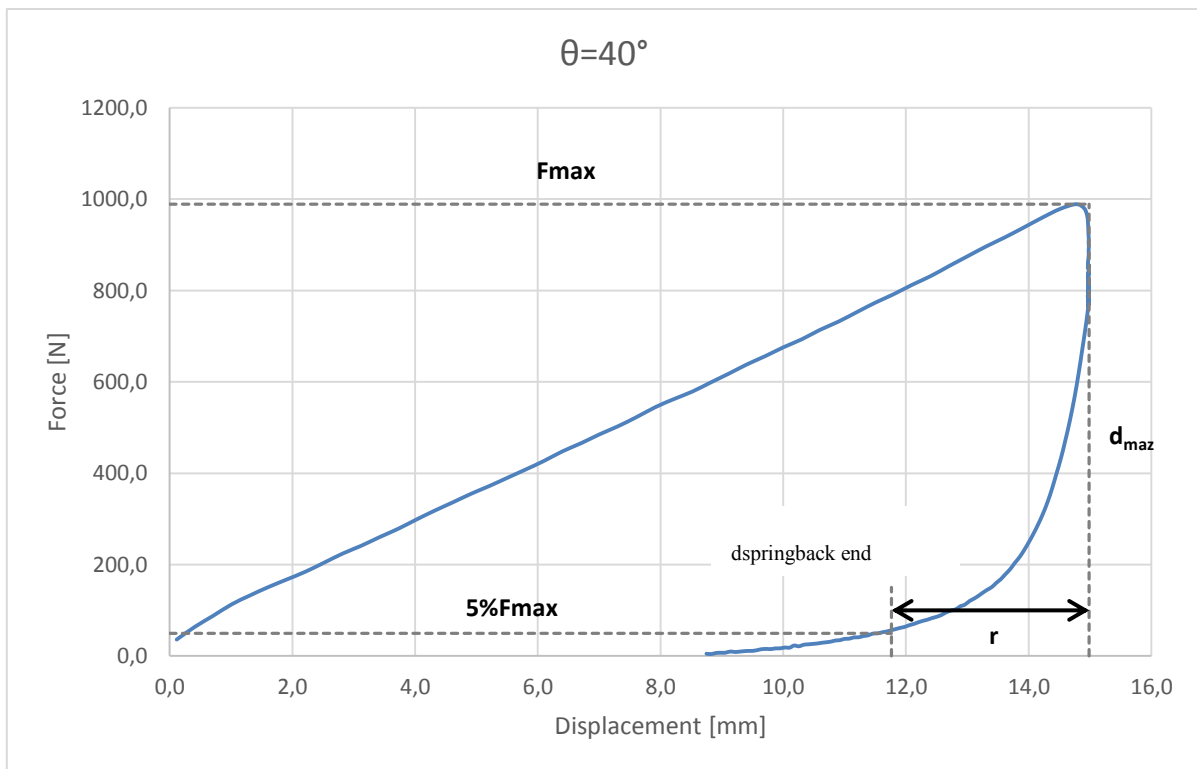


**Figure 5.10** Force versus displacement output for a foam tested at 40°

The curves are compared with the snow's curves obtained by Federolf in order to understand which material better simulated one of the three types of snow: soft (just fall), average ("tourism" snow) and hard snow (race snow).

## 5.4 Test and laser acquisition

### 5.4.1 Execution of the test

The keyboard foam panel is fixed over the Slytech bench so, more than one test can be developed without moving or modifying the position. Five tests has been done: one at 40°, two at 50° and two at 60°. When the ski is loaded and deformed the bending shape do not goes out of cell width, so it could be assume that all the load is transferred from the ski-foam

interaction to the load cell below. Therefore, in the same time, it is possible to perform a normal test and to imprint the foam. In results chapter these two output are compared.

At the end of the five tests the imprints are scanned to reveal how depth the imprints are, so how much force has been applied to obtain it.

First the Faro ScanArm acquisition has been done directly in laboratory, without moving the panel foam. Later on also with SmartScope Flash CNC300, but testing only three cells chosen as the most representative and interesting to study. The ski used for the test is a Blizzard SCS 170, with an elastic superstructure mounted, done by wood, designed by professor V. Quaggiotti. So, the cells studied were extracted under the front part of the ski, where the effect of the arm is more relevant.



**Figure 5.11** *Ski characterization with Slytech bench and innovative approach of foam snow mimic*

Once imprinted the foam panel the laser acquisition can start.

#### **5.4.2 Faro ScanArm laser acquisition**

With foam keyboard still fixed to Slytech bench, the Faro ScanArm has been positioned in front of the bench. One acquisition has been sufficient to scan all the surface of the imprinted foam. But in order to have lighter files, cell by cell is acquired.





**Figure 5.12** *Laser scan with Faro ScanArm*

The acquisition is one cell at a time so, in order to import the scan in a CAD software by maintaining the spatial position of each cell, the ScanArm has been placed on the floor by a tripod and has been paid attention not to move it during all the acquisitions.

### 5.4.3 *Faro ScanArm data analysis*

The Slytech Bench gives in output a text file with the number of the cells and the load registered by each. The values obtained are normalized to the ski length and then are plotted in a graph (one for each inclination) reporting the load values registered by the load cells in function of the ski length. These curves are compared with the curves of the same ski obtained previously without the interposition of any type of foam.

Instead, the point cloud scanned by the laser are meshed and then imported in Rhinoceros in STL format, Figure 5.13. By this software were generated sections spaced of 35.333 mm in such a way that the center of each cell is sectioned.

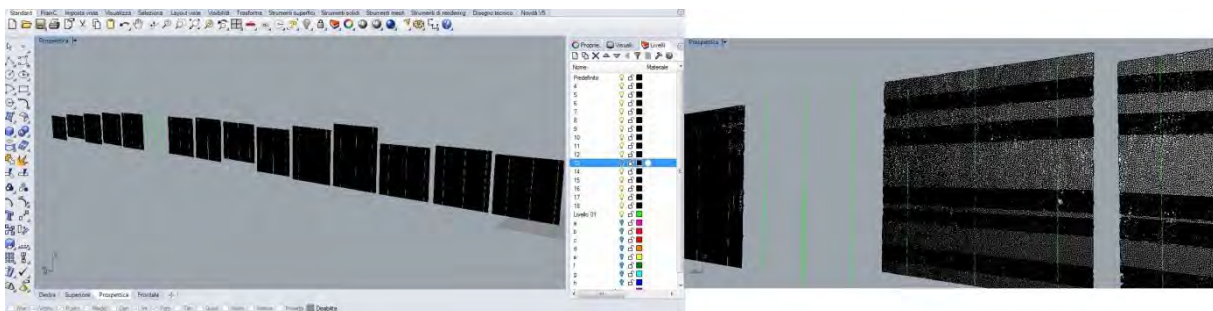


**Figure 5.13** *Rhinoceros screenshot of entire mesh foam panel and a detail.*

For each section the depth of each groove is acquired. In order to calculate the ski penetration depth  $d$  in the direction of the actuator axis, the groove's depths are divided by the cosine of the angle at which the test was executed. The obtained values were finally added with the spring back percentage.

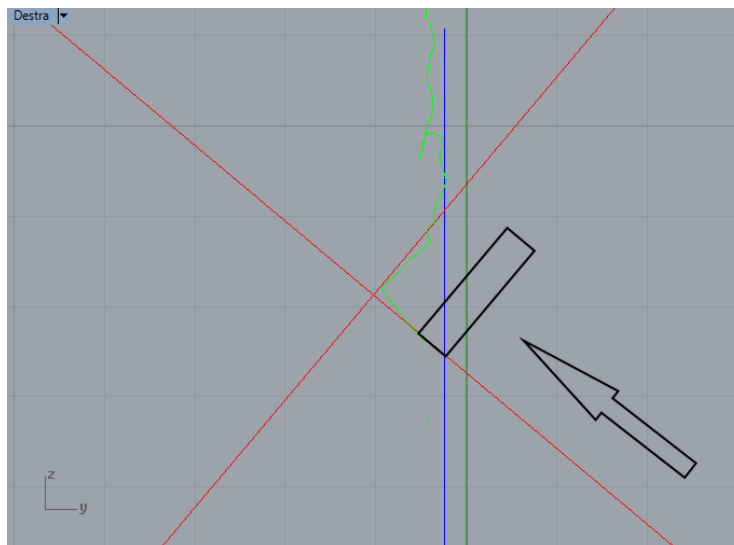


**Figure 5.14** Example of data analysis, imprint at 40°. In red the inclined guided line, in light green the imprint mesh

Once in possession of the values of the ski penetration depth, thanks to the results of the foam's characterization, it has been possible to obtain the value of the force at each point. Unfortunately, from the foam characterization the firsts millimeter must be estimated. It has been chosen a three polynomial approximation.

#### **5.4.4 SmartScope Flash CNC300 acquisition**

The analysis with SmartScope flash involved only three foam cells because of the geometric limitation of the machine. The cells extracted are the number 11, 12 and 13, that correspond at the same numbering of the cell's bench. These are extracted from the keyboard and analyzed in the laboratory. The scan time required is less compared to the previous work, and the file that come from is a collection of coordinates points, more easy to manage.

#### **5.4.5 SmartScope Flach CNC300 data analysis**

The .txt file that comes from the acquisition is imported in Rhinoceros as well and, some guided line are created that follows the angles of the ski. Knowing from which side the ski comes and, at which angle, the lines are drawn, Figure 5.15. Thanks to these, using the distance calculation tool of Rhinoceros, the penetration depth is found.

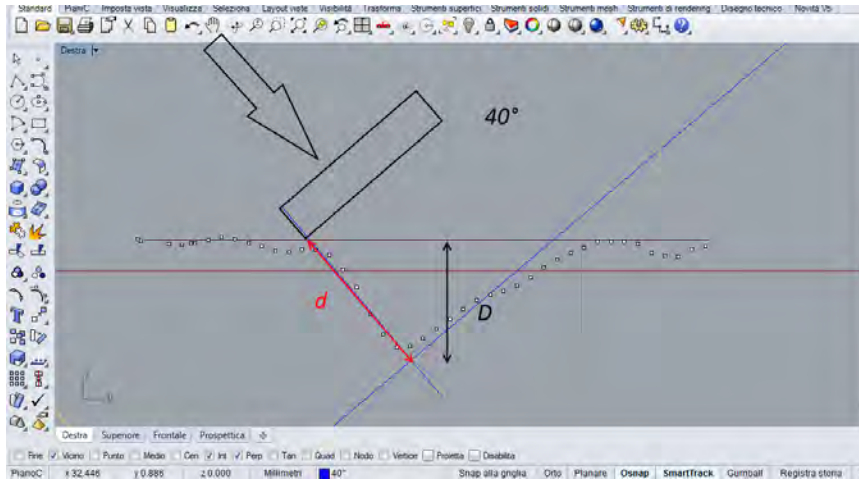


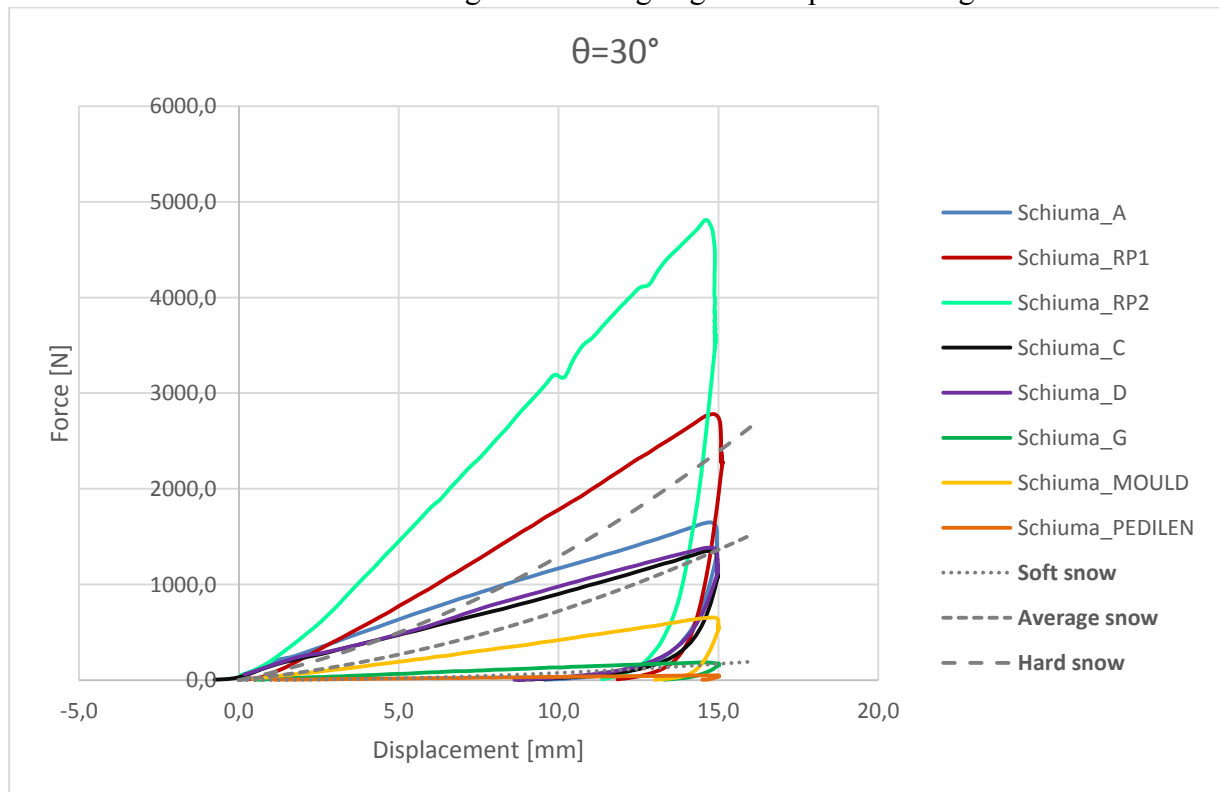
**Figure 5.15** Penetration depth calculation in Rhinoceros.

As before, once found the values of the ski penetration depth, thanks to the results of the foam's characterization, it is possible to obtain the value of the force in each point. Three values for each foam cell are collected, and the mean of these is compared with the value that comes out from the load cell of the bench.

## 5.5 Results

### 5.5.1 Foam characterization results

The F-d curves obtained after testing at increasing angle are reported in Figure 5.16.



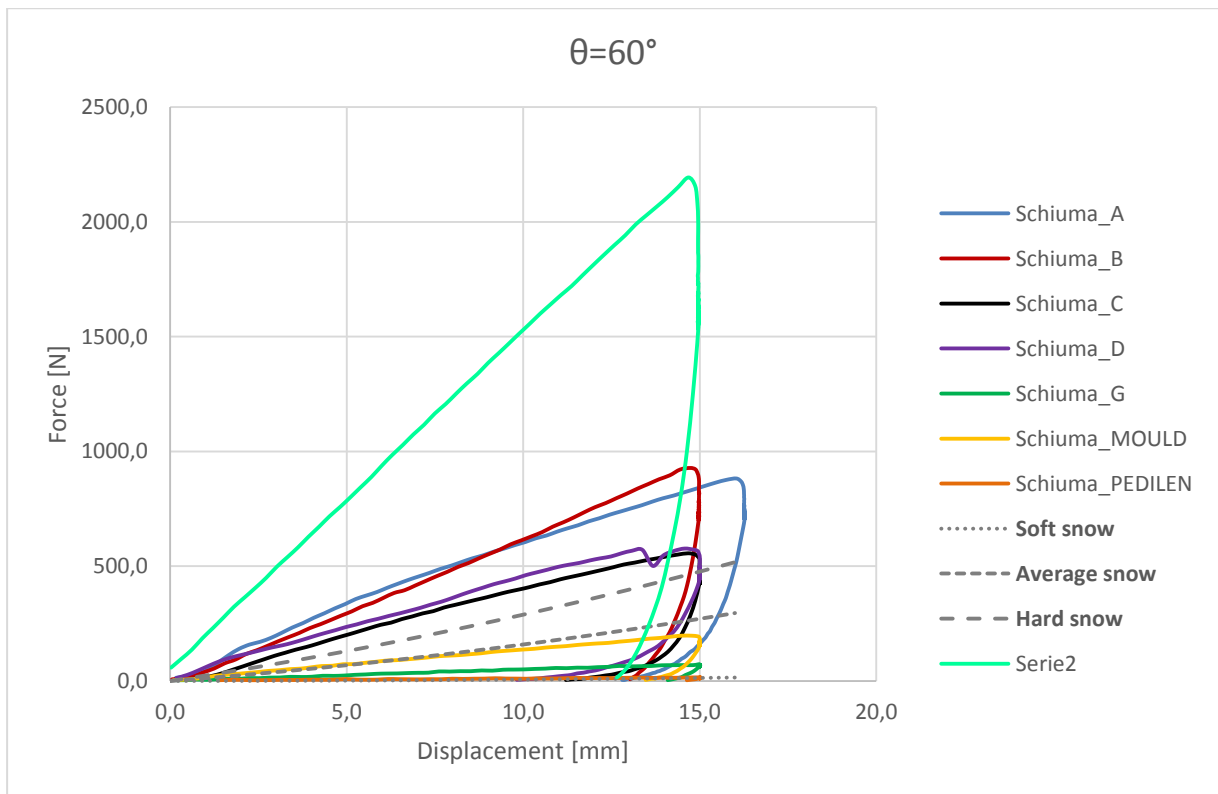
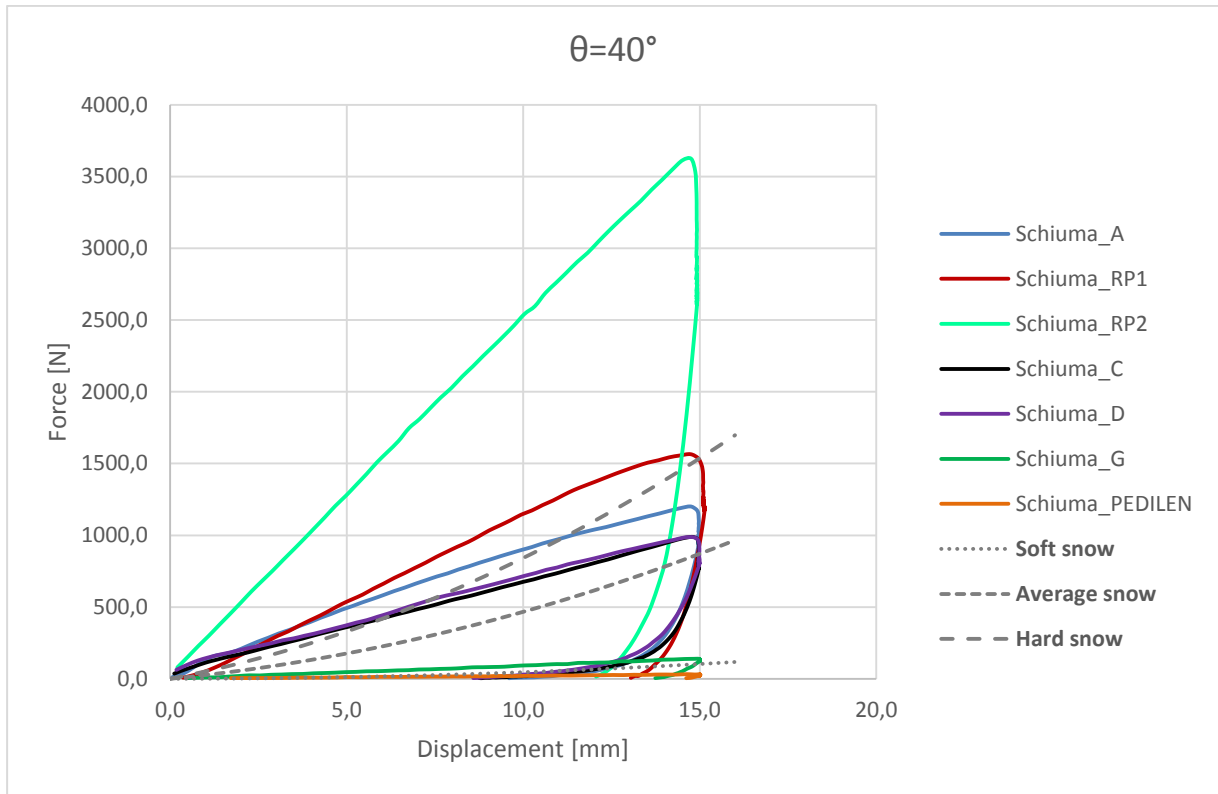


**Figure 5.16** Force over displacement at 30°, 40° and 60° for different foam

As Goldin observed in his work, it is evident that the F-d curves have a linear trend in the compression phase, in contrast to the snow curves.

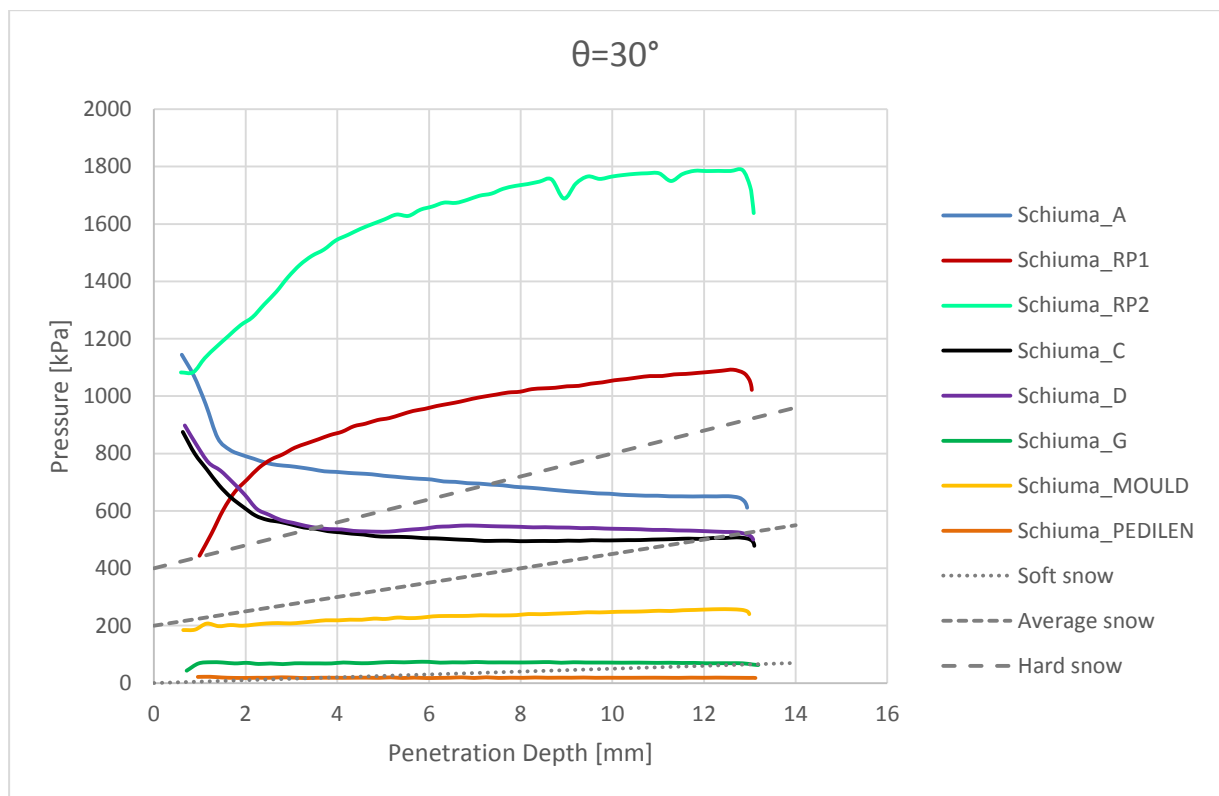
However, there are two aspects to note:

- The snow curves have a nearly linear trend that can be considered piecewise linear
- From tests on the Slytech Edge Pressure Bench is known that the maximum force acting on the edge profile of a section of ski of the same length of the actuator is less than 300 N, so, limiting to the first 300 N, the trend of the snow curves can be assumed linear with good approximation.

Therefore, the behavior of Federolf's empirical formulas in the F-d graph can be considered linear.

From the graphs comparisons it can be observed that the maximum forces are decreasing with the angle of incidence increasing. This fact is due to the internal phenomena of the material in each test typology: at lower angles the crushing effect is more predominant, while with the increasing of the angle, the crushing effect is gradually substituted by a shear effect.

Another comparison represents the resistance pressure as a function of penetration depth  $D$ .



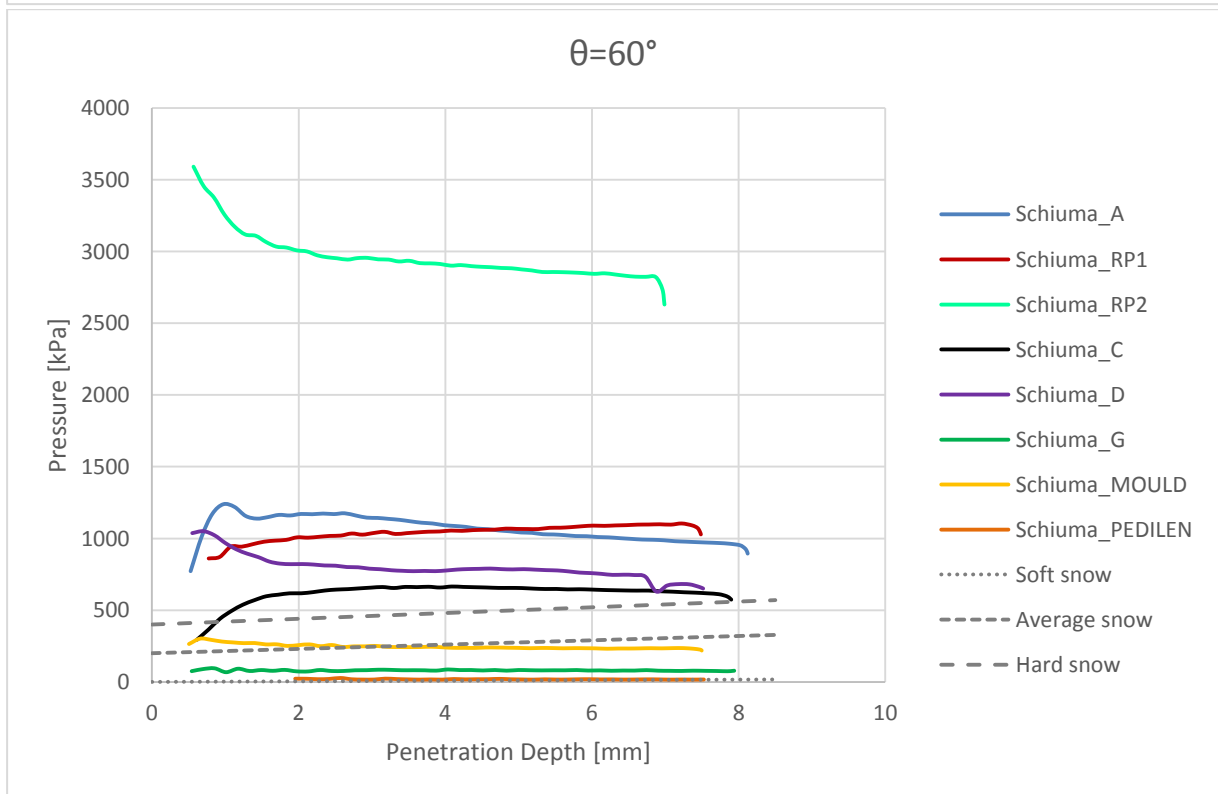
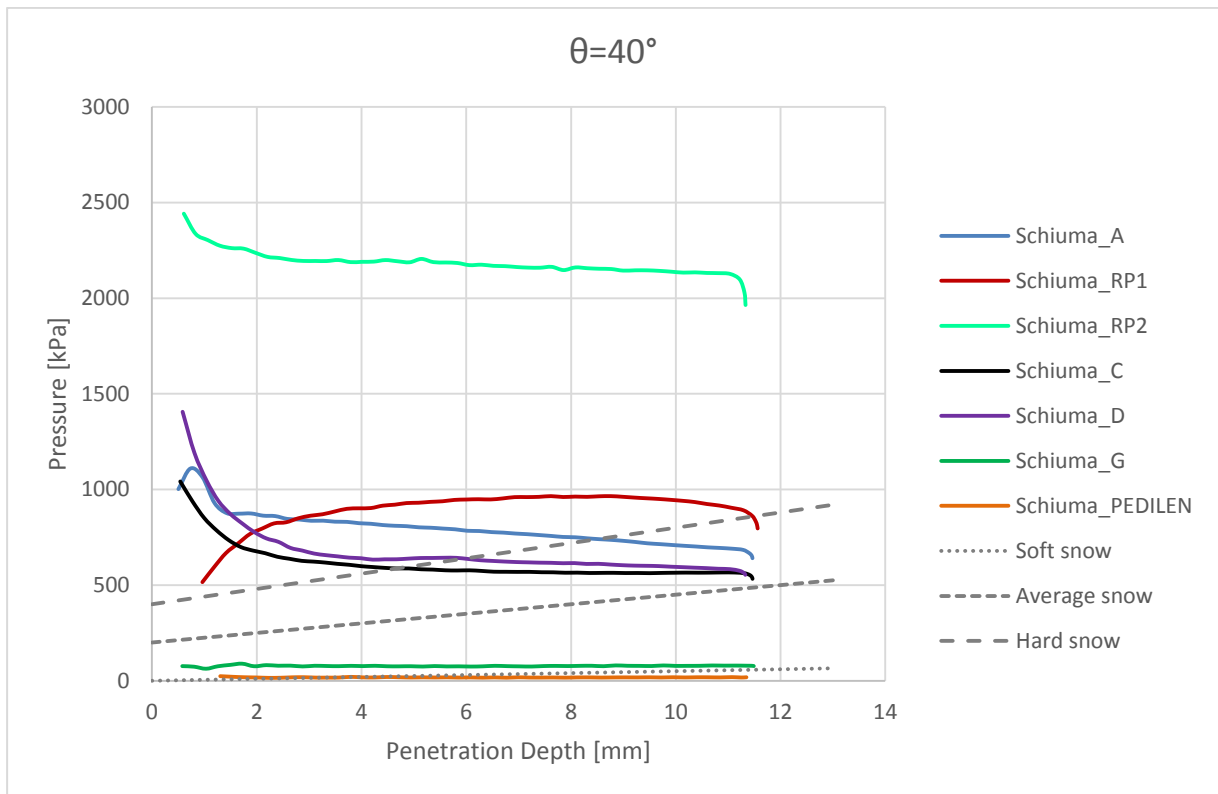


**Figure 5.17** Resistent pressure as a function of penetration depth at 30°, 40°, and 60°

For all material at each angle has been calculated also the percentage springback r

**Table 5-2** *Springback percentage*

Materiale	r%				
	20°	30°	40°	45°	60°
Schiuma_A		20,2%	18,8%		14,9%
Schiuma_RP1	10,7%	11,9%	10,2%	12,7%	10,7%
Schiuma_RP2	16,4%	14,4%	13,4%		11,8%
Schiuma_C	21,5%	22,3%	23,0%	21,8%	16,7%
Schiuma_D	22,2%	24,8%	26,6%		24,3%
Schiuma_G	7,0%	9,7%	7,8%		6,1%
Schiuma_MOULD	9,1%	7,4%		9,0%	9,1%
Schiuma_PEDILEN	5,7%	3,4%	2,7%		2,6%

Since the final target of this work was to test a ski on the Edge Load Profile Bench with the interposition of a foam panel and to acquire the footprint with a laser scan, material like Schiuma\_A, Schiuma\_C and Schiuma\_D, which have high springback, were immediately ignored.

From the graphs, it is also evident that the foam Schiuma\_RP2 is too hard to simulate any type of snow and has an average springback, so it was excluded.

The Schiuma\_MOULD foam is good to simulate the average snow because the two curves are close at each angle and has a very low springback as well as Schiuma\_G and Schiuma\_PEDILEN could simulate the behaviour of the soft snow.

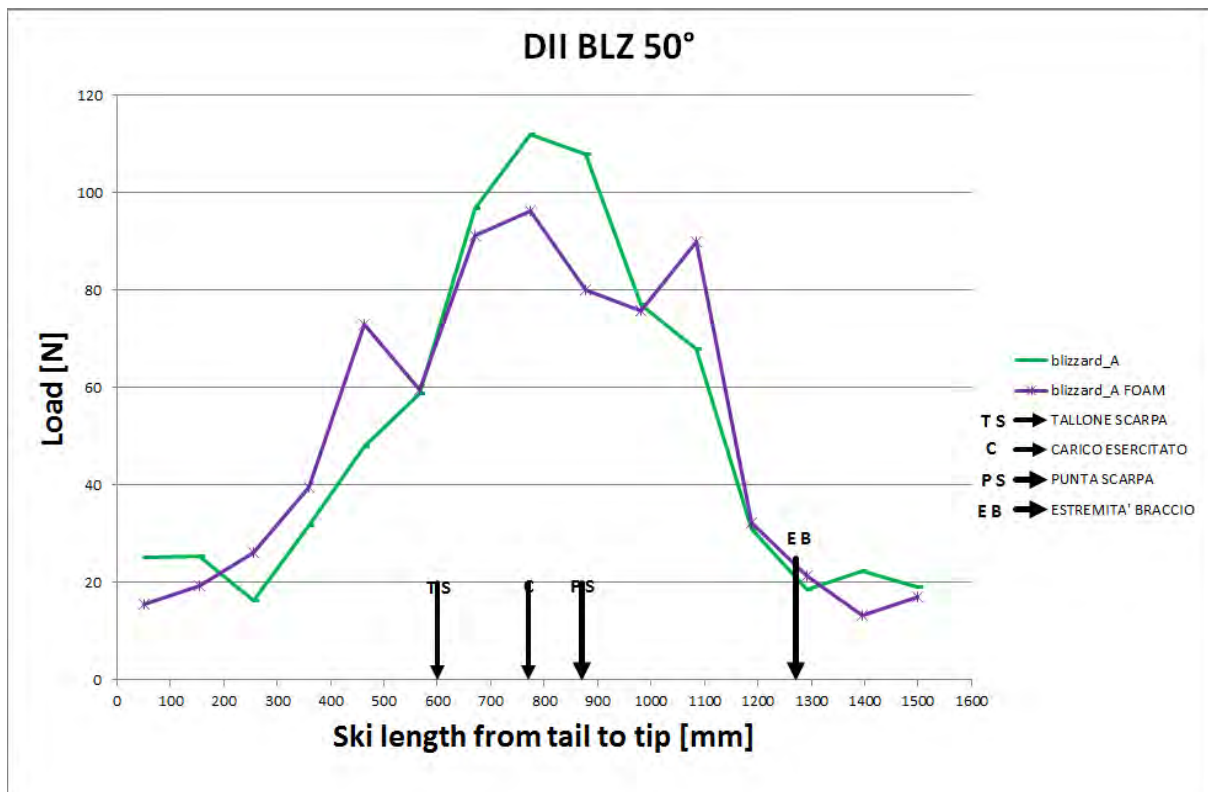
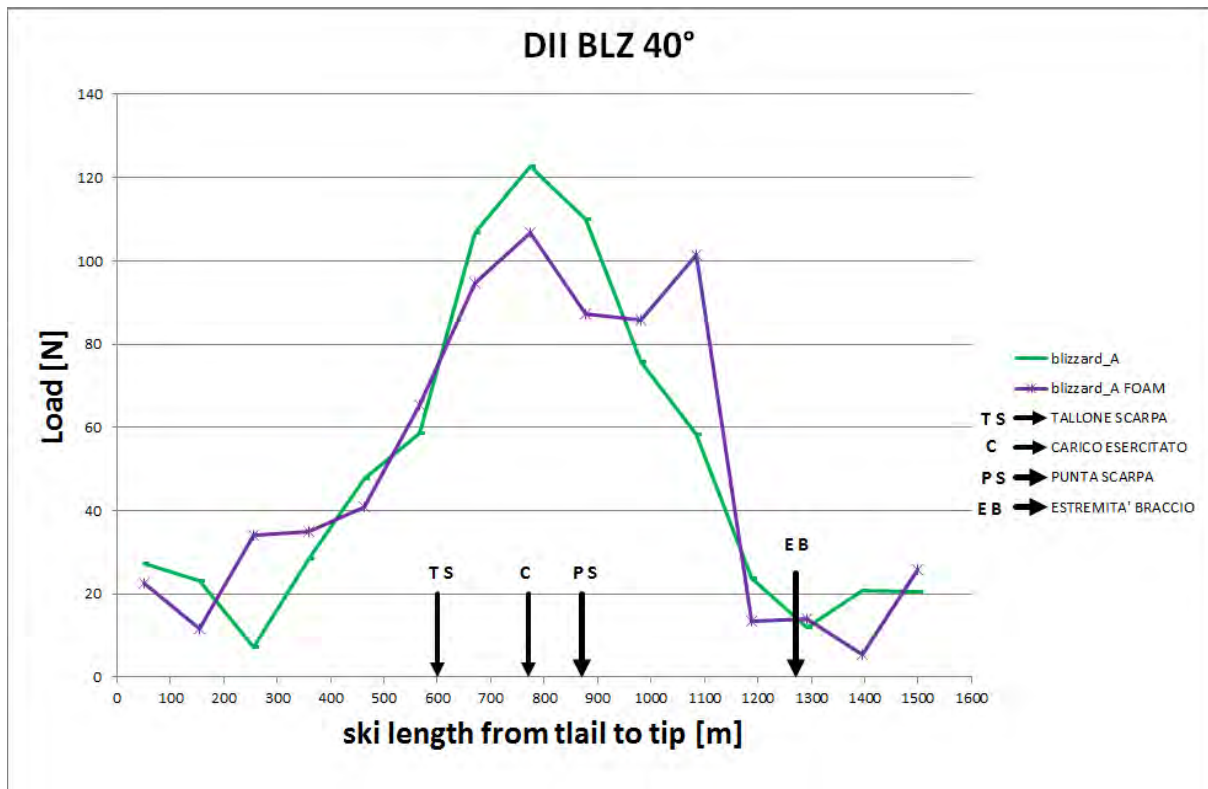
Finally, the foam Schiuma\_RP1 has been chosen because it has a low springback, its curves are close to hard snow curves and, in laboratory, there were panels of this foam already prepared for the test on the Edge Load Profile Bench. However, for angles greater than 40° the curves of Schiuma\_RP\_1 foam and hard snow diverge and this foam could be too much hard to simulate the snow.

### **5.5.2** *Slytech bench results*

During the foot imprinting, as said before, the Slytech bench works as usual. So, it's possible to make the comparison between the acquisition with and without panel foam.

Here the results for the angle tested, 40°, two at 50°, and two at 60° are presented (unfortunately one test at 50° it was not registered). As usual the diagram report the force register by the load cell along the ski length.





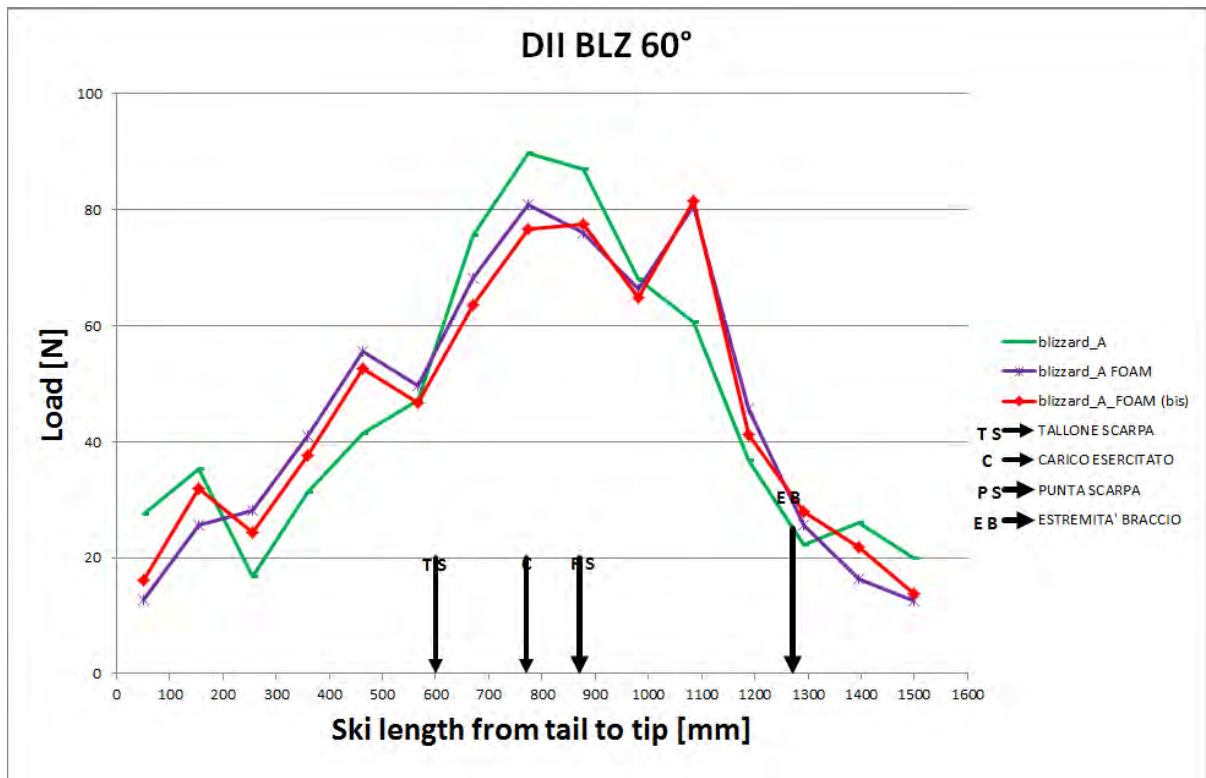


**Figure 5.18** Slytech bench results for the Blizzard SCS with and without panel foam interposition, at 40°, 50° and 60°

The load distribution along the ski reveals a discontinuity when there is the panel foam interposition.

The green line represents the ski during a normal characterization, as explained in Chapter 2.5.2. With the purple one, the load distribution is stored with the panel foam over the load cells. With this configuration, at cell number 14 correspond a peak, that it's not present with the green line. Probably this is justify by the non-perfect panel planarity. The 14 cell get an higher load that the other near cell, so it takes more load than usual. This corresponds to a peak registered and the following valley. Watching at the panel foam imprinted this effect is sensible visible, infect due to the hardness of the foam, the grooves depths have sized of a few millimeter, and in front of the cell 14 the mark is almost invisible.

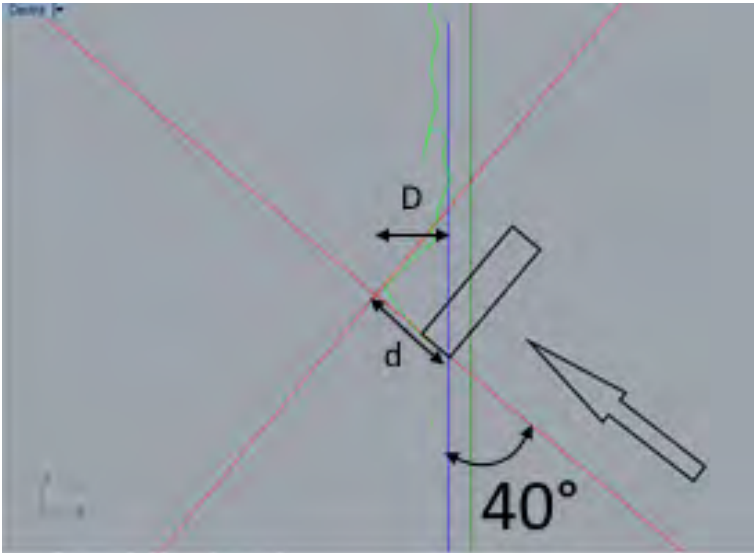
### 5.5.3 Scanarm results

The Scanarm has been positioned in front of the Slytech bench after the footprints, once synchronized all the grooves has been scanned. The rearrange file has been imported in Rhinoceros to reveal the grooves depth along the ski.

As said before, due to the non-uniform profile of the panel foam, the prints are not perfectly coherent from cell to cell. Therefore it has been decided to study only the cells 11, 12 and 13.

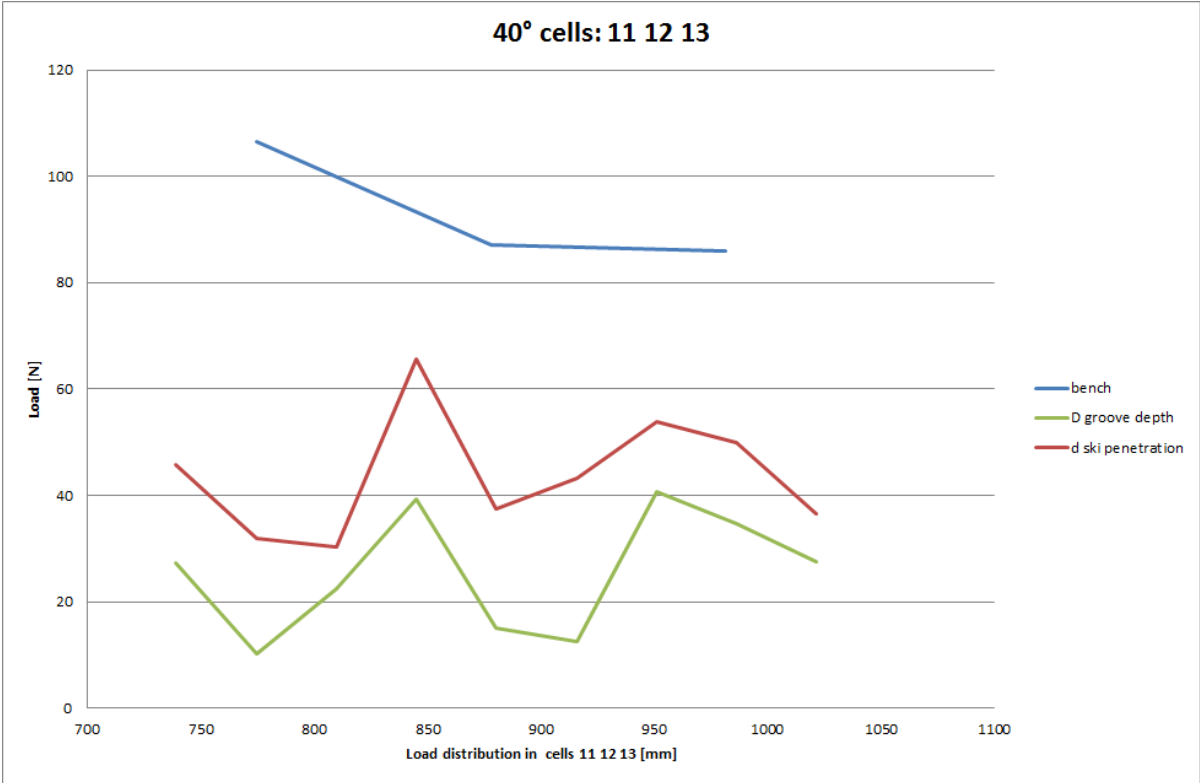
The results are presented with the overlapping of the Slytech load and extracted foam load, for the central cells 11, 12 and 13.

Both the technique used to find the print depth are presented and compared. Reminding the first method it provide the Newton applied by calculating the depth grooves  $D$ . Instead, the second method measure the penetration of the ski along the actuator axis  $d$ , with the creation of the guided line, in red in the next figure.



**Figure 5.19** The blue line represent the guided line foam surface, the red lines are the guided lines for the inclination,  $D$  is the groove depth,  $d$  the penetration depth

With the elaboration data form the Faroscan acquisition the prints present a lot of noise.



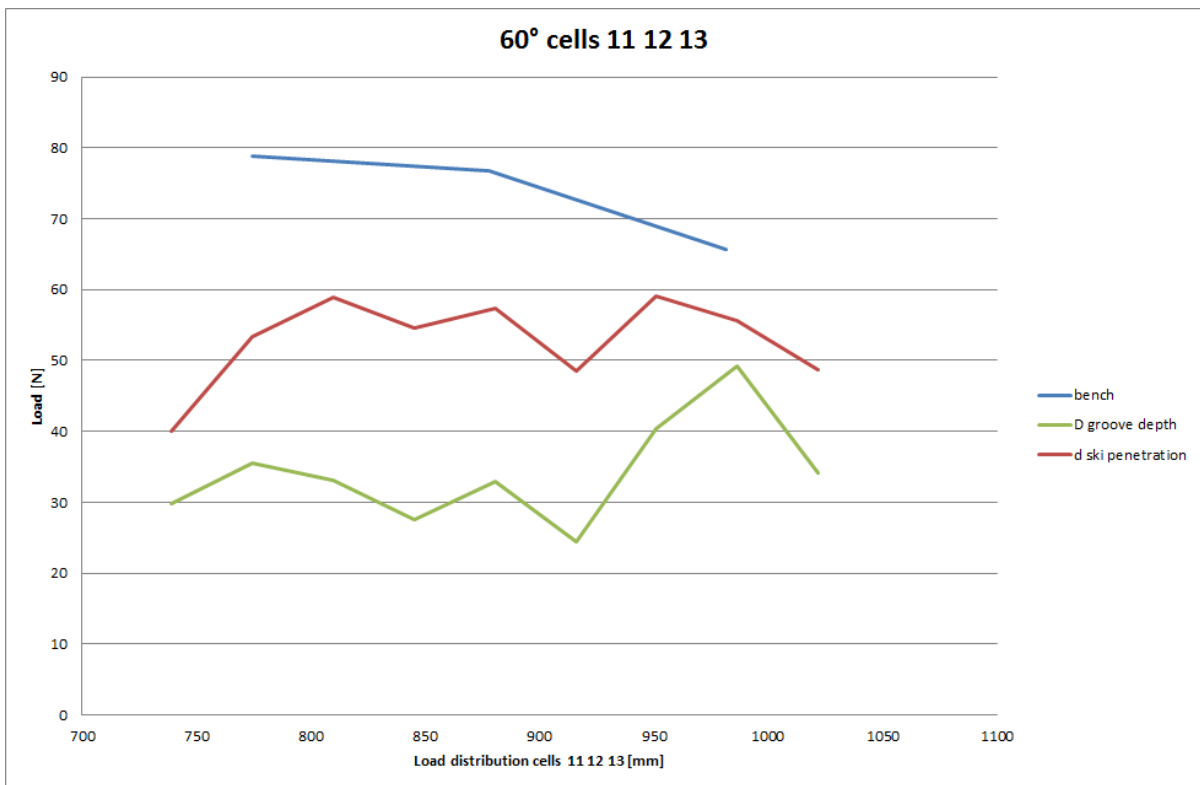
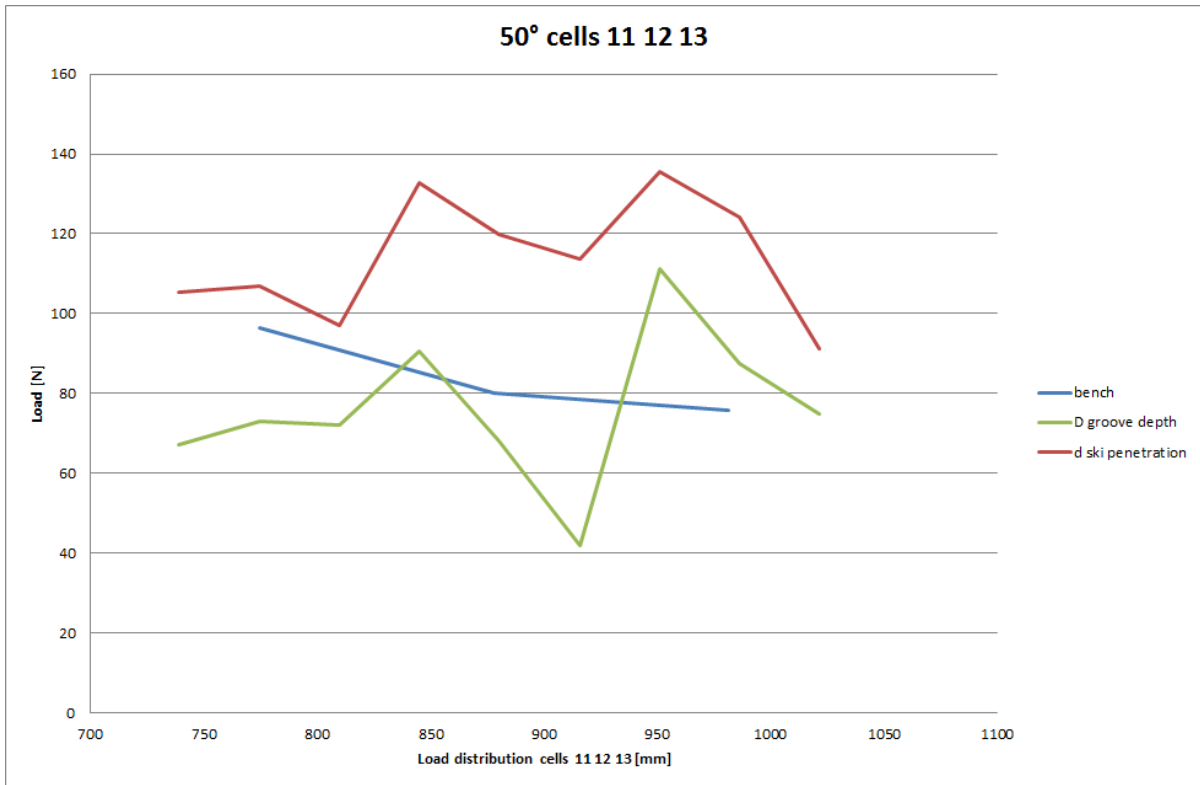


**Figure 5.20** Load distribution for Slytech bench, blue line, and foam characterization, in red and green, for cells 11, 12 and 13

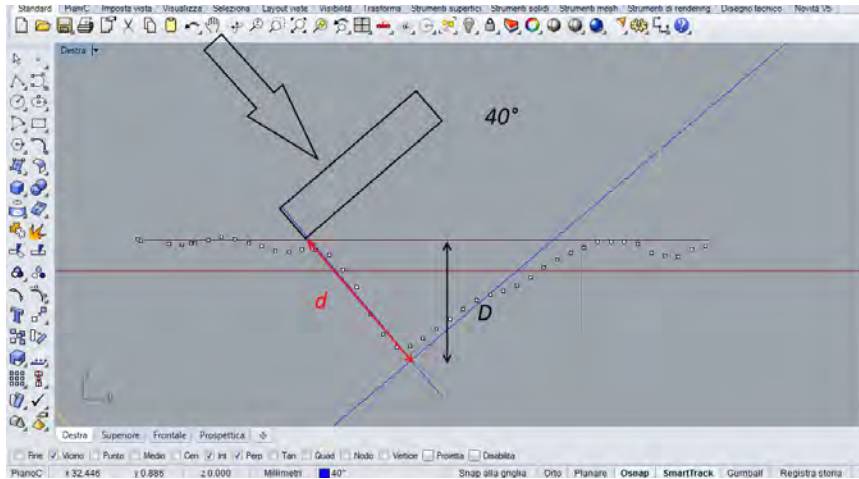
The lines are not perfectly matching, but some considerations are possible.

The green and red lines at 50° and 60° come from the mean of the two tests done per angle.

The method with the guided line, in red, better represents the distribution.

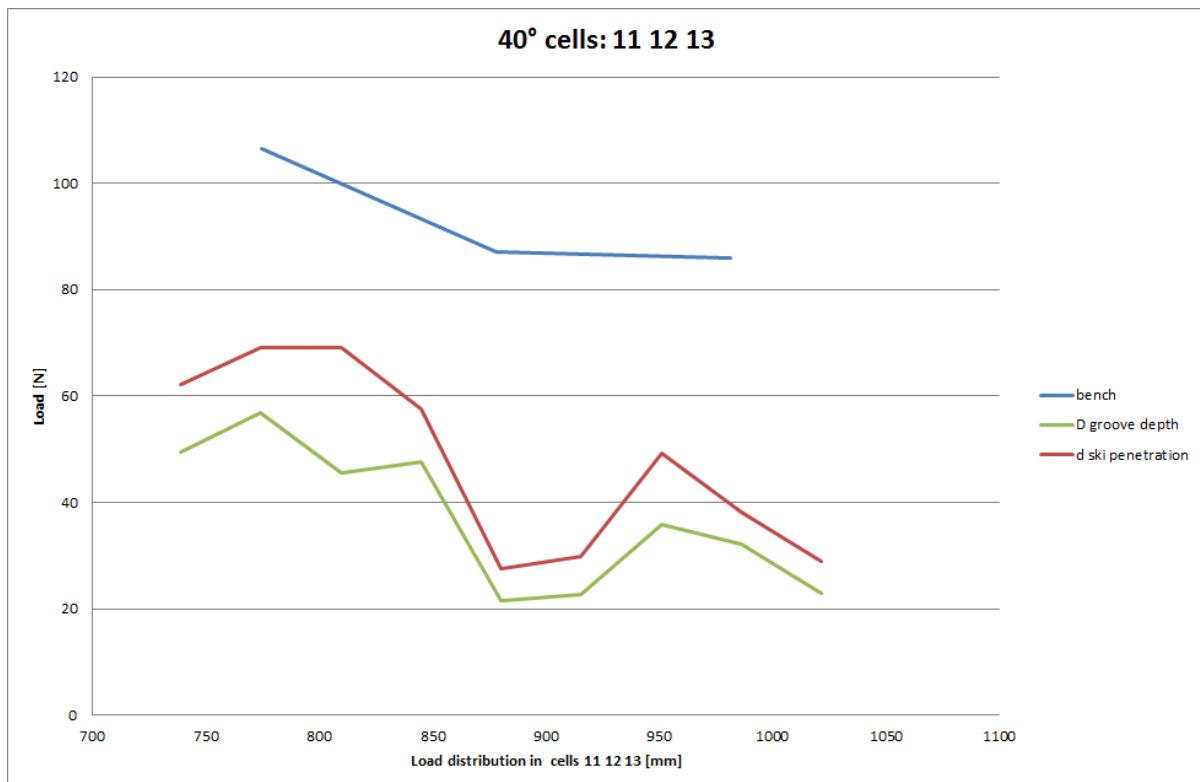
### 5.5.4 Smartscope results

Once scanned the total panel surface, the cells of interest have been extracted and analyzed in the laboratory by Smatscope ogp FLASH. Also in this case the file imported in Rhinoceros has been studied with the two technique, with and without guided line, here presented in blue



**Figure 5.21** Smartscope analysis data with Rhinoceros, in blue the guided line.  $D$  in the groove depth and  $d$  the ski penetration.

This method permits to obtain a points dispersion more easy to analyzed and more precise.



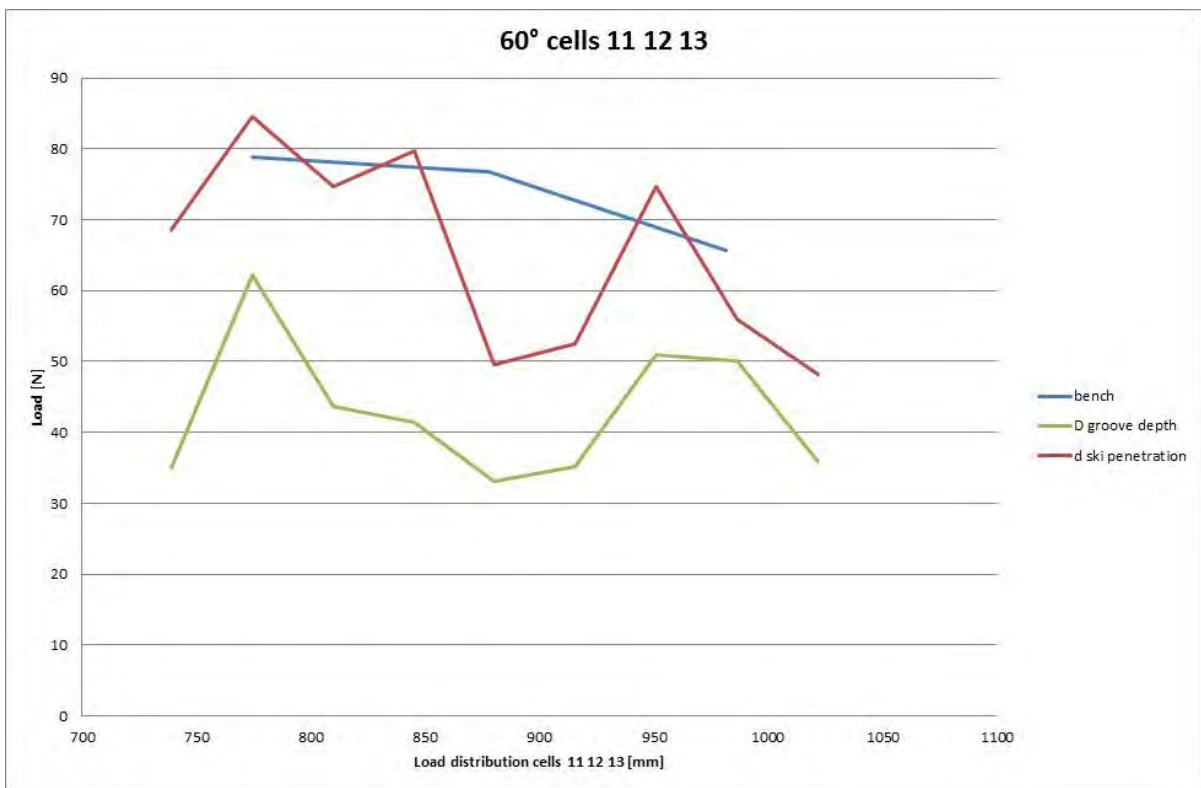
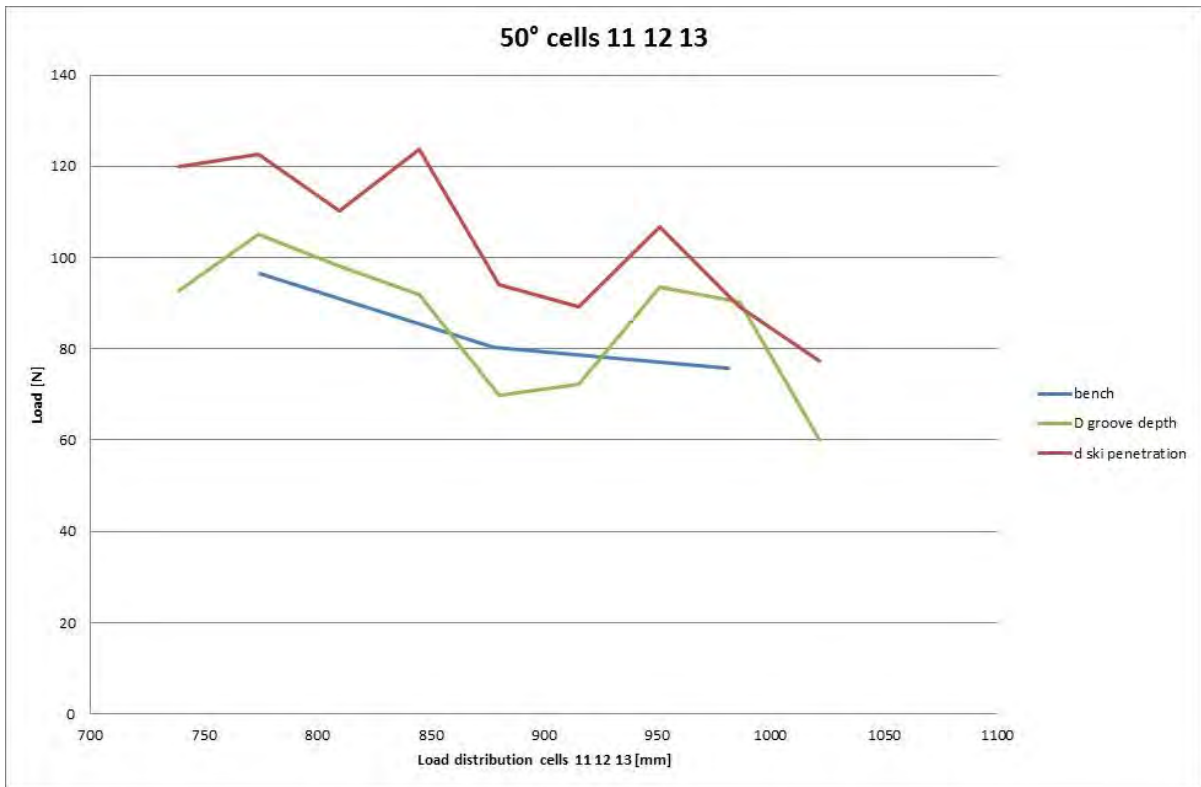
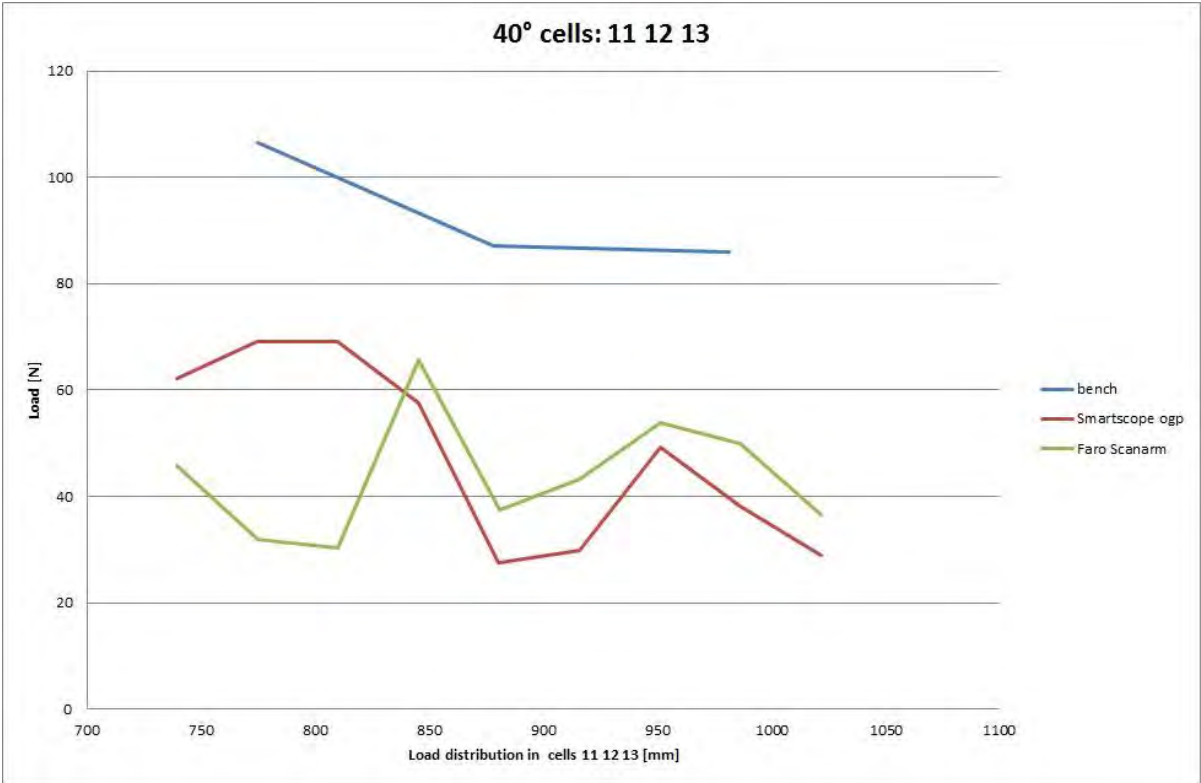


**Figure 5.22** Load distribution from Slytech bench, blue line, and foam characterization with Smartscope FLASH, at 40°, 50° and 60°, cells 11, 12 and 13

With Smartscope FLASH the characterization of the foam follows better the distribution of the load usually found with Slytech bench.

### 5.5.5 Smartscope and ScanArm results

The results that come from the two different foam characterization technique, Faro ScanArm and Smartscope ogp, are put in the graph. The method with the guided line during the data analysis is preferable for both.





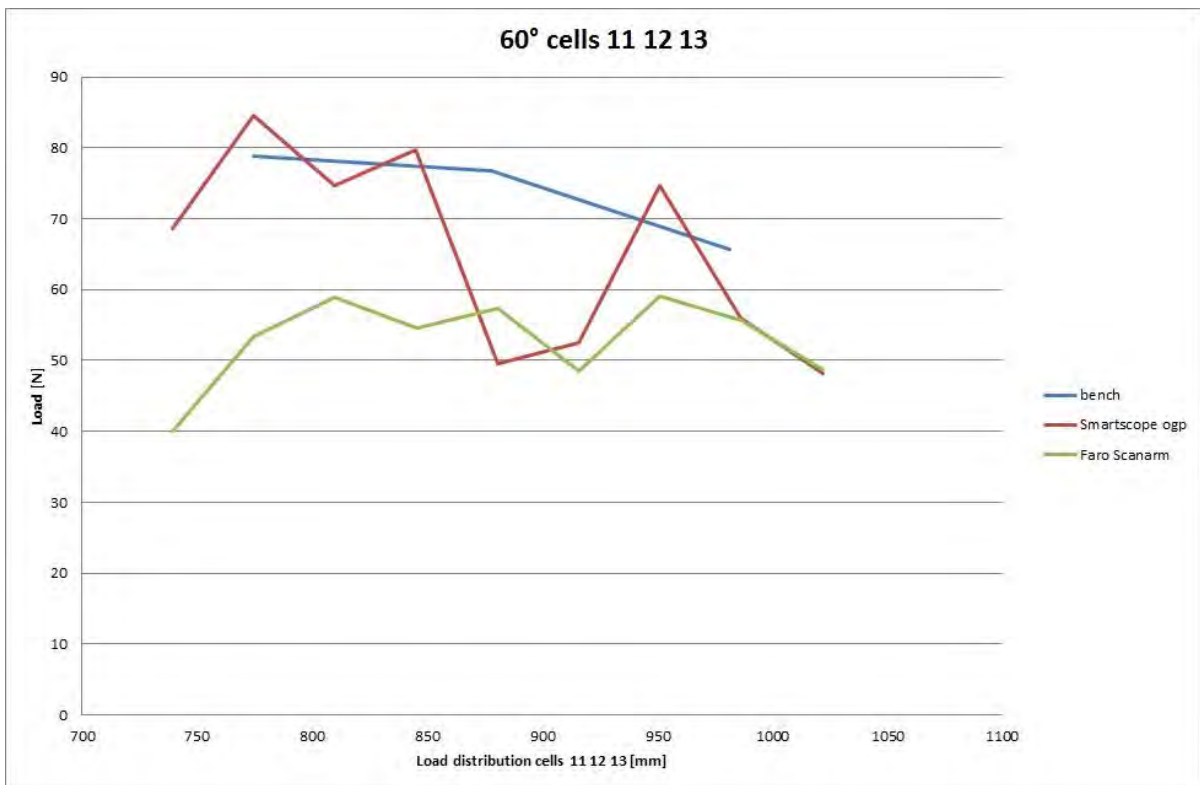
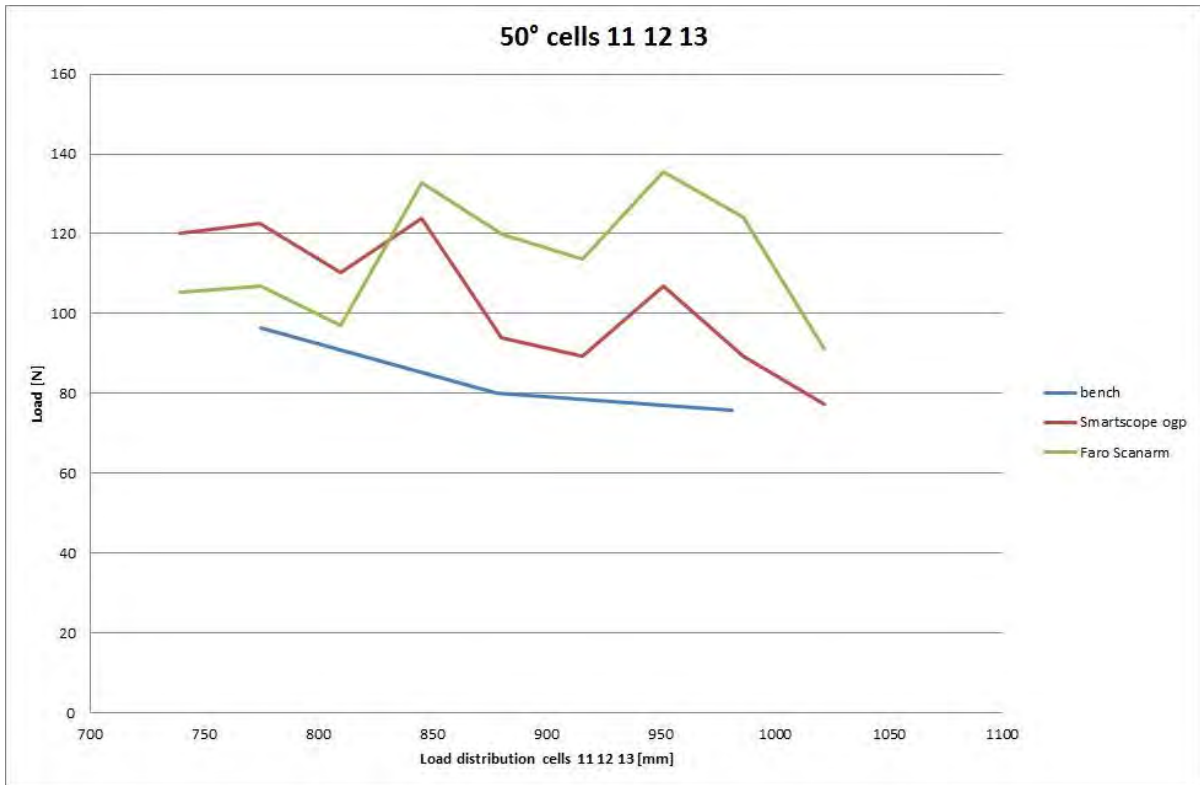


**Figure 5.23** Load distribution from Slytech bench, blue line, foam characterization with Scanarm, in green, and Smartscope in red, at 40°, 50° and 60°, for cells 11, 12 and 13

On average the Smartscope results better represent the load distribution along the ski. But some comment are necessary

## 5.6 Comments to the results

The new method presented in this thesis permits to obtain a ski load distribution along an artificial snow surface. The purpose of the technique is ambitious and some problems have been difficult to solve.

First of all it was almost impossible to find a foam product that presents the same characteristic of the snow. The choose one, RP1 in particular requires an high force to deform than the classified hard snow. This means that during imprinting the grooves that ski produce on the foam are sized of few millimeters. In this region of penetration the foam characterization is not so precise, and an interpolation function is necessary.

As said before, the thickness of the panel foam has to be constant.

The results are lines with an high dispersions of values, that reveals that there are some problems.

## 6. Conclusions

The accurate knowledge of ski structural and mechanical properties is very important for users and manufacturers. A key point for the comprehension of these properties is the distribution of pressure under the ski edge. Understanding the load distribution along the ski is one of the most important parameters to know in order to evaluate the ski performances.

The approach to load distribution investigations that was presented in Chapter 5 could introduce a new methodology to characterize the ski. The method involves testing of foam materials that could simulate the snow behaviour in a skiing slope, in order to obtain the edge pressure distribution of an alpine ski under realistic conditions. The results of this kind of “ski footprint” analysis were affected by some errors caused by the too heavy density of the foam and the disuniform thickness of the panel. In fact, the foam used was harder than the hard real snow, so the print depths were of the order of few millimetres, really small to be analysed with sufficient accuracy.

However, the innovative load analysis method introduced can also support the characterization of elastic compensation structures. The outcome of the arms characterization and in-field test experience can be summarized as follows:

- Each skier has a different feeling while skiing, and he can express it with different words. So, it’s really difficult to catch what the skier feels and tries to explain.
- Verbally the best quality felt by tester was the carving precision, that is the ability of the ski to follow the desired turning radius without skidding, with no evident side skidding.
- The best results were obtained with the WOOD arm, followed by CHB arm.

The elastic compensation structure is a promising innovation that needs a developing effort including more pairs of the same original ski, equipped with the aluminum supports and more samples of arms with the same characteristic. In this way more tests can be conducted in the same day with more people filling the evaluation form, so a statistically significant result can be obtained. Moreover, the tests will have to be conducted during the winter season with stable and good snow conditions.

Nevertheless, testers involved expressed positive comments especially for the stability during a carved turn. It seems like that not only the central zone under the bindings react with the snow, but also the complete ski does this. It’s like having a “longer ski” under the boot.

The wish is that the study here presented will support soon the production of such devices.



# Appendix

## PU details: Resina SG 95

COLORE		TRASPARENTE	TEST/ISO
RAPPORTO DI MISCELA	IN PESO (A : A/LP)	vedere istruzioni d'uso	
POT LIFE	SEC. (100 g A 25°C)	8-10 min.	
VISCOSITA' (CPS A 25°C)	COMP. A	1299	
	COMP. A/LP	1299	
	COMP. B	180	
PESO SPECIFICO (CPS A 25°C)	COMP. A	1,070	
	COMP. A/LP	1,070	
	COMP. B	1,190	
DUREZZA	SHORE A 23°C	82 D	868
	SHORE A 60°C	77 D	
	SHORE A 80°C	74 D	
RESISTENZA ALLA FLESSIONE	MPa (N/mm <sup>2</sup> )	88,6	178
MODULO DI ELASTICITA'	MPa (N/mm <sup>2</sup> )	2.195	178
RESISTENZA A TRAZIONE	MPa (N/mm <sup>2</sup> )	54	R 527
MODULO ELASTICO A TRAZIONE	MPa (N/mm <sup>2</sup> )	2.521	R 527
RESISTENZA ALL'URTO IZOD	Kj/m <sup>2</sup>	8,9	180
ALLUNGAMENTO A ROTTURA	%	12	R 527
RESISTENZA ALLA LACERAZIONE	N/mm <sup>2</sup>	---	34
CONDUCIBILITA' TERMICA	W/mK	208	BS 874
TEMPERATURA DI DEFLESSIONE provino 110x12,7x6,4 mm	°C	72	
RESISTENZA ALLO SNERVAMENTO	MPa (N/mm <sup>2</sup> )	64,2	R 527
ALLUNGAMENTO x SNERVAMENTO	%	6	
TEMPO DI VULCANIZZAZIONE	A 65°-70°C	vedere istruzioni d'uso	
RITIRO (secondo lo spessore della parete)	%	0,20	

**RESINA SG 95**

ISTRUZIONI D'USO	
Rapporto di miscela	100:150
Pot life (100 g a 25°C)	300 sec.
Temperatura della resina (nel forno)	40°C
Temperatura dello stampo (nel forno)	70°C
Tempo di miscelazione	30-60 sec.
Tempo di vulcanizzazione nello stampo a 70°C	45 min.
Trattamento post vulcanizzazione	no
Deareazione primaria	1-2 ore

Procedimento	<p>Pesare i 2 componenti. Calcolare il quantitativo di resina che rimane nella coppa "A". Sistemare le coppe all'interno della macchina ed azionare la pompa da vuoto. Azionare il motore di miscelazione. Una volta raggiunto il livello massimo di vuoto, attendere 5-15 minuti prima di colare il comp. A nel comp. B. Miscelare i componenti il più velocemente possibile. Colare la resina nello stampo in gomma siliconica fino a completo riempimento dello stesso. Aprire la valvola di ingresso aria nella camera da vuoto prima della fine del pot life.</p>
Note	<p>La temperatura dello stampo è importante. Sformare immediatamente dopo il tempo di vulcanizzazione raccomandato.</p> <p>Il quantitativo di pigmento che può essere utilizzato è l'1-2% max. del peso totale della resina.</p> <p>La resina SG 95 ha 2 tipi di componente A: componente A standard e componente A avente un pot life più lungo (SG 95 A/LP, pot life = 10 minuti).</p>
Quantitativo rimanente nelle coppe (coppa da 2 litri)	30 g - coppa A
Conservazione: - contenitori chiusi - contenitori aperti	15 - 20°C / Proteggere dal gelo. Posizionare le lattine (con il tappo) in forno a 40°C.
In caso di cristallizzazione del componente B	Posizionare la lattina del componente B nel forno a 70°C per 2-4 ore e mescolare la resina.

## Vittorio Quaggiotti Patent

### PRATICHE PER SIGLA

### "Monocorpo"

RIF	PAESE	CLIENTE	NUM DOMANDA	DATA DEPOSITO	NUM RILASCIO	DATA RILASCIO	DATA DEC	MESE RINN.
701.41	AT AUSTRIA	CERSAL S.R.L.	E 494.938	10/06/2004	1 841 541	12/01/2011	10/06/2024	8
701.76	FR FRANCIA	CERSAL S.R.L.		10/06/2004	1 841 541	12/01/2011	10/06/2024	8
701.84	DE GERMANIA	CERSAL S.R.L.		10/06/2004	1 841 541	12/01/2011	10/06/2024	8
701.122	CH SVIZZERA	CERSAL S.R.L.		10/06/2004	1 841 541	12/01/2011	10/06/2024	8
701.468	US USA	CERSAL S.R.L.	10/580.038	10/06/2004	7.559.571	14/07/2009	10/06/2024	1
701.473	JP GIAPPONE	CERSAL S.R.L.	Tokugan 2006-51	10/06/2004	4594303	24/09/2010	10/06/2024	9
701.476	CA CANADA	CERSAL S.R.L.	2.527.741	10/06/2004	2.527.741	17/01/2012	10/06/2024	8
801.331	ITE ITALIA	CERSAL S.R.L.	84106 BE/11	10/06/2004	1 841 541	12/01/2011	10/06/2024	8

### DEVICE FOR ANCHORING A BINDING TO A DOWNHILL SKI

in my patents list

**Inventor:** QUAGGIOTTI VITTORIO [IT]

**Applicant:** CERSAL S R L [IT] ;  
QUAGGIOTTI VITTORIO [IT]

**EC:** [A63C5/07](#); [A63C9/00D](#)

**IPC:** [A63C5/07](#); [A63C9/00](#); [A63C5/06](#);  
(+1)

**Publicatio** WO2008032349 (A1) - 2008-03-20

**Priority Date:** 2006-09-14

**n info:**

### *Influence of rubber inserts*

For this test a different rubber insert were used, and not the same configuration was tested. In particular for C H B arm was used a different one. Testing the arm with Slytech bench was used the rubber in figure A, during the characterization conducted in Tecnica the one reprints in figure B. Rubber insert influence the ski load distribution due to the fact that without it the arm do not preload the ski. Only when the ski is on bending there is some influence.

PU arm with and without rubber insert has been tested.



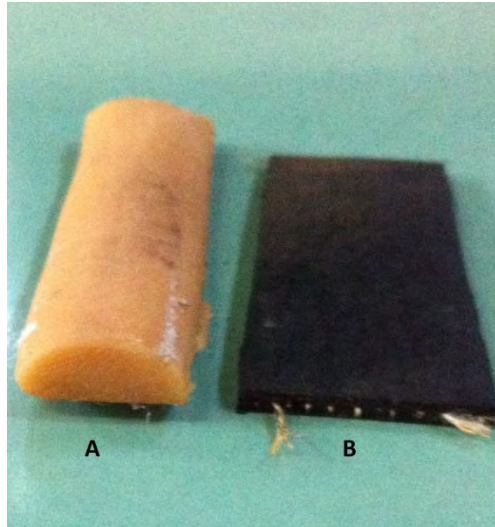


Figure 0.1 Rubber inserts

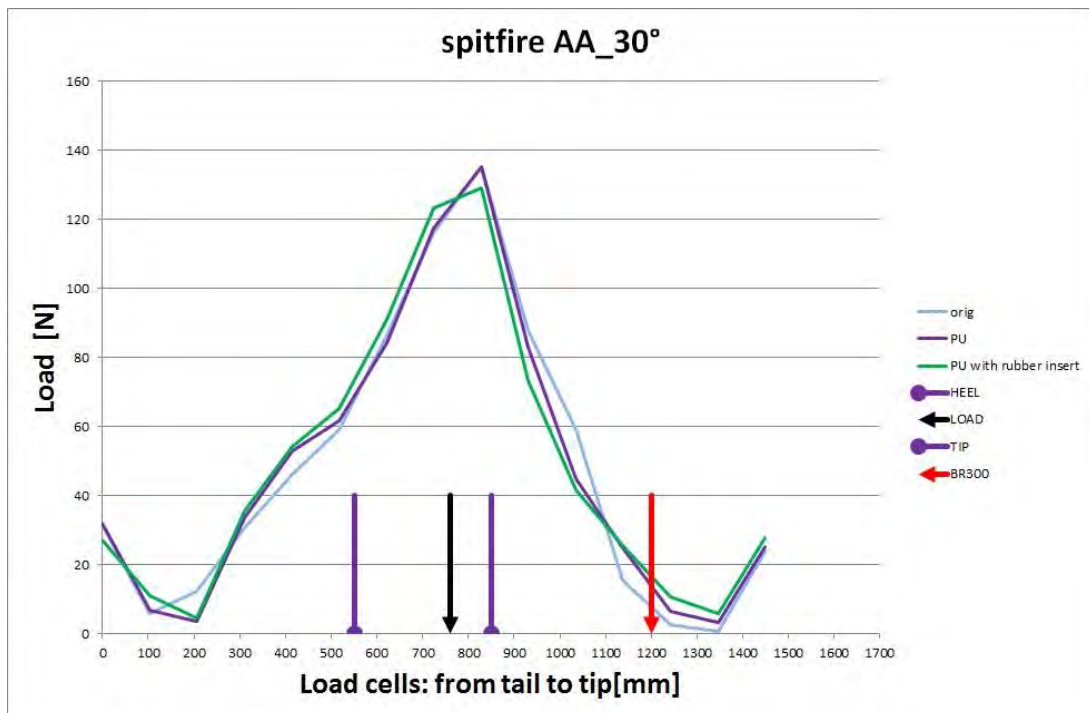


Figure 0.2 Influence of rubber insert in ski load distribution for PU arm

It can be noticed that the purple line is more similar to the original one, than the green one. The green line represents the effect of the arm with a rubber insert that permits to preload the ski more effectively.

The differences introduced are not so evident but not negligible. Preload introduced by the arm affects the total load distribution. As more rigid is the arm, more this effect is evident. An example is given in the next picture, where it represents the rubber insert influence for the aluminum arm.

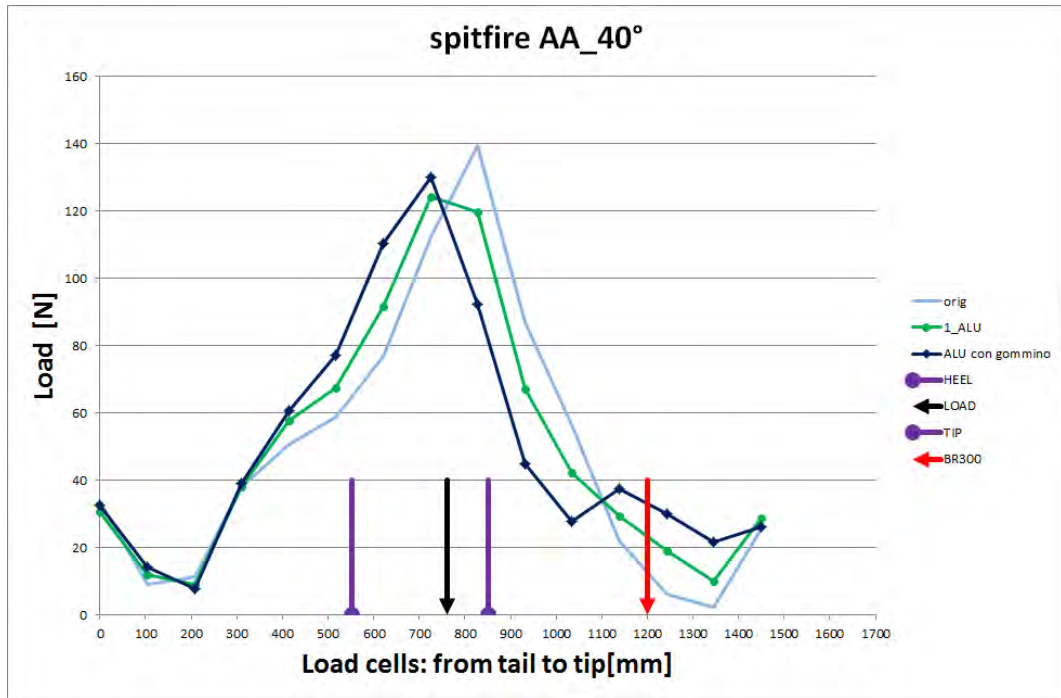


Figure 0.3 Influence of rubber insert for ALU arm



# Bibliography

*The use of an Edge Load Profile static bench for the qualification of alpine skis.* Nicola Petrone, 9th Conference of the International Sports Engineering Association (ISEA), 2012.

*Finite element simulation of a carving snow ski.* Peter Andreas Federolf, 2005.

*Pressure Distribution Under a Ski During Carved Turns,* P. Kaps, M. M<sup>o</sup>ssner, W. Nachbauer, and R. Stenberg, Science and Skiing, 2001.

*Structural behavior analysis of elastic compensation superstructure for innovative ski production.* Federico Signoretto, 2014.

*Analisi strutturale e prestazionale di sci innovativi con sovrastuttura di compensazione elastica.* Alberto Pillon, 2013.

*Numerical and experimental structural analysis of alpine skis with an innovative elastic compensation arm.* Riccardo Baldan, 2012.

*The modern alpine ski,* Bard Glenne, Anthony DeRocco, jim Vander, 1997.

*Reducing On-Snow Vibrations of Skis and Snowboards.* Gary C. Foss, Boeing Technology Services, Seattle, Washington Bard Glenne, K2 Corporation, Vashon Island, Washington, 2010.

*Mechanical Performance of Snow UnderLoading,* Fukue, 1979.

*Investigation on the ski-snow interaction in a carved turn based on the actual measurement.* Takeshi Yoneyama, Motoki Kitade, Kazutaka Osada, (ISEA), 2010.

Visited website:

<http://www.evo.com/how-to-choose-skis-size-chart-and-guide.aspx>

<http://skiing.about.com/od/downhillskiing/a/skiinghistory.htm>

<http://www.google.com/patents/US5647605>

[http://books.google.it/books?id=Nz\\_V2p3zG18C&pg=PA36&lpg=PA36&dq=ski+load+distribution&source=bl&ots=zFURkFwyJw&sig=ngCGfb2V7VXzTlqAQ9c8yoU5SiA&hl=it&sa=X&ei=oGnPU\\_S1Ce3Y7Abj14HYCg&ved=0CI4BE0gBMAw#v=onepage&q=ski%20load%20distribution&f=false](http://books.google.it/books?id=Nz_V2p3zG18C&pg=PA36&lpg=PA36&dq=ski+load+distribution&source=bl&ots=zFURkFwyJw&sig=ngCGfb2V7VXzTlqAQ9c8yoU5SiA&hl=it&sa=X&ei=oGnPU_S1Ce3Y7Abj14HYCg&ved=0CI4BE0gBMAw#v=onepage&q=ski%20load%20distribution&f=false)

<https://skiinghistory.org/history/timeline>

<http://www.mechanicsofsport.com/skiing/equipment/skis.html>



## RINGRAZIAMENTI

In primo luogo voglio ringraziare il professor Nicola Petrone: grazie dell'insegnamento che mi ha fornito, grazie delle esperienze ed opportunità che mi ha concesso di vivere.

Grazie a mamma e papà che mi hanno sempre incoraggiato e sostenuto.

Grazie a tutti i parenti, fratello, nonni, cugini, zii e non che sono sempre disponibili per ogni evenienza.

Grazie a Nicoletta che mi sta accompagnando in un percorso fantastico

Alex Persico